1963

Probable life of prestressed beams as limited by concrete fatigue, October 1963

F. S. Ople

PRESTRESSED CONCRETE BRIDGE MEMBERS

PROGRESS REPORT NO. 26

PROBABLE LIFE OF PRESTRESSED BEAMS AS LIMITED BY CONCRETE FATIGUE

F. S. Ople, Jr.

C. L. Hulsbos

DEPARTMENT OF CIVIL ENGINEERING
FRITZ ENGINEERING LABORATORY
LEHIGH UNIVERSITY
BETHLEHEM, PENNSYLVANIA

Part of an Investigation Sponsored By:

PENNSYLVANIA DEPARTMENT OF HIGHWAYS
U.S. DEPARTMENT OF COMMERCE
BUREAU OF PUBLIC ROADS
REINFORCED CONCRETE RESEARCH COUNCIL

Fritz Engineering Laboratory
Department of Civil Engineering
Lehigh University
Bethelehem, Pennsylvania

October, 1963

Fritz Engineering Laboratory Report No. 223.26A

TABLE OF CONTENTS

A B S T R A C T

Results of an investigation into the fatigue life of prestressed concrete flexural members are presented. A method for estimating the probable fatigue life of prestressed concrete beams where crushing of the concrete compressive block precedes fracture of the tension steel reinforcement when subjected to constant cycle fatigue loading is proposed. The solution is based on the results of an experimental study into the fatigue properties of plain concrete together with a theoretical analysis of the stresses and deformations in a prestressed concrete beam.

Particular attention is given to the effect of compressive stress gradient on the fatigue life of plain concrete. A relationship between the variables --- stress level, fatigue life, probability of failure, and stress gradient --- was established from results of constant load cycle tests on small plain concrete specimens.

The validity of the method is verified experimentally from results of a limited number of beam fatigue tests. The calculated and observed values of fatigue life for the test beams show reasonable agreement. The results of the beam fatigue tests provided information on the behavior of prestressed concrete beams failing by concrete fatigue.

1. INTRODUCTION

Prestressed concrete structural members subjected to repeated loads less than the static ultimate load may fail in fatigue by (1) fracture in tension of the prestressing reinforcement, (2) crushing of the concrete in the compression zone, (3) diagonal tension failure in the shear zone, or (4) progressive bond breakdown between steel and concrete. The particular type of fatigue failure that takes place depends on the stress conditions existing in the member due to repeated loading. Fatigue failure of prestressed concrete flexural members in a region of uniform bending moment or high moment-to-shear ratio is characterized by the occurrence of the first two types of failure, either separately or simultaneously. The present investigation is restricted to the study of the fatigue life of prestressed concrete flexural members failing by fatigue of the concrete in the compression zone.

1.1 BACKGROUND OF STUDY

A bibliography on fatigue of concrete has been published by the American Concrete Institute[1] in 1960 and a review of research was made by Nordby[2] in 1958. A recent publication by Venuti[3] includes a review of previous investigations on the fatigue of concrete beams. No detailed review will therefore be made here; however, previous

studies pertinent to the subject matter of the present investigation will be discussed.

The earliest reported investigations on fatigue of concrete can be traced to the studies on mortar specimens made by Considere[4] and De Joly[5] in 1898. Tests on plain concrete in compression were conducted by Van Ornum[6,7] starting in 1903, and in reporting his investigations, the use of S-N (stress-number of cycles) diagrams to represent concrete fatigue data was first introduced. Studies on the change of shape of the concrete stress-strain curves with load repetition and on permanent concrete deformations remaining after removal of the repeated loading were conducted by Probst[8] and his associates[1,2] in Germany. The use of a modified Goodman diagram (fatigue failure envelope) to illustrate the effect of range of stress in concrete fatigue was introduced by Graf and Brenner.[9] Results of previous investigations on fatigue of plain concrete have been summarized.[2]

The statistical nature of fatigue, as reflected by the variability of fatigue test results, is generally recognized. Several investigators[10,11,12,13,14,15] have applied statistical concepts in the interpretation of fatigue data of metals. That concrete fatigue results would exhibit a scatter, of magnitude at least in the same order as those observed in fatigue tests of metals, is to be expected. However, except for a few recent investigations,[3,16,21] it is surprising to note the lack of statistical treatment of fatigue data in most of the previous studies made on fatigue of concrete.[1]

The variability of concrete data was investigated by McCall[16] who applied statistical analysis to test results of plain concrete subjected to repeated loading in reversed bending. It was found that S-N-P (stress-number of cycles - probability of failure) relationships for concrete can be expressed reasonably well either graphically or mathematically.

Venuti[3] reported an experimental study on the variability of fatigue life of pretensioned prestressed concrete beams. Eighteen beam tests were replicated at each of five different maximum load levels ranging from 50 to 90 percent of the mean static ultimate load. The minimum load level was held constant at 10 percent. A relationship between the variables - load level, fatigue life, and probability of failure - was obtained from a regression analysis of the pooled data and expressed in the form of the cumulative normal distribution function. A study of the modes of fatigue failure was included. Although the test beams were classified as under-reinforced on the basis of static ultimate strength considerations, fatigue failures in the steel and in the concrete were observed. In general, steel fatigue occurred at low load levels and concrete crushing took place at high load levels. The scatter of test results increased with increasing load levels.

An early attempt at predicting the flexural fatigue resistance of prestressed concrete beams was made by Ekberg, et.al.[17,18,19,20] The procedure involves the use of the fatigue failure envelopes of the component steel and concrete together with the stress-moment relations

for the critical section of the beam. The method is simple and provides an approximate prediction of whether or not a failure will occur in either the steel or concrete for a given range of loading when repeated for one million cycles. Fatigue failure envelopes are required from repeated load tests of steel specimens in tension and plain concrete specimens in axial compression. In using the failure envelopes to describe the fatigue properties of the component materials in the beam, several factors are neglected, which are: (1) the wide scatter in fatigue test results, (2) presence of a stress gradient in the concrete compression zone of the beam, and (3) size effect.

Warner and Hulsbos[21] proposed a method for predicting the fatigue life of prestressed concrete beams failing by steel fatigue under constant cycle and cumulative damage loadings. The solution is based on the results of an experimental study on the fatigue properties of high strength steel prestressing strand and a theoretical analysis of the stresses and deformations in the beam induced by repeated loading. The S-N-P relationship for the strand was established from a regression analysis of the stress-fatigue life data together with an assumed log-normal frequency distribution of fatigue life. A generalized form of Miner's[22] cumulative damage theory was developed in order to apply at all probability levels. A series of beam fatigue tests was conducted to check the accuracy of the method. A comparison of the predicted fatigue lives with the results of the beam tests showed satisfactory correlation.

A means of obtaining a lower bound estimate of beam fatigue life as limited by fatigue failure of the concrete in compression is described by Warner and Hulsbos.[21] The presence of a stress gradient in the concrete compressive block is neglected and the problem is reduced to a case of fatigue failure of a concrete element subjected to repeated axial loading. The fatigue properties of the concrete in the beams are obtained from tests of plain concrete specimens with cross sectional area equal to the area of the compressive block and subjected to uniform compressive stresses equal to the extreme concrete fiber stress in the beam. Since the stress-moment relations for the concrete top fiber can be determined from the theoretical analysis, a lower bound estimate of fatigue life may be thus obtained.

1.2 OBJECT AND SCOPE

The object of this investigation was to develop a method to estimate the probable fatigue life of prestressed concrete flexural members as limited by the fatigue failure of the concrete in compression. The proposed method is based on the following information:

(1) Results of an experimental study into the fatigue properties of plain concrete with particular attention to the effect of compressive stress gradient on fatigue life, and

(2) A theoretical analysis of the stresses and deformations in a prestressed concrete beam presented in a previous study.[21]

A limited number of beams were tested under constant load cycles to check the validity of the proposed solution and to obtain information on the behavior of prestressed concrete beams failing by concrete fatigue. The calculated and observed values of fatigue life for the test beams show reasonable agreement.

An approximate design check against the possibility of concrete fatigue failure of beams subjected to repeated loading was formulated from the fatigue data. A relationship between the maximum concrete top fiber stress and the depth kd of the compressive block in the beam was established for a specified fatigue life N = 2,000,000 cycles and a probability "design limit" $P \leq 0.00001$.

2. FATIGUE PROPERTIES OF CONCRETE IN COMPRESSION

2.1 INTRODUCTION

A fairly extensive program of fatigue tests was conducted on small plain concrete specimens to study the fatigue properties of concrete in compression.

The main variables considered in the fatigue tests were stress gradient and maximum stress level. The following variables were held constant: concrete composition, frequency of cyclic loading, and minimum stress level. Only constant load cycle tests were conducted.

In the description of the small concrete specimen tests and analysis of results which follow, maximum and minimum stress levels are stated for convenience as percentages of the concrete static ultimate stress.

2.2 TEST SPECIMENS

The plain concrete specimens were 4- by 6-in. in cross section and 12 in. in height. Three concrete prisms were cast in 6- by 6- by 36-in. steel forms with a 2-in. plywood false bottom to reduce one breadth dimension to 4 in. Steel plates 1/4-in. thick divided each form into 12-in. lengths.

The specimens were manufactured in batches of 18 to 21 prisms and 12 to 14 6- by 12-in. cylinders. The batches were designated as AA, BB, CC, etc., in order of preparation. Eleven batches were manufactured at a rate of approximately one batch every twelve days. Table 1 lists the actual date of preparation, the number of prisms, and number of cylinders of each batch.

The concrete used in the manufacture of specimens was made from 3/4-in. maximum size crushed limestone, fine Lehigh river sand, and Type I ordinary Portland cement. Grading curves of the aggregates are shown in Fig. 12. The fineness modulus of sand was 3.03. The specific gravities of the fine and coarse aggregates were 2.57 and 2.77, respectively.

One batch of specimens required 6.5 cu ft of concrete. Except for the first three batches, the concrete mix was held constant with slight variation in the water content. A slump of approximately 2 in. was maintained for all batches. Details of the mix quantities are shown in Table 1.

The concrete prisms were vibrated; the cylinders were rodded. After the concrete had set, the specimens were covered with wet burlap. The specimens were stripped of the forms after three days and cured in a moist room until 28 days. Both prisms and cylinders were capped with carbo-vitrobond material and stored at room temperature until tested.

2.3 TEST SETUP

The testing arrangement is shown in Fig. 1. Cyclic loads were applied by an Amsler pulsator connected to a 110-kip hydraulic jack. The jack had spherical seatings at the base and at the end of the loading ram. The specimen was tested in a vertical position. Pairs of thick plates pivoting over cylindrical pins placed at both ends of the concrete specimen allowed jack loads to be applied at different eccentricities. The stress distribution was varied along the 6-in. dimension of the specimen. Figure 1(b) shows a close-up of a specimen under load applied at an eccentricity of one inch.

The spherical seats in the jack together with the pinned-end condition of the specimen made the setup very unstable in the plane perpendicular to the axes of the pins. Lateral braces consisting of a turn-buckle at one side and a spring at the other side were attached to the top plate. For carefully aligned specimens negligible amount of force, or none at all, was transmitted to the braces in the duration of the repeated load test.

2.4 PILOT TESTS

Before commencing the main experimental program, preliminary static and fatigue tests were conducted. These tests were made primarily to evaluate the performance of the test setup. The first

two batches of concrete specimens were used for this purpose. The following observations were obtained from these tests:

(1) The specimen size was adequate for the purpose intended.

(2) Linear strain distribution was obtained under static and dynamic loading.

(3) Lateral braces were required to maintain the alignment of the specimen under dynamic loading.

(4) Premature failures due to splitting in the longitudinal direction were remedied by capping the specimens with carbo-vitrobond material.

2.5 TEST PROCEDURE

2.5.1 Test Groups

The experimental program for plain concrete specimens was divided into static and fatigue tests. Static tests were conducted on prisms and cylinders to determine the stress-strain and ultimate strength properties of the concrete. Constant load fatigue tests were conducted on prisms to obtain maximum stress level versus fatigue life relationships for three types of stress distribution.

The following nomenclature for the test groups was adopted:

Numerals 1 and 2 referred to the static and fatigue tests, respectively. Lower case letters a, b, and c referred to the type of stress distribution the prisms were subjected to, thus:

Groups 1a, 2a - Tests with uniform stress distribution (e = 0)

Groups 1b, 2b - Tests with zero to maximum stress distribution (e = 1")

Groups 1c, 2c - Tests with one-half to maximum stress distribution (e = 1/3")

Group 1d - Static tests on cylinders.

The specimens from each batch were randomly assigned to the different test groups. The distribution of specimens is shown in Table 2.

2.5.2 Order of Tests

One batch of specimens was tested within approximately 15 days. The general order of testing was as follows:

(1) At 28 days: static tests on cylinders (Group 1d).

(2) Prior to commencing the fatigue tests: static tests on cylinders (Group 1d) and prisms (Group 1a).

(3) Fatigue tests on specimens of Group 2a.

(4) Approximately one week from the start of fatigue tests: static tests on cylinders (Group 1d) and prisms (Group 1b).

(5) Fatigue tests on specimens of Group 2b.

(6) Interspersed with the fatigue tests of Group 2b: static and fatigue tests on specimens of Groups 1c and 2c, respectively.

(7) At completion of fatigue tests: static tests on cylinders (Group 1d).

The above procedure was followed for each batch of specimens except for the first two batches which were used primarily as preliminary tests. Also, no specimens were tested under Groups 1c and 2c for the first five batches.

2.5.3 Static Tests

Static ultimate tests on cylinders and prisms were conducted in a 300-kip Baldwin Universal Testing Machine. Deformation measurements on cylinders were made using a mechanical compressometer over a 6-in. gage length with a multiplication factor of 2 and dial readings of 0.0001-in. Six-inch SR-4 gages were used to measure the strains on the prism. For eccentrically loaded prisms, only minimum and maximum strains were obtained since the linear variation of strain was established during the pilot tests. Deformations were observed at equal increments of load and the measurements were made without stopping the loading process. Total time of testing a cylinder or a prism was approximately five minutes.

In general, the static tests were carried to failure. However, because of the limited number of specimens per batch, static tests of Group 1c were conducted to approximately 90 percent of the static ultimate stress, and immediately after, the same specimens were fatigue tested under similar stress distribution (Group 2c). Static and fatigue tests on specimens of Groups 1c and 2c, respectively, were conducted in the dynamic test setup.

2.5.4 Fatigue Tests

Repeated load tests were conducted in the fatigue test setup shown in Fig. 1. The rate of loading was 500 cpm. The maximum and minimum loads were maintained throughout the fatigue test of a specimen. This necessitated adjustment of the loads from time to time over the test period as loads would drop off due to creep of concrete. The repeated loads were applied without interruption until failure or 2,000,000 cycles, whichever occurred first.

Tests were replicated at discrete maximum stress levels which varied for each group as follows: Group 2a - 65 to 80, Group 2b - 85 to 95, and Group 2c - 77.5 to 87.5. The specimens were assigned and tested at the different stress levels in a random manner.

The maximum and minimum load levels used during the fatigue tests of prisms were determined from the load-stress-strain relationships obtained from the static tests. The values of stress corresponding to the loads were therefore referred to the initial stress

condition of the concrete specimens. The loads for eccentrically loaded specimens were controlled by the stresses on the highest stressed surface of the prism. The method of establishing the loads is illustrated on Fig. 2 which shows the load-stress-strain curves of specimens from Batch HH. The loads that will induce a stress 80 percent of f'_c are given by P_a = 124.2 kips, P_b = 65 kips, and P_c = 95.5 kips, for Groups 1a, 1b, and 1c, respectively. Thus, for a stress level S_{max} = 80, the maximum loads required for fatigue tests of Batch HH specimens corresponding to Groups 2a, 2b, and 2c, respectively, are given by the preceding values. The loading portion of the stress-strain relation shown on Fig. 2 is an average of the curves of Groups 1a and 1b. The stress-strain curve for Group 1a (e = 0) is obtained by direct conversion of load to stress (f_c = P/A_c). The stress-strain curve for Group 1b(e = 1") is obtained by using a numerical differentiation procedure which is explained further in Sec. 2.7 and Appendix A.

2.6 TEST RESULTS

2.6.1 Static Tests

Static test results on cylinders and prisms are summarized in Tables 3 and 4, respectively. Average values of the different mechanical properties of concrete of each batch are listed.

In Table 3, two values of f'_c are listed for cylinders: f'_c at 28 days and at test. The age at test, being the time of fatigue tests of prisms, varied from batch to batch as shown in Table 4. No deformations were measured for cylinders tested at 28 days. The mechanical properties listed in Table 3 were therefore determined from the results of cylinders at test.

The mechanical properties of prisms are contained in Table 4. The values listed are the average results of Groups 1a and 1b.

The stress-strain relationships for cylinders and prisms are presented in tabular form in Tables 3 and 4. Furthermore, the stresses and strains are expressed in non-dimensional terms

$$F = \frac{f_c}{f'_c} \qquad \text{and} \qquad E = \frac{\epsilon_c}{\epsilon'_c}$$

where f'_c is the ultimate stress and ϵ'_c is the strain at ultimate stress. Only the loading portion of the stress-strain curve is presented, and in addition to the extreme points (E = 0, F = 0) and (E = 1, F = 1), four values of F are listed at E-values of 0.2, 0.4, 0.6, and 0.8. The F-values are the averages of the corresponding number of static tests conducted for each batch of specimens.

A typical load versus strain curve for Group 1b (e = 1") is shown in Fig. 2. In general the load-strain curves for Group 1b exhibited zero strains at the neutral face of the prism up to approximately 0.90 f'_c, after which tensile strains were observed. The magnitude of the tensile strain increased rapidly as the applied load

approached failure value. Maximum tensile strains recorded are contained in Table 5. Also contained in Table 5 are the maximum compressive strains with the corresponding failure loads.

A typical load versus strain curve for Group 1c (e = 1/3") is also shown in Fig. 2. Static tests of specimens of Group 1c were not carried to failure as was noted previously.

2.6.2 Fatigue Tests

Complete results of the constant load cycle tests on specimens subjected to three types of stress distribution are contained in Tables 6, 7, and 8. The same results are shown graphically on Fig. 5. The results are summarized in Table 9.

Loads corresponding to the maximum and minimum stress levels were applied taking into account the variation in the cross sectional area of the specimen. The nominal cross sectional dimensions of the prism were 4- by 6-in.; however, the actual dimensions of each specimen varied slightly.

Nine test specimens from Group 2a survived over two million load repetitions. The repeated load tests were discontinued and the specimens were tested statically to failure. A comparison of the ultimate static strengths of these specimens with that of specimens with no preloading was made. The results are contained in Table 10. The static strengths of the preloaded specimens were higher, the difference being greater at the lower maximum stress levels.

Typical specimen failures are shown in Fig. 3. Prior to complete crushing of the specimen, cracks were observed on the surface of the prism. This was particularly evident for tests with low maximum stress levels where the time interval between initiation of cracking and final failure was of long duration. In axially loaded specimens, cracking initiated at any one of the four vertical faces of the prism. The final failure mode is shown in Fig. 3(a). In eccentrically loaded specimens, cracks initiated at the highest strained surface and progressed toward the center of the specimen. At failure, a tensile crack appeared at the neutral surface, followed by spalling of a wedge-shaped section of the prism. Figure 3(b) illustrates this type of failure.

2.7 ANALYSIS OF STATIC TEST RESULTS

2.7.1 Concrete Stress-Strain Properties

A comparison of the stress-strain properties of cylinders and prisms was made from the results of the static tests. The ultimate static stress of prisms was found to be consistently higher than the cylinder ultimate stress, the average prism stress being 6 percent larger. The range varied from a minimum of 1 percent to a maximum of 11 percent.

The form or shape of the stress-strain curves were likewise investigated. A cubic parabola of the form

$$F = \alpha E + (3-2\alpha)E^2 + (\alpha-2)E^3 \qquad (2.1)$$

where stress and strain are expressed in non-dimensional terms

$$F = \frac{f_c}{f'_c} \quad \text{and} \quad E = \frac{\epsilon_c}{\epsilon'_c}$$

and the α term is the initial slope of the curve, $\alpha = E_c \frac{\epsilon'_c}{f'_c}$, where E_c is the modulus of elasticity, was proposed for representing the loading portion of the concrete stress-strain relation. The behavior of this equation had been studied[21] and it was found that for this equation to represent a monotonically increasing curve for values of E between zero and unity, the maximum value of α is limited to 3. Correlation with previous test data showed that values of α less than 3 was adequate for most types of concrete.

Equation 2.1 was used to represent the stress-strain relations for both cylinders and prisms. A best fit was made and the test results were well approximated by Eq. 2.1 for values of α of 2.20 and 1.85 for cylinders and prisms, respectively. The equations are compared with averaged test results in Fig. 4. Note that in Fig. 4(b) the abscissa is actual strain instead of non-dimensionalized strain E in order to show that the difference in F for the same ϵ_c is quite small. The experimental values plotted in Fig.4(b) were obtained from Tables 3 and 4. It must be pointed out that the best fit equation may not necessarily be that which is obtained by using the α value from the observed initial slope of the stress-strain curve but that equation with a chosen α value which pro-

vides the best fit at all levels of stress, as demonstrated in the two cases investigated here.

Only the loading portion of the stress-strain curve was treated in the analysis of the static test results, since stresses induced by repeated loads are in general restricted within this region. If the unloading portion of the curve is of importance, as in static ultimate strength studies, then the load-strain test results of Group 1b (e = 1") may be used to determine the shape of the unloading portion in a manner similar to that performed by Hognestad, Hanson, and McHenry.[23] Although the experimental procedures differed, the numerical differentiation method of calculating the stress-strain relationship from flexural tests can still be applied with slight modifications. The method of testing adopted by Hognestad, et al. provided a means for maintaining zero strain at the neutral surface throughout the duration of the test. Thus the zero-to-maximum strain distribution was strictly adhered to up to failure. In the corresponding tests reported here tensile strains were observed at the so-called neutral surface near ultimate stress. In order for the numerical differentiation procedure to be applicable to the test data obtained here, the equations were modified[24] to include the effect of the observed tensile strains. The equations are summarized in Appendix A.

The stress-strain curve as calculated by the numerical differentiation procedure from tests of eccentrically loaded specimens compared very well with the stress-strain curve for axially loaded

specimens in the loading portion of the curve. Because of the flatness of the load-strain curve and the rapid increase of tensile strains, the unloading portion of the curve as determined by the numerical differentiation procedure was not too reliable. However, the computed results gave an approximate picture of the shape of the unloading portion which compared well enough with Hognestad's findings. Figure 2 shows a stress-strain relation which includes the unloading portion of the curve.

2.7.2 Analysis of Variance

An analysis of variance[25] was performed on the cylinder tests from batches DD to KK to investigate the sources of variation of concrete strength. Only results from batches DD to KK were included because the concrete mix was the same for these batches and, furthermore, specimens prior to batch DD were used mostly for pilot tests. Cylinder test results obtained at test (Art. 2.6.1) were used in the analysis. An estimated overall variance of 0.1368 was obtained from the analysis of variance. It was found that 71 percent of the overall variance was contributed by the batch-to-batch differences and only 6 percent from specimen-to-specimen (within batch) differences. The remainder was attributed to the residual. The small variation in concrete strength of specimens within each batch indicated negligible increase in strength due to age, therefore, no correction of the fatigue loads was necessary. The batch-to-batch variation was not critical since the fatigue loads were

referred to the mean prism stress of each batch which was not affected by the variation between batches. The overall mean cylinder stress f'_c was 5.59 ksi.

2.8 ANALYSIS OF FATIGUE TEST RESULTS

The results of the constant load cycle tests on plain concrete specimens subjected to three types of stress distribution are shown in Fig. 5. These data gave an indication of the scatter of test results, the effect of stress gradient on fatigue strength, and the trend of the mean S-N curves.

The results obtained from the constant load cycle tests on small concrete specimens show quite vividly the non-reproducible aspect of fatigue testing. Scatter in fatigue test results arises in part from imperfect experimental technique, but the main contribution to the scatter is attributed to the considerable variability inherent in the phenomenon of fatigue failure itself. This statistical nature of fatigue is now generally recognized so much so that the prevalent practice of presenting fatigue data as a simple S-N (stress level-number of cycles) relationship is being supplanted by a more adequate representation in three dimensional form, S-N-P, where P is the probability of failure at a number of cycles equal to or less than N. Included in the analysis of test results therefore are attempts at fitting theoretical frequency distribution functions to the data

obtained. The scatter of test results show a tendency to increase in magnitude with decreasing maximum stress level for the same stress distribution. In addition, the scatter of test points failing within the same range of N are approximately of the same order of magnitude in different stress distributions. An examination of the computed standard deviations contained in Table 9 will substantiate this observation.

The effect of stress gradient on the fatigue strength of plain concrete is exhibited in Fig. 5. A significant difference in fatigue strength exists between tests of specimens with uniform stress distribution and specimens with varying stress distribution, the fatigue strength of the latter being higher. The fatigue strength of Groups 2a and 2b test results show a difference of approximately 15 to 18 percent over a range of fatigue life of 40,000 to 1,000,000 cycles. The lower fatigue strength of uniformly stressed specimens forms the basis for using such data as a lower bound estimate of the fatigue life of flexural members as limited by concrete fatigue in compression.[17,21] It is easily seen that substantial improvement of the lower bound method can be accomplished by taking the effect of stress gradient into account.

Two important observations are easily noted with respect to the trend of the mean S-N curves which have been drawn in Fig. 5:

(1) The mean S-N curves are approximately parallel to one another.

(2) The slopes of the curves are quite "flat".

The first observation suggests a possible existence of a relationship among the variables -- stress (S), fatigue life (N), and stress gradient (θ) -- which may be obtained empirically from this set of experimental data. The second observation points out the importance of determining the stress level as accurately as possible because a small change in the value of the stress reflects a large change in fatigue life. A change in stress of only 7.5 and 5 percent for Groups 2a and 2b, respectively, is required to change the fatigue life from approximately 40,000 to 1,000,000 cycles.

These observations gathered from the experimental results are considered in the analysis of data which follows.

2.8.1 S-N-P Relationships

Recent studies have been made to investigate the frequency distributions that may be associated with the phenomenon of fatigue failure. The logarithmic-normal distribution has been used by several investigators[12,21] and has been found to approximate the distribution of fatigue test results satisfactorily. Another type of distribution proposed[11,14,15] is one that is based on the statistical theory of extreme values. The logarithmic-normal and extreme value distributions both fit fatigue test data satisfactorily in the vicinity of the mean value ($P = 0.50$); however, appreciable difference between the two distributions may exist in the vicinity of the limiting values of P, such as $P \rightarrow 1.0$ and $P \rightarrow 0$. McCall[16] attempted to

describe the S-N-P relationship of test data of plain concrete beams loaded in reversed bending by a mathematical model which allowed for the variables S, N, and P to be contained in a single equation.

The frequency, or "plotting position", of each test result was determined[11,12,14] by ranking the specimens in the order of cycles to failure and calculating the probability of failure P of each specimen by

$$P_r = \frac{r}{n+1} \tag{2.2}$$

where r is the rank of the specimen and n is the total number of specimens tested at a particular stress level. (Note: The terms "frequency", "plotting position", and "probability" as used here are inter-changeable.) The range of the frequencies of all data plotted in this manner is $0 < P < 1$. The plotting position of each specimen included in the analysis is listed in Tables 6, 7, and 8.

S-N-P relationships were established from the fatigue data of small plain concrete specimen tests. Three types of frequency distribution functions were investigated and are discussed in the following:

Logarithmic - Normal Distribution

The log-normal distribution has the probability density function

$$f(X) = \frac{1}{\sigma\sqrt{2\pi}} e^{-\frac{(X-\mu)^2}{2\sigma^2}} \tag{2.3}$$

and the cumulative distribution function

$$P = F(X) = \frac{1}{\sigma\sqrt{2\pi}} \int_{-\infty}^{X} e^{-\frac{(X-\mu)^2}{2\sigma^2}} dX \qquad (2.4)$$

where $X = \log N$

and the parameters μ and σ are estimated by the mean and standard deviation, respectively, of the log N values. The functions f(X) and F(X) are completely determined when the values of μ and σ have been obtained.

The "goodness-of-fit" of the log-normal distribution was investigated by plotting the results of the constant load cycle tests of Groups 2a and 2b on logarithmic-normal probability paper as shown in Fig. 7. The observed values of fatigue life at each specified stress level should be randomly distributed about a straight line. In addition, in order for a theoretical probability function to be valid over all ranges of stress levels, the functions should not intersect. The log-normal distribution appears to fit the test data reasonably well within the range shown in Fig. 7.

The observed mean and standard deviation of log N values at each stress level are contained in Table 9. Least squares method was applied to establish a relationship between stress level and mean of log N values ($\overline{\log N}$), and likewise, between stress level and standard deviation (D). A simple straight line equation was used and the following relationships were obtained:

Group 2a:

$$\overline{\log N} = 18.20011 - 0.18139\ S \qquad (2.5a)$$

$$D = 1.0770 - 0.0115\ S \qquad (2.6a)$$

$(67.5 \leq S \leq 75)$

Group 2b:

$$\overline{\log N} = 28.47683 - 0.26468\ S \qquad (2.5b)$$

$$D = 1.6841 - 0.0165\ S \qquad (2.6b)$$

$(85 \leq S \leq 90)$

Group 2c:

$$\overline{\log N} = 20.19196 - 0.18442\ S \qquad (2.5c)$$

$$D = \text{----------}$$

$(77.5 \leq S \leq 85)$

The least squares fit for each test group was restricted within the limits of stress level indicated in the list of equations. In terms of fatigue life N, these limits lie approximately between 40,000 and 1,000,000 cycles. The equations for mean fatigue life and standard deviation are plotted in Figs. 5 and 6, respectively. Note that no relationship for standard deviation was obtained for Group 2c, since not enough replications were available to justify an analysis of this type.

The S-N-P relationships for the constant load cycle tests based on an assumed log-normal distribution are obtained from Eq. 2.4 where μ and σ are estimated by $\overline{\log N}$ from Eq. 2.5 and D from

Eq. 2.6, respectively. Evaluation of probability values in Eq. 2.4 is facilitated by the use of standard tables available in most texts on statistics.

Extreme Value Distribution

The statistical theory of extreme values may be applied to the analysis of the distribution of fatigue test data if it is assumed that the specimens that fail at various numbers of load cycles, tested at the same stress amplitude, are considered as forming a group of the weakest specimens out of (large) samples of the population tested.[14] The works of Freudenthal, Gumbel[14,15] and Weibull[11] have shown that the extreme value distribution agreed quite well with fatigue data from tests of different types of metals. The use of extreme values to represent the frequency distribution of fatigue data allows for the extrapolation of the S-N curve to the limiting values of the probability of failure, $P \rightarrow 0$ and $P \rightarrow 1.0$.

An asymptotic probability function of the type

$$L(N) = e^{-\left(\frac{N-N_o}{V_s-N_o}\right)^{\beta}} \qquad (2.7)$$

with the properties

$$L(V_s) = 1/e \qquad \text{and} \qquad L(N_o) = 1$$

has been proposed by the above investigators. The function L(N) is the probability of survival of a specimen at or before N cycles, thus

related to the probability of failure P(N) by the expression, $L(N) = 1 - P(N)$.

The parameters V_s, β, and N_o in Eq. 2.7 are defined as follows: V_s, or "characteristic number", is the mode of log N values with probability of survival $L(V_s) = 1/e$, $1/\beta$ is the "geometric standard deviation" proportional to the standard deviation of log N values, and N_o ("sensitivity limit", "threshold value", or "minimum life") is the number of cycles up to which all specimens survive for a given stress amplitude.

Equation 2.7 constitutes what Freudenthal and Gumbel have referred to as the "general theory".[15] If the minimum life N_o is assumed to be zero, then Eq. 2.7 reduces to

$$L(N) = e^{-\left(\frac{N}{V_s}\right)^{\beta}} \tag{2.8}$$

with boundary conditions $L(0) = 1$ and $L(\infty) = 0$.

This is the probability function used in the so-called "linear theory".[14] Equation 2.8 plots as a straight line on extremal probability paper, the coordinates of which may be expressed by $\log\left[-\log L(N)\right]$ versus $\log N$. In contrast, Eq. 2.7 plots as a curve on extremal probability paper, and becomes asymptotic to the limiting value N_o. Freudenthal and Gumbel have shown that fatigue data agreed well with the linear theory at high stress levels and

with the general theory at low stress levels, as in the case of nickel tested in reversed torsion.[15]

The linear theory was used in the analysis of the fatigue data obtained from the present investigation. Equation 2.8 was expressed in linear form

$$Y = a + bX$$

where $Y = \log(-\log L)$, $X = \log N$ and the parameters a and b were obtained from the experimental data by using the method of least squares. The following equations were obtained:

Group 2a:

$$\begin{aligned} S = 75.0: \quad & \log(-\log L) = -10.8079 + 2.2153\ (\log N) \\ S = 72.5: \quad & \log(-\log L) = -\ 8.0592 + 1.4822\ (\log N) \\ S = 70.0: \quad & \log(-\log L) = -\ 8.6731 + 1.5096\ (\log N) \\ S = 67.5: \quad & \log(-\log L) = -\ 8.4486 + 1.3180\ (\log N) \end{aligned} \tag{2.9}$$

Group 2b:

$$\begin{aligned} S = 90.0: \quad & \log(-\log L) = -\ 9.0160 + 1.8033\ (\log N) \\ S = 87.5: \quad & \log(-\log L) = -10.6945 + 1.9116\ (\log N) \\ S = 85.0: \quad & \log(-\log L) = -\ 8.1422 + 1.2536\ (\log N) \end{aligned} \tag{2.10}$$

No relationships were obtained for Group 2c because of the limited test results available.

The "goodness-of-fit" of the theory with the test results was checked graphically in Fig. 8. For each specified stress level,

the test values appear to be scattered randomly about the straight line. Except for S = 75 of Group 2a and S = 85 of Group 2b, the requirement that the functions should be parallel is fairly well satisfied. In addition, the linear theory is acceptable if the observed and estimated values of the geometric standard deviations are the same, at least within the errors of random sampling. The estimated standard deviation can be calculated by the method presented in Refs. 14 and 15. A comparison is made in Table 11 for the two test groups. Except for S = 67.5 of Group 2a and S = 87.5 and 90 of Group 2b, agreement between estimated and observed values is quite good.

The discrepancy between test and theory at some of the stress levels may be explained by the following reasons. Freudenthal and Gumbel suggests equal number of replicates with at least twenty specimens tested at each stress amplitude. The data analyzed in this investigation obviously did not meet this requirement. Furthermore, run-outs or specimens that did not fail after two million load cycles were not included in the analysis. Part of the anomalies between theory and test could therefore be explained by the limited number of test data. Another possible explanation may be due to the small interval between stress levels. Also, the assumption of zero minimum life ($N_o = 0$) for all stress levels may not hold true. However, because of the limited number of test replications at each stress level, it was deemed unnecessary to proceed with the analysis using the general theory. It is interesting to note that McCall,[16] in

applying both the linear and general theories to the analysis of fatigue data of plain concrete beams tested in reversed bending arrived at the conclusion that the extreme value distribution did not fit the data.

Mathematical Model (McCall)

McCall[16] proposed a mathematical model to describe the S-N-P relationship of fatigue data. An equation of the form

$$L = 10^{-aR^b(\log N)^c} \tag{2.11}$$

with properties

$$N = 1 \text{ for } L = 1$$
$$N \to \infty \text{ for } L \to 0$$

and

$$R = 0 \text{ for } L = 1$$
$$R \to 1 \text{ for } L \to 0$$

where a, b, and c are experimental constants, R is the stress level expressed as a ratio of static ultimate stress, N is the fatigue life, and L is the probability of survival, L = 1 - P. The use of L instead of P simplifies the form of Eq. 2.11.

Equation 2.11 can be linearized by taking the logarithms of the logarithms of both sides of the equation, thus reducing it into the form

$$Z = A + BX + CY$$

where X = log S, Y = log(-log L), Z = log(log N), and constants A, B, and C. Instead of the stress ratio R, the maximum stress level S was used and expressed as percent of the static ultimate stress in order to be consistent with the other methods of analysis presented here. The experimental constants were evaluated by a regression analysis of the test data from Groups 2a and 2b. The data from Group 2c were not included for reasons previously stated. The following relationships were obtained:

Group 2a:

$$\log(\log N) = 4.9092 - 2.2470(\log S) + 0.0538 \log(-\log L) \qquad (2.12)$$

Group 2b:

$$\log(\log N) = 9.3083 - 4.4076(\log S) + 0.0435 \log(-\log L) \qquad (2.13)$$

where L = 1 - P. The values of the experimental constants a, b, and c in Eq. 2.11 were obtained and the corresponding equations are:

Group 2a:

$$P = 1 - 10^{-4.97 \times 10^{-92} S^{41.80} (\log N)^{18.60}} \qquad (2.14)$$

Group 2b:

$$P = 1 - 10^{-1.11 \times 10^{-214} S^{101.31} (\log N)^{22.98}} \qquad (2.15)$$

Test results and theoretical equations are compared in Fig. 9. A measure of the degree of association among the variables S, N, and L

(or P) was obtained by calculating the multiple correlation coefficients for each test group. The correlation coefficients are 95.5 and 99.1 percent for Group 2a and Group 2b, respectively. It can therefore be concluded that the S-N-P relationships for plain concrete tested in fatigue with different compressive stress distributions can be described by a mathematical equation of the form presented in Eq. 2.11.

The foregoing analyses have shown that fatigue data from the small concrete specimen tests can be adequately represented by different types of S-N-P relationships. The results will be used in conjunction with the discussions on size and stress gradient effects following.

2.8.2 Statistical Approach to Size and Stress Gradient Effects

In recognition of the statistical aspect of fatigue, several researchers have applied probability theory to explain certain characteristics of fatigue such as the effects of size and stress gradient. A statistical theory was proposed by Weibull[11] originally applied to explain the effect of size of specimen on the ultimate strength of brittle materials and later extended to the problem of size effect in fatigue. Weibull verified his theory by applying it to test results of rotating-beam endurance tests on specimens with two different effective lengths. Stulen[13] obtained satisfactory agreement between

theory and test results of specimens with three different effective volumes. The fatigue specimens that Stulen investigated were prepared from the same steel and subjected to similar treatments prior to testing; however, the specimens were not geometrically similar. As a first approximation, an effective volume enclosing the region wherein a failure was most likely to originate was estimated by taking the volume where the oscillating stress was within 15 percent of the maximum stress on the specimen. In effect, the effective volume constituted a correction for both size and stress gradient. In a study of the fatigue failure of strand reinforcement in prestressed concrete beams, Warner and Hulsbos[21] used probability theory to account for the varying amount of strand reinforcement in a beam.

The distribution functions of two sizes of specimens which are geometrically similar and tested with the same stress distribution are related by means of the following equation

$$P_1 = 1 - (1 - P_o)^{v_1/v_o} \tag{2.16}$$

where P_o is the probability of failure of a specimen with volume v_o and P_1 is the probability of failure of a specimen with volume v_1. From Eq. 2.16 it is seen that if v_1 is greater than v_o, then P_1 is greater than P_o; in other words, the probability of failure at or before N cycles increases with size. Viewed from the standpoint of equal probability of failure, a larger specimen will have a lower fatigue life (or strength) compared with a smaller specimen. Thus with Eq. 2.16, it is only necessary to know the distribution function,

say P_o, of a specimen with volume v_o in order to obtain the distribution function of a different size specimen.

The effect of stress gradient observed in the results of the current investigation was expected since on the basis of probability theory the specimens with varying stress distribution had less material subjected to the maximum stress level, thus the fatigue strength is increased. Hence, it may be possible to use probability theory to non-uniformly stressed specimens if allowance is made for the fact that different volumes within the specimen are stressed at different levels.

Fowler[10] proposed a statistical approach to the stress gradient problem which Stulen[13] described in connection with the endurance limit of a specimen subjected to non-uniform alternating stress. In treating the problem of stress gradient, the specimen is thought of as consisting of small elementary volumes, for which the stresses may be determined. From the statistical theory of size effect, once the cumulative frequency distribution of uniformly stressed specimens of a given volume is known, the frequency distribution of the elementary volumes may be calculated by using Eq. 2.16. Note that the frequency distribution may be in terms of either endurance limit, fatigue strength, or fatigue life. The probability of a failure or no failure, whichever applies, of the whole specimen subjected to varying stress distribution is found by taking the products of the corresponding probabilities of the elementary volumes.

On this basis, Fowler derived the following formula:

$$P_\theta(S,N) = 1 - e^{\frac{1}{v_o}\int \ln\left[1 - P_o(fS,N)\right] dv} \qquad (2.17)$$

where $P_\theta(S,N)$ is the probability of failure of a non-uniformly stressed specimen, $P_o(fS,N)$ is the probability of failure associated with an elementary volume having a stress fS, f is the ratio between the elementary volume stress and the maximum stress S in the specimen, v_o is the volume of the uniformly stressed specimens, and N is the number of cycles to failure. Equation 2.17 may be integrated for a specified N value if an S-N-P equation is known for uniformly stressed specimens and the stress ratio f can be expressed in terms of the volume for a given specimen. Thus the S-N-P relationship for a specimen of any size subjected to any type of stress distribution may be obtained by using Eq. 2.17.

Equation 2.17 is actually a general expression for both size and stress gradient effects. It can be shown that for uniformly stressed specimens where f is constant with respect to volume, Eq. 2.17 reduces to the form of Eq. 2.16.

The set of data obtained from tests of small concrete specimens subjected to three types of stress distribution provided a means of checking the applicability of Eq. 2.17. S-N-P relationships were established for uniformly stressed specimens, such as Eq. 2.14. The stress distribution in the non-uniformly stressed specimens could be

expressed in terms of specimen volume knowing the concrete stress-strain equation and the linear strain variation in the specimen. However, because of the form of the S-N-P relation as given by Eq. 2.14, the integration process remained quite complicated. As a first approximation, the effective volume approach used by Stulen could have been resorted to.

It was however found unnecessary to go further into the effective volume approximation to show that the statistical approach to the stress gradient effect did not apply in so far as the set of data obtained in this investigation was concerned. According to the statistical theory of size and stress gradient there exist limiting S-N curves which correspond to infinitesimally small (upper limit) and infinitely large (lower limit) volumes of specimen. The S-N curves of specimens of any size and subjected to any type of stress distribution should fall within these limits.

The limiting S-N curves may be obtained from the known S-N-P relationship for uniformly stressed specimens by letting $P \rightarrow 1.0$ and $P \rightarrow 0$ for the upper and lower limits, respectively. Practical limits[14] may be taken as those corresponding to $P = 0.99999$ and $P = 0.00001$, respectively. Using Eq. 2.12, the following limiting curves are obtained:

Upper S-N Limit:

$$\log(\log N) = 4.9468 - 2.2470 (\log S) \qquad (2.18)$$

Lower S-N Limit:

$$\log(\log N) = 4.6402 - 2.2470 (\log S) \qquad (2.19)$$

With reference to the data shown in Fig. 5, the mean S-N curves of Groups 2a, 2b, and 2c should fall within the region bounded by the upper and lower limiting S-N curves. However, it can be shown by plotting Eqs. 2.18 and 2.19 on Fig. 5 that the experimentally determined mean S-N curves of Groups 2b and 2c fall outside the upper limit. This was sufficient evidence to reject the validity of the statistical theory of stress gradient as applied to the fatigue results of tests on small plain concrete specimens.

The discrepancy between test and theory may be explained by examining the manner of testing the concrete specimens in this investigation. The fatigue tests were conducted at constant load instead of constant stress cycles. While it was recognized that constant stress cycle tests would have been preferable, the difficulty of maintaining constant stress throughout a test was such that it was considered impractical to do so. Thus, the loads were maintained throughout the fatigue test of a specimen while allowing the stresses to change with load repetition. In this connection it should be noted that the stress level associated with a particular test specimen was referred to the initial stress condition of the specimen, or N = 1, since the stress-strain relation was obtained from static tests without preloading. The rate of change of stress with respect to load repetition is a force-and time-dependent phenomenon. The time effect was minimized by conducting all of the tests at a single frequency rate and without rest periods. The rate of change of stress was influenced primarily by the loading condition. It is conceivable that a difference in the

rate of change of stress existed between tests on uniformly stressed and non-uniformly stressed specimens, and that a more rapid rate of change occurred in the former, it being a more severe loading condition for the same maximum stress level. Therefore, an additional effect of the stress gradient on the fatigue life (or strength) may be attributed to the difference in rate of change of stress between uniformly and non-uniformly stressed specimens. As a consequence, the statistical theory of stress gradient as proposed by Fowler did not apply since no account was made of the effect of change of stress with load repetition.

It has been shown in the preceding discussion that the statistical theory of stress gradient is not applicable to the set of fatigue data obtained in this investigation. It must however be emphasized that no experimental evidence has been obtained here to likewise invalidate the statistical theory of size effect. It is believed that the theory of size effect may still hold true as long as such requirements of similarity in specimen geometry, stress distribution, and manner of testing are fulfilled.

2.8.3 S-N-P-Θ Relationship

The set of data obtained in this investigation may be utilized in developing an empirical approach to account for the effect of compressive stress gradient on the fatigue life of plain concrete prismatic specimens. If it is stipulated that the stress varies in one

direction only, then a stress gradient θ can be defined as the slope of the stress function at the point of maximum stress. An expression for the stress gradient θ can be derived knowing the stress-strain equation

$$F_x = \alpha E_x + (3-2\alpha) E_x^2 + (\alpha-2) E_x^3 \qquad (2.1)$$

and the linear strain relationship

$$E_x = \frac{E_{max}}{t} x$$

where F_x and E_x are the non-dimensional stress and strain at x, respectively, and E_{max} is the non-dimensional maximum strain corresponding to the maximum stress at t. The distances x and t are measured from the point of zero strain or stress. (Reference can be made to Fig. 21(b).) The above equations can be combined to give

$$F_x = \alpha\left(\frac{E_{max}}{t}\right)x + (3-2\alpha)\left(\frac{E_{max}}{t}\right)^2 x^2 + (\alpha-2)\left(\frac{E_{max}}{t}\right)^3 x^3$$

Differentiating F_x with respect to x and putting x = t

$$\theta = \left(\frac{dF_x}{dx}\right)_{x=t} = \frac{E_{max}}{t}\left[\alpha + 2(3-2\alpha)E_{max} + 3(\alpha-2)E_{max}^2\right]$$

Note that the expression inside the brackets can be obtained from Eq. 2.1 by taking $\frac{dF_x}{dE_x}$ and letting $E_x = E_{max}$. Thus, the stress gradient θ can be expressed as

$$\theta = \frac{E_{max}}{t}\left(\frac{dF}{dE}\right)_{E_{max}} \qquad (2.20)$$

The value of θ vanishes for each of the following conditions:

(1) $E_{max} = 0$

(2) $\left(\frac{dF}{dE}\right)_{E_{max}} = 0$

(3) $t = \infty$

The first condition is a trivial case when no strain is applied. The second condition occurs when E_{max} is equal to the strain at ultimate stress. A specimen subjected to a stress gradient and tested at a maximum stress level equal to the ultimate stress will fail at a very low number of cycles which is beyond the range of fatigue life considered in this investigation. The third condition corresponds to a case of uniform stress distribution where t may be taken as infinite in magnitude.

The stress gradient θ was calculated for specified values of F and t using the stress-strain relation in Eq. 2.1 with $\alpha = 1.85$ (α-value for prisms). The values of t were chosen to correspond to the three different stress distributions used in this investigation. The results are plotted as θ versus S_{max} curves in Fig. 10.

Knowing the S-N-P relationships for the different stress distributions, it is possible to superimpose on Fig. 10 curves of equal fatigue life N for a specified probability level P. N-curves were drawn for P = 0.50 and P = 0.37. In effect, each graph in Fig. 10 is a three-dimensional representation of S-N-θ for a specified value of P. Since other similar families of N-curves can be drawn for values

of P other than P = 0.50 and P = 0.37, an S-N-P-θ relationship is obtained. As a first approximation therefore, the S-N-P-θ relationship of concrete specimens subjected to stresses varying in one direction only may be determined by means of this graphical approach.

The empirical approach to stress gradient effect was developed using the test results obtained from specimens with the same size. The applicability of the method is however not limited to the size of the specimen tested here. For prismatic specimens, the following approximation may be used to account for size effect. A change in size (depth) in the direction of the stress variation is already accounted for in the stress gradient expression, for a change in t results in a change in θ which, in turn, reflects a change in fatigue life N. For instance, an increase in t decreases the fatigue life N. A change in size in the other two directions (width and length) may be corrected for by using the statistical theory of size effect. Equation 2.16 is reduced to the following form

$$P_1 = 1 - (1 - P_o)^{u \cdot w} \qquad (2.21)$$

where u and w are the width and length ratios, respectively, of the two different sizes of specimens.

2.9 SUMMARY

From the results of an experimental program conducted on small plain concrete specimens subjected to constant load cycles, a graphical

solution to account for the effect of compressive stress gradient on the fatigue life of plain concrete was obtained. The solution has been generalized to apply to specimens of different sizes by using a statistical explanation of size effect.

The results of the foregoing study may be utilized in estimating the fatigue life of concrete structural components which are critical in fatigue of the concrete in compression when subjected to repeated flexural loading. Concrete slabs and beams, conventionally reinforced or prestressed, may be treated if the concrete top fiber stresses and the stress gradient of the compressive concrete block induced by the repeated loading can be determined.

In this investigation, the results of the fatigue tests on small plain concrete specimens are used to estimate the probable fatigue life of prestressed concrete flexural members as limited by the fatigue failure of the concrete in compression. The procedure is presented in Chapter 4.

3. BEAM FATIGUE TESTS

3.1 INTRODUCTION

The main purpose of the beam fatigue tests was to obtain experimental verification of the proposed method for estimating beam fatigue life described in Chapter 4, and, at the same time, to obtain information on the behavior under repeated loading of prestressed concrete beams failing by concrete fatigue. Of the four beams tested, one was tested statically to failure and the other three were subjected to constant load cycle tests. The repeated load tests were carried to failure except for one beam which was statically tested to failure after having sustained approximately half a million load repetitions.

3.2 TEST SPECIMENS

The test beams were 12 ft long with a rectangular cross section approximately 6 in. wide and 12 in. deep. Six 7/16 in. diameter high strength steel strands were used as prestressing elements. These were placed in two layers of three strands each with the center of gravity of the total steel area approximately 7-3/4 in. from the top surface of the beam. The nominal initial prestressing force was 18.9 kips per strand corresponding to approximately 70 percent of the

static ultimate strength of the steel. The effective prestressing forces in the beams varied from 57 to 60 percent of the static ultimate strength.

Details of the test beams are contained in Fig. 11 and in Table 12. The test section was located in the middle 4-ft section of each beam. No stirrup reinforcement was included in the test region, however, two-legged stirrups of 3/8-in. intermediate grade reinforcing bar were placed in the shear spans of each beam as shown in Fig. 11.

3.2.1 Materials

The same aggregates were used for the beams as was used in the manufacture of the small concrete specimens, the grading curves of which are shown in Fig. 12. Type III, high early strength Portland cement was used.

Details of the mix quantities are contained in Table 13. Except for slight adjustments in the water content, the nominal concrete mix was held constant. A slump of approximately 3 in. was maintained. Five 7-cu ft mixes of concrete were required to fabricate four beams.

The mechanical properties of the concrete are contained in Table 14 which has been set up in the same manner as Tables 3 and 4. Five 6- by 12-in. cylinders and three 4- by 6- by 12-in. prisms were made from each of the five concrete mixes. Two cylinders from each

mix were tested at release of prestress force, the other three together with the three prisms were tested at the commencement of the beam tests. No prisms were made from Mix V because of lack of forms.

The reinforcement was 7/16-in. diameter seven wire uncoated stress relieved high strength prestressing strand manufactured by Bethlehem Steel Company. A load-strain curve for the strand from laboratory test is shown in Fig. 13. Failure occurred in the testing machine grips at a load of 29.6 kips. The load-strain curve provided by the manufacturer specified a minimum ultimate break load of 27.0 kips and a minimum elongation over a 24-in. gage length of 3.5 percent. The modulus of elasticity was 26.4×10^3 ksi.

3.2.2 Fabrication

Four test beams were cast end to end in a prestressing bed on the laboratory test floor. The prestressing steel was positioned straight throughout the length of the bed in two layers of three strands each. A special jacking arrangement was used to tension each strand to the required initial prestressing force. Formwork consisting of steel channel sides and plywood bottoms were assembled after the stirrups were positioned for four beams.

The concrete was mixed in a horizontal drum, positive action mixer and transported by buggies to the prestressing bed. The sequence of placing and mixing the five mixes of concrete was such

that no interruption occurred until the four beams were completed. The amount of concrete from one mix was not sufficient to cast a single beam, therefore concrete from only one mix was placed in the test section of each beam to achieve uniformity. Companion cylinders were cast from the different mixes as mentioned previously. The concrete in the beams was vibrated.

The specimens were covered with wet burlap for five days after which time the forms were removed. The beam surfaces were prepared for deformation measurements. The beams were allowed to cure under room temperature and humidity. At 14 days the prestressing force was released and the strands between the beams were burned off. The beams were stored in the laboratory until tested.

3.2.3 Prestress Data

The prestress was developed by jacks at one end of the bed with dynamometers placed at the other end to measure the force. The dynamometers, used extensively in beam fabrication in Fritz Laboratory and described in a previous report,[21] were placed at each strand. The measured force in each strand varied by at most 0.2 kips from the required value of 18.9 kips.

A 10-in. gage length Whittemore deformeter was used to measure elastic as well as creep and shrinkage deformations on the beam.

Prior to release of the prestressing force, aluminum targets were cemented to the surfaces of the beams in a pattern shown in Fig. 11. The beams were cast and tested along an east-west longitudinal direction, and for convenience the gage lengths were designated E, R, and RR proceeding east of the centerline, and W, L, and LL proceeding west of the centerline. Gage lines were placed at six different levels on the north and south faces of the beam. Thus, deformeter readings for WN-4 and WS-4 would correspond to the gage lengths on the west (W) section at level 4 on the north and south faces of the beam, respectively. This grid system allowed for the measurement of deformations at the top surface and along the C.G.S. of the beam and, in addition, provided data for determining the strain distribution in the vertical direction at the center of the beam.

Elastic and inelastic concrete strains obtained from deformeter measurements made before and after release of prestress and at the commencement of the beam tests were used to determine the elastic and inelastic concrete prestress losses. Prestress data are contained in Table 15. Strains and effective prestress forces with the corresponding percentages of total losses are given for the two levels of steel reinforcement and also for the C.G.S. The elastic strains due to the initial prestressing force were practically the same for the four beams. The inelastic strains however were different because the beams were tested at different ages.

Elastic strains determined from measurements made before and after release of prestress were different for the north and south

faces of the beams. The strains on the south face were larger than those on the north face for all the four beams. A comparison of the strains at the C.G.S. line is contained in Table 16. The percentage difference with respect to the average strain varied from 4 to 12 percent.

The difference in strains at release of prestress was attributed to a slight eccentricity of the center of gravity of the strand forces with respect to the centerline of the beam width. The magnitude of the total prestressing force was very large such that a small deviation in the location of the force could easily cause a big difference between the stresses in the north and south faces of the beam. Although care was taken to position the strands symmetrically about the vertical axis of the beam cross section by means of steel end plates with holes drilled for the strands, it is not inconceivable that a small deviation may have occurred. The fact that the south face strains were consistently larger than the north face strains for all beams seemed to justify this explanation.

Further observation showed that the difference in north and south face strains for Beam Nos. 1, 2, and 4 was practically the same and much larger than that of Beam No. 3. This may be explained by examining the concrete strengths at release of prestress force as contained in Table 14. The cylinder strengths of Beam Nos. 1, 2, and 4 varied from 4.37 to 4.62 ksi while that of Beam No. 3 was 5.04 ksi. As would be expected the beams with lower strength were strained more severely.

3.3 TEST PROCEDURE

3.3.1 Test Setup

The beam tests were conducted in a loading frame assembled on the dynamic test bed of the laboratory floor. An overall view of the test setup is shown in Fig. 14. The beams were simply supported over a 10-ft span; the supports consisted of a hinge at one end and a rocker at the other end. Concentrated loads symmetrically located 3 ft away from the supports provided a constant moment region of 4 ft over the central portion of the beam. This was the test section of each beam. The static and dynamic loads were applied by two 22-kip capacity Amsler hydraulic jacks with spherical seatings at both ends. A 1/2-in. thick homosote pad was placed between steel distributor plates and the top surface of the beam.

3.3.2 Static Ultimate Test

Beam No. 3 was tested statically to failure at 28 days. Loads were applied and measured by a pendulum dynamometer connected to the hydraulic jacks. During the test, the load was applied in two-kip increments up to cracking load and in one-kip increments from cracking to ultimate load.

Data obtained during the static test included deflection and Whittemore deformation readings at each load increment. Crack patterns were marked on the surface of the beam. At high loads consid-

erable creep occurred; the deflection and deformation measurements were recorded after the readings settled down to relatively steady values.

3.3.3 Constant Load Cycle Tests

Constant load cycle tests were conducted on Beam Nos. 1, 2, and 4. An Amsler pulsator was used to apply pressure to the jacks during the tests. The repeated loads were applied at a frequency of 250 cpm.

Fatigue loading was maintained throughout the beam tests to failure except for interruptions at specified intervals to conduct static tests. Also, prior to the commencement of each fatigue test, two static tests were conducted on the beam. These static tests were carried to loads somewhat higher than the intended maximum load level of the repeated load test. Deformation and deflection measurements were made during the static tests. Crack development was observed and recorded.

During the fatigue loading maximum dynamic mid-span deflections were obtained by Ames dial gage readings. The Ames dial is shown in Figs. 14 and 18(c). The manner of taking the deflection reading was as follows: the plunger was manually controlled and allowed to extend slowly upwards until it made contact with the bottom surface of the beam at its position of maximum deflection.

Readings were taken at regular intervals during the fatigue test. When not in use, the dial gage plunger was taped down out of contact with the moving test beam. The same dial gage was used during the static tests and the initial reference position remained the same throughout the fatigue test.

3.4 BEAM TEST RESULTS

3.4.1 Static Ultimate Test

Cracking and ultimate loads of Beam No. 3 are contained in Table 17. The load versus mid-span deflection curve is shown in Fig. 15. Concrete top fiber strains and C.G.S. deformations plotted in Figs. 16 and 17, respectively, were averaged over gage lengths EN, ES, WN, and WS. Beam No. 3 failed by crushing of the concrete in compression before yielding of the steel, a typical failure of an over-reinforced beam. Cracking was confined within the test region. These flexure cracks were initially vertical up to the level of the strand reinforcement after which they branched out into two opposing horizontal cracks and progressed along the steel level. The cracks were practically evenly spaced and at least one crack formed within each gage length. The cracking patterns for both sides of the beam were almost identical. A view of the failure zone for Beam No. 3 is shown in Fig. 18(a).

3.4.2 Fatigue Test Results

The results of the repeated load tests on Beam Nos. 1, 2, and 4 are contained in Table 17. Deflection and concrete deformation measurements are shown graphically in Figs. 15, 16, 17, and 19. Only the loading portion of the curves are plotted and the values at zero load indicate the remaining deflection or deformation upon immediate removal of the repeated loading and elastic recovery of the beam. Note that the remaining deflection or deformation is not necessarily permanent since partial recovery takes place during rest periods. Values of the applied loads shown in the table and figures include corrections for inertial effects obtained by comparing the dynamic deflections with the load-deflection curves from the static tests conducted at intervals during the fatigue test of the beam. The three beams were tested in the following order -- Beam No. 1, 4, and 2.

3.5 BEAM BEHAVIOR UNDER REPEATED LOADING

Deflection and deformation measurements together with crack development observations provided information on beam behavior under fatigue loading.

3.5.1 Mid-span Deflections and Concrete Deformations

Mid-span deflections measured under dynamic loads are plotted against number of cycles for each beam in Fig. 19. Load-deflection curves obtained from static tests at specified number of cycles are shown in Fig. 15. Deflections increased with number of cycles, the rate of increase depending on the severity of the fatigue loading. The rate of increase was quite rapid at the early stages of fatigue loading and just prior to failure. At failure the mid-span deflection was observed to approach the maximum static deflection of 0.87 in. obtained from the static ultimate test of Beam No. 3. This was indicated by the dynamic deflection curves of Beam Nos. 1 and 2 in Fig. 19.

Concrete strains measured at the top surface of the beam are plotted against jack loads in Fig. 16. Strain values were averaged over the four gage lengths EN, ES, WN, and WS. The shape of the load-strain curves changed with load repetition from an initially concave downward direction to a more or less straight one near failure. The remaining inelastic strains at zero load increased, and the total strains increased with number of cycles. At failure, the total strain -- elastic and inelastic -- corresponding to the maximum applied load indicated a tendency to approach a maximum strain value of approximately 0.0034 in. per in. which was observed during the static ultimate tests of Beam Nos. 3 and 4.

Concrete deformations at the center of gravity of the steel reinforcement (C.G.S.) are plotted against jack loads in Fig. 17.

There was variation in the deformation measured from one gage length to another depending on whether a flexure crack had formed between the gage points. In the east and west gage sections however, quite uniform deformations were observed since at least one crack had formed in each of the four gage lengths. The values plotted in Fig. 17 were therefore averaged over the gage lengths EN, ES, WN, and WS. Small deformations were observed at loads below that causing the opening of the cracks. Values of P_{crk} shown in Fig. 17 correspond to the cracking at the first static test. Of course cracks opened at loads lower than P_{crk} at subsequent static tests. There was very little remaining inelastic deformation at zero load which indicated that very slight reduction occurred in the magnitude of the prestressing force with load repetition. The curve for the last static test (N = 525,000) of Beam No. 4 indicates an increase in prestress force. This was attributed to the severe cracking of the beam and upon removal of the loads, the cracks did not close completely.

3.5.2 Cracking and Failure Patterns

Cracking of the beams followed a common pattern. The crack patterns after the initial static tests were similar to that observed in the static ultimate test. Subsequent applications of repeated loading caused the flexure cracks to extend along a longitudinal path more or less following the level of the steel reinforcement. A strong tendency was noted for adjacent cracks to link

together and form an essentially single longitudinal crack. This longitudinal cracking at the steel level may be attributed to the fact that the neutral axis was approximately located at the C.G.S.

During the test of Beam No. 4 which was subjected to the least severe fatigue loading, this longitudinal cracking became pronounced after 500,000 cycles, and soon after, the horizontal crack formed completely within the test region on both sides of the beam. The crack pattern on the south face of Beam No. 4 after 525,000 load repetitions is shown on Fig. 18(c). The longitudinal crack tended to separate the concrete below the steel reinforcement from the main body of the beam. This cracking phenomenon was unexpected.

It was previously mentioned that the mid-span dynamic deflections were measured with the Ames dial plunger in contact with the bottom surface of the beam. The increase in width of the longitudinal crack just above the dial gage was therefore registered with the mid-span deflection readings. The considerably large readings obtained were erroneously interpreted as an indication of beam failure and it was decided to discontinue the fatigue test of Beam No. 4 at 525,000 cycles.

A static test to failure was conducted on Beam No. 4 after having sustained 525,000 load repetitions. The beam failed by crushing of the concrete in compression at an ultimate load of 18 kips per jack. This value is 90 percent of the static ultimate load of Beam No. 3. Mid-span deflections and concrete deformations

obtained during the static test to failure correspond to the curves with N = 525,000 cycles in Figs. 15, 16, and 17.

Results of the static ultimate test indicate that Beam No. 4 could have sustained additional applications of repeated loading before crushing of the concrete in compression occurred. However, the total number of cycles would be drastically reduced once the concrete below the steel level separated completely from the main body of the beam. Although the stress condition at maximum load level may not be affected, the removal of the bottom concrete section would introduce a severe change in the stress condition at minimum load level. A large reduction in the concrete area and moment of inertia together with a considerable increase in eccentricity of the total prestress force would create tensile stresses at the top fiber of the beam. Hence, the increase in the range of stress variation under repeated loading would have shortened the fatigue life of Beam No. 4.

The close-up view of the failure zone of Beam No. 2 in Fig. 18(b) also shows a similar longitudinal crack along the steel level. However, this crack formed more or less simultaneously with the complete crushing of the concrete compressive block.

Crushing of the concrete in the compression zone was taken as the condition of fatigue failure of a beam. Crushing of the concrete was preceded by the appearance of intermittently short hairline cracks on the top surface of the beam as shown on Fig. 18. The hair-

line cracks propagated from the top towards the neutral axis and were oriented along the longitudinal direction of the beam. Considerable number of load repetitions separated the initial appearance of the hairline cracks and the complete crushing of the compression zone. In all three beams hairline cracks had formed when the last static test was conducted. The fatigue failure of Beam No. 2 is shown in Fig. 18(b). A disc-shaped portion of the top concrete zone spalled off and a wedge-shaped region of crushing within the test section was evident.

4. ESTIMATION OF BEAM FATIGUE LIFE

4.1 INTRODUCTION

A method for estimating the probable fatigue life of beams as limited by fatigue failure of the concrete compressive block was developed using the information obtained from the study of the fatigue properties of small concrete specimens in Chapter 2 together with a known stress analysis.[21] Results of the beam fatigue tests in Chapter 3 provided experimental information for checking the accuracy of the proposed method.

4.2 REVIEW OF STRESS ANALYSIS

In order to use the results obtained from the small concrete specimen tests to estimate beam fatigue life, it is necessary to know the stresses in the concrete compressive block in the beam induced by a system of repeated loadings. In Ref. 21 equations were derived for the stresses and deformations in the steel reinforcement and in the concrete of prestressed beams with rectangular cross section and with one horizontal layer of steel reinforcement. Other cases such as beams with I sections and beams with steel reinforcement located at several levels were briefly treated. In particular, the equations were used to

establish the relationship between steel stress and applied moment or load since the study was concerned mainly with the fatigue failure of strand reinforcement in prestressed concrete beams. The same stress analysis is used in this investigation to establish the relationship between concrete top fiber stress and applied moment. A brief review of the theoretical analysis follows.

The analysis is divided into two parts depending on the range of loading; zero moment to M_{oN} and M_{oN} to static ultimate moment, where M_{oN} is the moment at which cracks begin to open. In the first loading stage, both steel and concrete are assumed to behave elastically. In the second loading stage, the analysis is complicated by the cracked condition of the beam section. The analysis of beam behavior is based on a consideration of the following:

(1) Stress-strain relations for concrete and steel,

(2) An assumed pattern of deformation in the beam in the region of flexural cracking,

(3) Equilibrium of forces and moments.

The equations are summarized below:

4.2.1 First Loading Stage, $M \leq M_{oN}$

With tensile stresses taken as positive, the total stresses at moment M in the N-th cycle are

$$f_{cN}^{t} = -F_N \left[\frac{1}{A_c} - \frac{he}{2I_c} \right] - \frac{M}{I} \left[\frac{h}{e} + e - \bar{x} \right] \tag{4.1}$$

$$f_{cN}^{b} = -F_N \left[\frac{1}{A_c} + \frac{he}{2I_c} \right] + \frac{M}{I} \left[\frac{h}{2} - e + \bar{x} \right] \tag{4.2}$$

$$f_{sN} = \frac{F_N}{A_s} + m \frac{M}{I} \bar{x} \tag{4.3}$$

where f_{cN}^{t} and f_{cN}^{b} are the top and bottom concrete fiber stresses, respectively, f_{sN} is the steel stress, F_N is the prestressing force, m is the modular ratio, A_s, A_c, I_c, I, h, e, and $\bar{x}$ are cross sectional properties of the beam (See NOMENCLATURE for definition of terms).

At N = 1 (first load cycle), F_N is equal to the effective prestressing force F_{se}. Cracking in the first load cycle occurs when f_{c1}^{b} is assumed equal to the concrete modulus of rupture f_t', thus from Eq. 4.2,

$$M_{o1} = I \frac{f_t' + F_{se} \left[\frac{1}{A_c} + \frac{he}{2I_c} \right]}{\frac{h}{2} - e + \bar{x}} \tag{4.4}$$

At $N > 1$, cracks will open when $f_{cN}^{b} = 0$, thus

$$M_{oN} = I \frac{F_N \left[\frac{1}{A_c} + \frac{he}{2I_c} \right]}{\frac{h}{2} - e + \bar{x}} \tag{4.5}$$

Note that the prestressing force F_N will vary slightly with load repetition. Correction may be made by estimating creep and shrinkage losses and other possible effects.

4.2.2 Second Loading Stage, $M = M_{oN}$

Details of the derivation of the equations for the cracked section are not included here. Brief explanations are made where they are found necessary. Equations for steel and concrete stresses in a prestressed concrete beam of rectangular cross section with reinforcing steel placed horizontally at one level are summarized below:

$$\frac{f_{s1} A_s}{bd\ k_3\ f'_c} = k\left[\frac{\alpha}{2} E_1 + \frac{3-2\alpha}{3} E_1^2 + \frac{\alpha-2}{4} E_1^3\right] \tag{4.6}$$

$$M_1 = f_{s1}\ A_s\ d\ (1 - k_2 k) \tag{4.7}$$

$$\epsilon_{s1} = \epsilon_{sF} + \epsilon_{cF} + \frac{1-k}{k}\ \epsilon_{c1}\psi \tag{4.8}$$

$$k_2 = \frac{\alpha + (1.5 - \alpha)\ E_1 + (0.3\alpha - 0.6)\ E_1^2}{3\alpha + (6 - 4\alpha)\ E_1 + (1.5\alpha - 3)\ E_1^2} \tag{4.9}$$

These equations, together with a known steel stress-strain relation, may be used to evaluate, for a moment $M_1 = M_{oN}$, the unknowns f_{s1}, ϵ_{s1}, k, k_2 and E_1 (or ϵ_{c1}). The value of F_N must be known or estimated in

order to determine values for ϵ_{sF} and ϵ_{cF}. (See NOMENCLATURE for definition of terms.)

Equations 4.6 and 4.7 were obtained from the conditions of equilibrium. The total compressive force in the concrete was expressed in terms of the volume of the stress block, the shape of the stress block being approximated by a cubic parabola of the form given in Eq. 2.1. The equations of equilibrium were derived neglecting concrete tensile stresses below the neutral axis of the section.

Equation 4.8 is the compatibility condition derived by assuming an idealized deformation pattern in the beam in the region of flexural cracking. The non-dimensional compatibility factor ψ may be regarded as a bond parameter. In the idealized case of perfect bond, $\psi = 1.0$. For the other extreme of zero bond, ψ approaches zero. A theoretical evaluation of the bond parameter ψ in Eq. 4.8 is not possible at the present time. In this investigation, an attempt was made to obtain an empirical value of ψ from the concrete deformation data of the beam tests in Chapter 3. A wide range of scatter of ψ-values was obtained. Furthermore, it was found from the empirical evaluation of ψ that for conditions intermediate between the two extremes of perfect and zero bond, ψ may not necessarily lie between zero and unity. In this investigation, $\psi = 1.0$ is assumed. Note that in the stress analysis of the type of prestressed concrete beams treated in Ref. 21, $\psi = 1.0$ was found satisfactory.

It must be pointed out that the values of ϵ_{s1} and ϵ_{c1} obtained from Eq. 4.8 are the maximum values of the steel strain and the concrete top fiber strain, respectively, at the cracked section. At sections away from the crack, the corresponding strains will be less in value, the magnitude of the difference depending on the degree of bond breakdown between steel and concrete at the cracked section.

Equation 4.9 gives the location of the point of application of the total compressive force in the concrete referred to the top fiber of the beam. Equation 4.9 was derived assuming a cubic parabola for the concrete stress-strain relation (Eq. 2.1) and linear strain variation with respect to the depth of the compressive region of the beam.

4.3 APPLICATION OF STRESS ANALYSIS

The equations presented in Sec. 4.2 were used to establish the relationship between concrete top fiber stress and applied moment of the prestressed concrete test beams described in Chapter 3. Since the maximum applied moments were greater than the cracking moment M_{oN}, the portion of the stress-moment curve within the second loading stage, $M = M_{oN}$, was of main concern.

4.3.1 Concrete Stress-Strain Relation

In the derivation of the equations for the second loading stage, $M \rightarrow M_{oN}$, a cubic parabola was assumed for the loading portion of the stress-strain relation of the concrete in the beam. The value of α in Eq. 2.1 was obtained by fitting the equation to the cylinder test data given in Table 14. It was found that the stress-strain curve could be represented by Eq. 2.1 with an α-value of 2.0. Thus Eq. 2.1 is reduced to the form

$$F = 2E - E^2 \tag{4.10}$$

In using Eq. 4.10 to represent the stress-strain relation of the concrete in the beam, the non-dimensional terms F and E are defined as follows:

$$F = \frac{f_c}{k_3 f'_c} \qquad \text{and} \qquad E = \frac{\epsilon_c}{\epsilon'_c}$$

where $k_3 f'_c$ is the ultimate stress of the concrete in the beam. In ultimate strength theory, k_3 is usually taken as 0.85. Hognestad, Hanson, and McHenry[23] obtained an empirical relationship for k_3 as a function of f'_c

$$k_3 = \frac{3900 + 0.35\, f'_c}{3000 + 0.82\, f'_c - \frac{f'^2_c}{26{,}000}} \tag{4.11}$$

For f'_c = 5,000 psi, k_3 = 0.92 is obtained from Eq. 4.11. In this investigation, stress-moment curves were calculated for values of

k_3 equal to 1.0, 0.92, and 0.85. The effect of k_3 on the results of the stress calculation is further discussed in Art. 4.3.5.

4.3.2 Steel Stress-Strain Relation

The load-strain relation of the strand reinforcement used in the test beams is shown in Fig. 13. The load-strain curve is essentially a straight line up to approximately 80 percent of the ultimate load. The stress-strain relation can therefore be represented by the following equation

$$f_s = E_s \epsilon_s \tag{4.12}$$

for $f_s \leq 0.80\ f_{su}$, where E_s is the modulus of elasticity of steel. For the type of prestressed concrete test beams treated in Chapter 3, the steel stress at ultimate load was less than $0.80\ f_{su}$. Hence, the stress-moment calculation was considerably simplified since no trial-and-error procedure was necessary.

4.3.3 Procedure for Stress-Moment Calculations

The following procedure was found expedient in calculating the stress-moment curve of the test beams for $M \geq M_{oN}$. By combining Eqs. 4.6, 4.8, and 4.12, the following equation is obtained,

$$\frac{E_s A_s}{bd\ k_3 f'_c} = \frac{k\left[\frac{\alpha}{2} E_1 + \frac{3-2\alpha}{3} E_1^2 + \frac{\alpha-2}{4} E_1^3\right]}{\epsilon_{sF} + \epsilon_{cF} + \frac{1-k}{k} \epsilon_{c1}\ \psi} \qquad (4.13)$$

for $f_{s1} \leqslant 0.80\ f_{su}$. In Eq. 4.13, the unknowns are k and E_1. By specifying E_1 (or ϵ_{c1} or F_1, since concrete stress-strain Eq. 4.10 is known), k is found from Eq. 4.13. The value of k_2 is obtained from Eq. 4.9 for a specified E_1. With E_1 and k known, the steel stress f_{s1} is obtained from Eq. 4.6. The moment M_1 corresponding to the concrete strain E_1 is solved from Eq. 4.7. The process is repeated for other specified values of E_1 until enough points are known to establish the M versus E (or F) curve.

Stress-moment calculations for Beam No. 2 are contained in Appendix B and stress-moment curves in the region $M \geqslant M_{oN}$ are plotted in Fig. 20.

4.3.4 Remarks on Stress-Moment Calculations

Stress-moment relationships were calculated for the fatigue test beams of Chapter 3 taking values of k_3 equal to 1.0, 0.92, and 0.85 with $\alpha = 2.0$ and $\psi = 1.0$. The effect of k_3 on the computed concrete stresses is illustrated by the stress-moment curves for Beam No. 2 plotted in Fig. 20. Significant variation in stress was observed for different values of k_3. In order to arrive at a value of k_3 which would be appropriate for predicting the stresses in the

beam, the calculated concrete top fiber stresses were compared with the observed average concrete top fiber stresses. The observed stresses were determined from the concrete deformation measurements made during the beam tests. Since the concrete strains were measured over a 10-in. gage length, the measured values represented the average concrete strains at the top fiber of the beam. The observed strains were converted to stresses by means of Eq. 4.10. As previously noted, the steel and concrete strains or stresses obtained from the stress analysis correspond to the maximum values at the cracked section of the beam. Hence it is reasonable to expect that the computed concrete stresses should be greater than the observed average concrete stresses. An examination of Fig. 20 shows that the stresses computed for $k_3 = 0.85$ fulfill this expectation. The same trend was noted for similar comparisons made of the other test beams. The magnitude of the difference between the actual maximum and average stresses is not known, hence the exact value of k_3 can not be determined. For purposes of the present investigation, on the basis of the observations made from the comparison of the stress-moment curves and in the absence of more reliable information, the stress-moment curve calculated for $k_3 = 0.85$ was adopted.

The test beams used in this investigation were prestressed with two horizontal layers of strand reinforcement. In Ref. 21 equations were derived for a beam with rectangular section with steel reinforcement at different levels. The stress-moment calculation becomes involved since simultaneous equations must be solved. In

most cases, however, a simplification is made by assuming that all strands are grouped at the center of gravity of the steel (C.G.S.). This simplification was used in calculating the stress-moment curves of the test beams since the top fiber concrete stress was of main concern and not the steel stress, and by referring the steel stress to the C.G.S. the resulting computed concrete stress is not affected.

Stress-moment relationships for the concrete top fiber of the test beams were calculated for the first load cycle (N = 1), that is, the calculated stresses were referred to the state of stress in the beam without preloading. Thus, the value of F_N is equal to the effective prestressing force F_{se} and the term $(\epsilon_{sF} + \epsilon_{cF})$ is determined from the corresponding value of $(\epsilon_{se} + \epsilon_{ce})$. Observations made during the beam fatigue tests in Chapter 3 indicated considerable variation in beam response with load repetition as reflected in the measured deflections and concrete deformations. It follows that the actual stress-moment relations of the test beams changed under fatigue loading. It has been suggested[21] that if the beam response varies with load repetition, several stress-moment curves calculated at intervals spread over the fatigue life are needed in order to transform load history to stress history for the beam. Such a procedure is however very complicated because it requires quantitative evaluation of changes taking place in the beam elements with load repetition which is not possible at the present time. These changes occur in the following: (1) stress-strain characteristics of the concrete, (2) magnitude of prestressing force due to creep

and relaxation, and (3) bond characteristics between the strand reinforcement and concrete. In addition, in the small concrete specimen fatigue tests described in Chapter 2, the concrete stresses were also referred to the initial state (without preloading) of the specimens. Therefore, since the experimental information obtained from the small specimen tests will be used to estimate beam fatigue life, the concrete stresses in the beam were likewise referred to the state of no preloading.

4.4 BEAM FATIGUE LIFE

Before the fatigue data obtained from the small concrete specimen tests can be applied to estimate the probable fatigue life of the test beams, the effects of size and stress gradient must be considered.

4.4.1 Size Effect

The concrete compressive block within the region of constant moment in a beam is thought of as a prismatic plain concrete specimen subjected to a stress gradient. The difference in size between this concrete beam section and the test specimen can be accounted for by using Eq. 2.21. Note that the size effect correction involves

only two dimensions, width and length, since the difference in depth is accounted for in the stress gradient considerations.

Although the beam section considered is within the constant moment region, the distribution of stresses in the longitudinal direction is not constant because of the presence of the flexural cracks. It was noted previously that the maximum concrete and steel stresses existed at the vicinity of the cracks and that the stresses calculated from the theoretical analysis represented these maximum values. An accurate consideration of the longitudinal size effect requires the determination of the stress variation along the beam which is not feasible at present. Hence, it will be assumed that fatigue failure in the beam will occur in the region of maximum concrete top fiber stress and no longitudinal size effect correction will be included. Equation 2.21 reduces to the form

$$Q = 1 - (1 - P)^{u} \tag{4.14}$$

where Q is the probability of beam failure at or before N cycles, P is the corresponding probability of specimen failure, and u is the ratio of the width of the beam to the width of the test specimen.

Using the nominal widths of the test beam and the concrete test specimen, u = 6/4. Substituting this value of u and Q = 0.50 in Eq. 4.14 gives a value of P = 0.37. Thus, the mean fatigue life of the test beam is equal to the fatigue life at P = 0.37 of the small concrete specimen subjected to an equivalent stress gradient (θ) and the same stress level as the concrete compressive block in

the beam. The S-N-θ diagrams shown in Fig. 10 will be used to estimate the mean fatigue life of the test beams.

4.4.2 Stress Gradient Effect

The stress gradient (θ) of the compressive block in a beam can be evaluated by using Eq. 2.20. As a first approximation, the value of t may be taken as equal to kd, thus Eq. 2.20 becomes

$$\theta_k = \frac{E^t_{max}}{kd} \left(\frac{dF}{dE}\right)_{E^t_{max}} \tag{4.15}$$

where E^t_{max} is the non-dimensional top fiber concrete strain at maximum stress level and $\left(\frac{dF}{dE}\right)_{E^t_{max}}$ is the derivative of the stress-strain equation (Eq. 4.10) of the concrete in the beam evaluated at E^t_{max}. The value of θ_k can be determined since k is found from the stress-moment calculations.

For prestressed concrete beams, the use of Eq. 4.15 gives conservative estimates of mean fatigue life because of the presence of the prestressing force. The effect of the prestressing force will be discussed with the aid of Fig. 21 which shows the stress distributions in the prestressed concrete beam and in the concrete test specimen under repeated loading. The stress distribution in the prestressed concrete beam represents the total stresses due to beam load and prestressing force. In both cases, the solid and dash lines indicate the

stress distributions under maximum and minimum load levels, respectively; hence, the cross-hatched regions show the range of stress variation under repeated loading. Note that for the same minimum concrete stress in the extreme fibers, $(f_c^t)_{min} = (f_c)_{min}$, the stress distribution in the prestressed concrete beam is different from that of the concrete test specimen as shown by the dash lines. For the same maximum concrete stress, $(f_c^t)_{max} = (f_c)_{max}$, and t = kd, the regions subjected to stress variation in the beam is less than that of the concrete specimen. With the above conditions, it is reasonable to expect a higher fatigue life for the beam. Therefore, in order to improve the estimate of beam fatigue life using the results of the small concrete specimen tests, the difference in stress conditions due to the prestressing force in the beam must be taken into account.

In this investigation a satisfactory correction was found by using in Eq. 2.20 a value of t less than kd. An effective depth k'd is introduced which can be defined as

$$k'd = \frac{kd + d_e}{2} \tag{4.16}$$

where the depth d_e is as indicated on Fig. 21(a). An expression for d_e can be derived from the strain distributions in the beam. Referring to Fig. 21(a), the following relationships can be established

$$\frac{(\epsilon_c)_x}{kd - d_e} = \frac{(\epsilon_c^t)_{max}}{kd}$$

and

$$\frac{(\epsilon_c)_x - (\epsilon_c^t)_{min}}{d_e} = \frac{(\epsilon_c^b)_{min} - (\epsilon_c^t)_{min}}{h}$$

The preceding equations can be solved for d_e by eliminating $(\epsilon_c)_x$, thus

$$d_e = \frac{(\epsilon_c^t)_{max} - (\epsilon_c^t)_{min}}{\frac{1}{h}\left[(\epsilon_c^b)_{min} - (\epsilon_c^t)_{min}\right] + \frac{(\epsilon_c^t)_{max}}{kd}}$$

The strains can be non-dimensionalized and the expression for d_e becomes

$$d_e = \frac{E^t_{max} - E^t_{min}}{\frac{1}{h}(E^b_{min} - E^t_{min}) + \frac{E^t_{max}}{kd}} \tag{4.17}$$

Substituting Eq. 4.17 into Eq. 4.16 and rearranging

$$k'd = \frac{kd}{2}\left[1 + \frac{1 - \frac{E^t_{min}}{E^t_{max}}}{1 + \frac{kd}{h}\left(\frac{E^b_{min} - E^t_{min}}{E^t_{max}}\right)}\right] \tag{4.18}$$

where E^t_{max} is the non-dimensional concrete top fiber strain at maximum stress level, E^t_{min} and E^b_{min} are the non-dimensional concrete top and bottom fiber strains, respectively, at minimum stress level. The values of the strains are found by converting the stresses calculated from the stress analysis using a known concrete stress-strain relation (Eq. 4.10). Note that compressive strains are taken as positive in the above equations.

For prestressed concrete beams therefore, the modified stress gradient θ_k, is obtained from Eq. 4.15 by replacing kd by k'd, thus

$$\theta_{k'} = \frac{E^t_{max}}{k'd} \left(\frac{dF}{dE}\right)_{E^t_{max}} \qquad (4.19)$$

where k'd is given by Eq. 4.18. For conventionally reinforced concrete beams, the use of Eq. 4.15 should provide a reasonable estimate of beam fatigue life.

The calculated values of stress gradients θ_k and $\theta_{k'}$ of each fatigue test beam of Chapter 3 are listed in Table 18.

4.4.3 Comparison of Calculated and Observed Fatigue Lives

An estimate of beam fatigue life can now be made since the concrete stresses induced by the repeated loads have been calculated and the effects of size and stress gradient have been considered. The mean fatigue lives of the test beams in Chapter 3 can be obtained from the S-N-P-θ diagrams shown in Fig. 10 and the procedure for using the diagram is explained and illustrated in Appendix B. Mean fatigue lives were determined for two values of stress gradient, θ_k and $\theta_{k'}$, as given by Eqs. 4.15 and 4.19, respectively.

A comparison of the estimated mean fatigue lives ($\bar{N}_k$ and $\bar{N}_{k'}$) and the observed fatigue life (N_{obs}) for each test beam is made in Table 18. The mean fatigue lives ($\bar{N}_{k'}$) estimated by using the modified stress gradient $\theta_{k'}$ agree reasonably well with the observed values for Beam Nos. 1 and 2. Note that estimates of fatigue life are included for Beam No. 4 although it did not fail by concrete fatigue

at N = 525,000 cycles. The comparison likewise shows that beam fatigue lives obtained by using Eq. 4.15 provide a good lower bound estimate of the observed values. The satisfactory agreement obtained between computed and observed values, although based on limited test data, indicates the appropriateness of the proposed method for estimating the probable fatigue life of prestressed concrete flexural members failing by fatigue of the concrete in compression.

4.5 DISCUSSION

Several important aspects of the present investigation into the probable fatigue life of prestressed concrete flexural members failing by concrete fatigue are discussed in this section.

4.5.1 Accuracy of Proposed Method

The extreme sensitivity of concrete fatigue life with respect to small changes in stress levels was pointed out in Sec. 2.8 from an examination of the stress - fatigue life data plotted in Fig. 5. In estimating beam fatigue life therefore, it is important that the top fiber concrete stresses induced by the repeated loading be determined as accurately as possible. The accuracy of the stress calculations depends on the precise evaluation of such quantities as k_3, f'_c, ϵ'_c, α,

and ψ which are subject to variation. Instead of treating these quantities as single-valued parameters, they should be considered as statistics with associated frequency distributions.[21] However, extensive experimental work is needed in order to establish the frequency distribution of each of the variables.

In addition, the stress analysis requires knowledge of the magnitude of prestress losses due to creep and shrinkage which can not be determined with exactitude under field conditions. In actual practice, these losses are usually assumed. In the stress calculations of the test beams in this investigation, reliable information on the magnitude of prestress losses was obtained from deformation measurements. It is therefore reasonable to expect that estimates of beam fatigue life in practical situations would be subject to greater variability than that indicated by the results of this investigation. Hence, it may be advisable in applying the proposed method to check the safety against fatigue failures of structures under repeated loads to use an estimate of fatigue life less than the mean value.

The mean fatigue life of a beam is estimated by specifying a probability level $Q = 0.50$. To insure against fatigue failure, a probability level less than $Q = 0.50$ must be specified. Theoretically, no fatigue failure will occur at a number of cycles only if the probability of failure $Q = 0$. Practically, a very low probability of beam failure, say $Q = 0.01$, may be specified for design purposes.

Thus, the probability of a fatigue failure occurring at a certain number of cycles is 1 out of 100. For example, the "design" life (Q = 0.01) of Beam No. 2 under the loading condition used in the test is found equal to 50,000 cycles. This is obviously a conservative estimate of the observed fatigue life of 350,000 cycles for Beam No. 2.

4.5.2 Practical Application of Concrete Fatigue Data

A possible application of the proposed method for estimating beam fatigue life to actual design practice was briefly indicated in the preceding discussion. As presented thus far, the procedure for determining the probable fatigue life of prestressed concrete beams involves a rigorous analysis as illustrated in Appendix B. For practical purposes however, a simplified means for checking the design of concrete flexural members against the possibility of fatigue failure of the concrete in compression is preferable.

Concrete fatigue data obtained in this investigation can be presented in a form more suitable for practical application, both as a tool for the designer and as a guide for the specification writer. From the S-N-P-θ diagrams (Art. 2.8.3), a relationship between maximum stress level S and stress gradient θ can be obtained by specifying values for fatigue life N and probability of failure P. Furthermore, the stress gradient θ as given by Eq. 2.20 or Eq. 4.15 can be

expressed in terms of kd, the depth of the compressive block in the beam. Hence, a relationship between maximum concrete top fiber stress and compressive depth kd can be shown graphically, as given on Fig. 22 for arbitrarily specified values of fatigue life N = 2,000,000 cycles and of probability levels P = 0.00001 and P = 0.01.

The curves plotted on Fig. 22 illustrate the effect of compressive stress gradient (in terms of the compressive depth kd) on the fatigue strength (in terms of the maximum concrete top fiber stress). The fatigue strength of concrete in compression varies inversely with the depth kd and becomes a minimum for kd = ∞. The minimum values of fatigue strength (N = 2,000,000 cycles) for the curves with P = 0.00001 and P = 0.01 are 51 and 59 percent, respectively, as shown on Fig. 22. These minimum values, in effect, represent the fatigue strength of uniformly stressed specimens (kd = ∞) for the specified values of N and P.

The effect of specifying different levels of probability of failure is indicated by the difference between the two curves shown on Fig. 22. The choice of the level of probability of failure is arbitrary; however for design purposes, a probability level as close to zero as possible must be specified. Freudenthal[12] has quoted a "design limit" of $P \leq 0.01$. In order to account for other uncertainties which may be associated with the results obtained from this investigation, a probability level of $P \leq 0.00001$ is recommended. Note that with reference to the discussion on size effect (Art.2.8.2), the probability level P = 0.00001 when associated with the S-N-P

relationship of uniformly stressed specimens represents the lower limiting S-N curve (Eq. 2.19) corresponding to an infinitely large specimen. Therefore, by specifying $P \leqslant 0.00001$, size effect is accounted for, size referring to the longitudinal and transverse dimensions of the beam.

With Fig. 22, it is only necessary to know the maximum concrete top fiber stress and the corresponding depth kd induced by the repeated loading in order to make an approximate check against fatigue failure of the concrete in compression. The calculation of the concrete top fiber stress and depth kd for a specific problem can be accomplished by using any conventional stress analysis procedure. Thus, the information presented in Fig. 22 may be incorporated into current design practice quite readily.

The procedure for carrying out the design check is as follows: The point representing the values of the concrete top fiber stress and the corresponding depth kd induced by the maximum repeatedly applied loading can be plotted on Fig. 22. If the point plots on the solid curve, the probability of failure of the particular flexural member at or before 2,000,000 load cycles is $P = 0.00001$. If the point plots above the curve, the corresponding probability of failure $P > 0.00001$; on the other hand, if the point plots below the curve, then $P < 0.00001$. It follows that for a specified "design limit" of $P \leqslant 0.00001$, then the "safe" region on Fig. 22 is the area below the solid curve. Thus, the probability of concrete fatigue

failure occurring at or before N = 2,000,000 cycles associated with any point plotting within this region is equal to or less than 1 in 100,000.

Note that on Fig. 22 the maximum top fiber stress is expressed as percent of the ultimate compressive stress of the concrete in the beam, $k_3 f'_c$, where $k_3 \leq 1.0$. In order to account for the difference in concrete strength between the beam and the test specimen, k_3 is usually taken as less than unity. In this investigation, $k_3 = 0.85$ was assumed. The current AASHO allowable concrete stress in compression of $0.40f'_c$ can be compared with the information on Fig. 22. For $k_3 = 0.85$, the AASHO allowable stress corresponds to $0.47k_3 f'_c$. It is seen that the current allowable stress is less than the minimum fatigue strength ($kd = \infty$) of $0.51k_3 f'_c$. Indeed, according to Fig. 22, for realistic values of the compressive depth kd, say $kd \leq 15$ in., the fatigue strength is greater than $0.60k_3 f'_c$ which would permit a stress at the top fibers of $0.51f'_c$.

The fatigue strength versus compressive depth kd relationship presented on Fig. 22 was established for a minimum extreme fiber stress of 10 percent of the ultimate compressive stress. It is known that the fatigue strength of concrete increases with increasing minimum stress level, thus the design check will give conservative results when applied to cases where the minimum top fiber stress is greater than 10 percent. For prestressed concrete beams, the minimum stress condition at the top fibers would be taken as the

stress caused by the combination of dead load and prestressing which is usually not less than 10 percent.

4.5.3 Need for Further Experimental Studies

The proposed method for estimating beam fatigue life requires concrete fatigue data in the form of S-N-P-θ relationship which can only be established by experimentation. In this investigation, fatigue data were obtained from tests on plain concrete specimens of one particular type of mix proportion; therefore, the results may be limited in general applicability. More extensive experimental work is needed in order to investigate the effects on fatigue life of variation in the physical properties of the concrete.

The range of fatigue life investigated varied from approximately 10,000 to 2,000,000 cycles, thus no information was obtained on whether or not a fatigue limit exists for concrete in compression with different stress distributions. This however was not of main concern in this investigation. By arbitrarily setting a cut-off point of 2,000,000 cycles, adequate number of test replications at discrete maximum stress levels were made which permitted a statistical analysis of the results obtained. In this connection, it must be emphasized that the S-N-P-θ relationship obtained in this investigation is only applicable within the range of fatigue life for which it was established. Extrapolation is not recommended, however if it becomes necessary to do so, a greater factor of uncertainty should be associated with the extrapolated value.

In this investigation, fatigue tests were conducted using constant cycle loading only. In actual field conditions, structures are usually subjected to varying repeated loadings. Constant load cycle fatigue represents a more severe case of loading condition if the maximum stress level is equal to the maximum stress that occurs in the structure for the same minimum stress level. However, if the maximum stress is repeated very infrequently over the fatigue life of the structure, the estimate of fatigue life assuming constant load cycles would be over conservative. In order to investigate the effect on fatigue life of variable repeated loading, a cumulative damage study is necessary. A review of cumulative damage theories and a study of the cumulative damage of prestressing strand are reported in Ref. 21. It was found that Miner's[22] linear accumulation theory may be used to predict the mean fatigue life of strands subjected to varying magnitudes of repeated loading. A similar study should be made on plain concrete specimens. This however, is beyond the scope of this investigation.

4.6 SUMMARY AND CONCLUSIONS

A study has been made into the fatigue life of prestressed concrete flexural members failing by fatigue of the concrete in compression. The investigation can be summarized as follows:

Constant cycle fatigue tests were conducted on small plain concrete specimens to study the effect of stress gradient on the

fatigue life of concrete in compression. Statistical methods were used in analyzing the test results and an empirical relationship between the variables -- stress level, fatigue life, probability of failure, and stress gradient -- was established from the fatigue data.

A method for estimating the probable fatigue life of prestressed concrete beams as limited by concrete fatigue was developed. The proposed method is based on the information obtained from the plain concrete specimen tests together with a stress analysis derived in a previous work.[21] The procedure for determining beam fatigue life is illustrated by a numerical example of an actual test beam.

A design recommendation was formulated for a specified fatigue life N = 2,000,000 cycles and a probability "design limit" $P \leq 0.00001$. The possibility of concrete fatigue failure can be checked when the maximum top fiber stress and the corresponding depth kd of the compressive block in the beam induced by the repeated loading are known.

Fatigue tests were conducted on a limited number of beams to verify experimentally the accuracy of the proposed method for estimating beam fatigue life. Information on the behavior under repeated loading of prestressed concrete beams failing by concrete fatigue was obtained from the beam tests.

As a result of this investigation, the following conclusions can be drawn:

(1) Stress gradient has a significant effect on the fatigue strength (or life) of plain concrete in compression. For the same maximum stress level, fatigue strength of specimens tested with zero-to-maximum stress distribution (Group 2b) is higher than that of specimens tested with uniform stress distribution (Group 2a) by approximately 17 percent of the static ultimate stress.

(2) Concrete fatigue life is highly sensitive to small changes in maximum stress levels. A change in stress of only 7.5 and 5 percent for Groups 2a and 2b, respectively, causes the fatigue life to change from approximately 40,000 to 1,000,000 cycles.

(3) A large degree of variability is associated with fatigue life of plain concrete. Fatigue data should be treated statistically and presented in the form of S-N-P relationship.

(4) The statistical theory of stress gradient by Fowler[10] does not apply to the fatigue data obtained from tests of small plain concrete specimens.

(5) An empirical S-N-P-θ relationship can be obtained from the fatigue data and generalized to apply to specimens of different sizes by using a statistical explanation of size effect.

(6) Crushing of the concrete compressive block may precede fracture of the tension steel in over-reinforced prestressed concrete beams when subjected to repeated loading. Beam response can be expected to vary with load repetition, the rate of change depending on the severity of the applied loading.

(7) Severe cracking along the longitudinal steel reinforcement may occur under repeated loading if the neutral axis is located close to the center of gravity of steel area. This longitudinal cracking may cause the separation of the concrete below the steel reinforcement from the main body of the beam and could reduce considerably the fatigue life of the prestressed concrete beam.

(8) Good agreement is obtained between calculated and observed values of fatigue life if the difference in the minimum stress distribution in the concrete test specimen and in the concrete compressive block due to prestressing in the beam is accounted for. The calculated mean fatigue life neglecting the influence of prestressing gives conservative estimate of the observed beam fatigue life.

(9) The current AASHO allowable concrete compressive stress of $0.40f'_c$ is a conservative estimate of the fatigue strength of concrete in compression. The results of this investigation indicate that for a fatigue life N = 2,000,000 cycles, a

probability of failure P = 0.00001, and a minimum compressive top fiber stress of $0.10f'_c$, a maximum compressive stress of $0.50f'_c$ may be permitted at the top fibers of prestressed flexural members subjected to repeated loading.

5. ACKNOWLEDGEMENTS

This work has been carried out in the Department of Civil Engineering at the Fritz Engineering Laboratory, under the auspices of the Institute of Research of Lehigh University, as part of an investigation currently sponsored by: Pennsylvania Department of Highways; U.S. Department of Commerce, Bureau of Public Roads; and Reinforced Concrete Research Council.

The authors wish to express their thanks to Mr. Wilfred F. Chen for his assistance during the experimental phase of the project.

6. NOMENCLATURE

A_c	cross sectional area of concrete
A_s	cross sectional area of longitudinal tension steel
b	width of rectangular beam; width of concrete test prism
C.G.S.	center of gravity of longitudinal tension steel
d	effective depth of beam measured from top surface to C.G.S.
d_e	distance from top surface of beam to the point of zero stress variation
$D, D_{(\log N)}$	standard deviation of log N
D_N	standard deviation of N
e	eccentricity of load; eccentricity of C.G.S. with respect to centroidal axis of beam cross section
E	non-dimensional concrete strain; $E = \frac{\epsilon_c}{\epsilon_c'}$
E_c	modulus of elasticity of concrete
E_{max}	non-dimensional concrete strain corresponding to the maximum stress in the concrete test specimen
E^t_{max}, E^t_{min}	non-dimensional top fiber concrete strains of beam at maximum and minimum load levels, respectively
E^b_{min}	non-dimensional bottom fiber concrete strain of beam at minimum load level
E_s	modulus of elasticity of steel

E_1 non-dimensional top fiber concrete strain of beam for $M_1 \geq M_{oN}$

f ratio between the elementary volume stress and the maximum stress in the specimen

f_c concrete compressive stress

f'_c static ultimate stress of concrete

$(f_c)_{max}$, $(f_c)_{min}$ concrete stresses at highest strained surface of test prism at maximum and minimum load levels, respectively

$(f^t_c)_{max}$, $(f^t_c)_{min}$ top fiber concrete stresses of beam at maximum and minimum load levels, respectively

$(f^b_c)_{min}$ bottom fiber concrete stress of beam at minimum load level

f^t_{cN}, f^b_{cN} top and bottom fiber concrete stresses of beam, respectively, for $M \leq M_{oN}$

f_s steel stress

f_{sN} total steel stress at C.G.S. for $M \leq M_{oN}$

f_{su} static ultimate stress of steel

f_{sl} total steel stress at C.G.S. for $M_1 \geq M_{oN}$

f'_t modulus of rupture of concrete

F non-dimensional concrete stress; $F = f_c/f'_c$ for concrete in cylinders and prisms; $F = f_c/k_3 f'_c$ for concrete in beams

F_N prestressing force in beam during the N-th load cycle

F_{se} effective prestressing force just prior to the first load cycle

h	total depth of beam
I	moment of inertia of transformed section about the centroidal axis
I_c	moment of inertia of concrete area about its centroidal axis
k	dimensionless factor defining depth to neutral axis at a cracked section
k'	dimensionless factor defining depth of beam to be used in the modified stress gradient expression
k_2	dimensionless factor defining location of total force in the concrete compressive stress block
k_3	dimensionless factor defining relationship between concrete strength in beam and cylinder
L	probability of specimen survival at or before N cycles; $L = 1 - P$
m	modular ratio; $m = E_s/E_c$
M	moment
M_{max}, M_{min}	maximum and minimum repeatedly applied moments, respectively
M_{oN}	moment in N-th load cycle at which cracks begin to open
M_{o1}	cracking moment in first load cycle
M_1	moment after cracks have opened; $M_1 \geq M_{oN}$
n	number of specimens
N	number of cycles

$\bar{N}$	mean fatigue life
$\overline{\log N}$	mean of log N
$\bar{N}_k$	estimated mean fatigue life of beam corresponding to stress gradient θ_k
$\bar{N}_{k'}$	estimated mean fatigue life of beam corresponding to modified stress gradient $\theta_{k'}$
N_o	number of cycles up to which all specimens survive for a given stress amplitude (minimum life)
N_{obs}	observed beam fatigue life
p	proportion of steel in cross section; $p = A_s/bd$
P	probability of specimen failure at or before N cycles
P_{crk}	observed cracking load in first load cycle
P_{max}, P_{min}	maximum and minimum load levels, respectively
P_r	plotting position; $P_r = \frac{r}{n+1}$
Q	probability of beam failure at or before N cycles
r	rank of specimen
R	stress level expressed as ratio of the static ultimate stress
S	stress level expressed as percent of the static ultimate stress
S_{max}, S_{min}	maximum and minimum stress levels, respectively
t	thickness (or depth) of concrete test prism

t' distance from N.A. to the highest strained surface of the concrete prism

u width ratio between beam and test specimen or between two different prismatic specimens

v volume

V_s mode of log N (characteristic number)

w length ratio between two different prismatic specimens

$\bar{x}$ center of gravity of transformed section measured from C.G.S.

α dimensionless quantity defining the shape of the concrete stress-strain relation; $\alpha = E_c \frac{\epsilon_c'}{f_c'}$

β reciprocal of the "geometric standard deviation" which is proportional to $D_{(\log N)}$

ϵ strain

ϵ_c concrete compressive strain

ϵ_c' concrete strain in cylinder and prism at f_c'

$\Delta\epsilon_c$ inelastic concrete strain at C.G.S. due to creep and shrinkage

ϵ_{ce} elastic concrete strain at C.G.S. due to effective prestressing force F_{se}

ϵ_{cF} elastic concrete strain at C.G.S. due to prestressing force F_N

$(\epsilon_c)_{max}, (\epsilon_c)_{min}$ concrete strains at highest strained surface of test prism at maximum and minimum load levels, respectively

$(\epsilon_c^t)_{max}$, $(\epsilon_c^t)_{min}$ top fiber concrete strains of beam at maximum and minimum load levels, respectively

$(\epsilon_c^b)_{min}$ bottom fiber concrete strain of beam at minimum load level

ϵ_{cl} top fiber concrete strain of beam for $M_l \geq M_{oN}$

ϵ_s steel strain

ϵ_{se} steel strain at C.G.S. due to effective prestressing force F_{se}

ϵ_{si} steel strain at C.G.S. due to initial prestressing force

ϵ_{sF} steel strain at C.G.S. due to prestressing force F_N

ϵ_{sl} total steel strain at C.G.S. for $M_l \geq M_{oN}$

ϵ_t concrete tensile strain

θ compressive stress gradient in prismatic concrete specimen

θ_k stress gradient of compressive block in the beam

$\theta_{k'}$ modified stress gradient of compressive block in the prestressed concrete beam

μ, σ mean and standard deviation of the population of log N, respectively

ψ bond parameter

7. APPENDIX A - SUMMARY OF EQUATIONS FOR STRESS-STRAIN CALCULATIONS

7.1 ASSUMPTIONS

In Refs. 23 and 24, equations were derived for calculating the complete stress-strain curves of concrete in flexure. The derivation involves a consideration of the equilibrium of forces and moments together with the following assumptions:

(1) The strain is linearly distributed across the test section.

(2) Concrete stress is a function of strain only, $f_c = F(\epsilon)$.

(3) The stress function is the same for tension and compression, $F(-\epsilon) = -F(\epsilon)$. (24)

A relationship between concrete stress and the continuously measured quantities strain, load, and moment is established by differentiating the equilibrium equations with respect to the strain. The differentials may be closely approximated by finite differences.

The equations which apply to the types of test conducted on the small plain concrete specimens in this investigation are presented in the following sections.

7.2 GROUP 1b TESTS (e = 1")

From equilibrium of forces and moments together with the assumed linear strain variation, the following equations are established:

$$P = \frac{bt'}{\epsilon_c}\left[\int_o^{\epsilon_c} F(\epsilon_x)d\epsilon_x \quad - \quad \int_o^{\epsilon_t} F(\epsilon_x)d\epsilon_x\right]$$

$$= f_o'bt' \tag{7.1}$$

and

$$M = \frac{bt'^2}{\epsilon_c^2}\left[\int_o^{\epsilon_c} \epsilon_x F(\epsilon_x)d\epsilon_x + \int_o^{\epsilon_t} \epsilon_x F(\epsilon_x)d\epsilon_x\right]$$

$$= m_o'bt'^2 \tag{7.2}$$

where $f_o' = \frac{P}{bt'}$ and $m_o' = \frac{M}{bt'^2} = \frac{P(e + t' - \frac{t}{2})}{bt'^2}$

Differentiating Eqs. 7.1 and 7.2 with respect to ϵ_c, combining the resulting equations by eliminating $d\epsilon_t/d\epsilon_c$, and rearranging, the following equation is obtained

$$f_c = \frac{1}{\epsilon_c + \epsilon_t}\left[\epsilon_c^2 \frac{dm_o'}{d\epsilon_c} + 2m_o'\epsilon_c + \epsilon_c\epsilon_t \frac{df_o'}{d\epsilon_c} + f_o'\epsilon_t\right] \tag{7.3}$$

In the above equations, f_c is the concrete stress in the highest strained surface, ϵ_c and ϵ_t are the compressive and tensile strains, respectively, b and t are the width and thickness (or depth),

respectively, and t' is the distance from the neutral axis to the highest strained surface of the specimen. Note that if no tensile strains are present in the so-called neutral surface of the specimen, then $\epsilon_t = 0$ and $t = t'$.

By calculating in small increments, the differentials can be replaced by the finite differences $\Delta f_o'/\Delta \epsilon_c$ and $\Delta m_o'/\Delta \epsilon_c$. The f_o' versus ϵ_c and m_o' versus ϵ_c curves can be drawn using the load-strain curves obtained from static tests of Group 1b such as that shown in Fig. 2. Thus, the loading and unloading portions of the stress-strain curve can be obtained.

7.3 GROUP 1c TESTS (e = 1/3")

By a similar procedure as was indicated in Sec. 7.2, the following equations are established:

$$P = \frac{bt}{\epsilon_{c_1} - \epsilon_{c_2}} \int_{\epsilon_{c_2}}^{\epsilon_{c_1}} F(\epsilon_x) d\epsilon_x$$

$$= f_o bt \tag{7.4}$$

and

$$M = \frac{bt^2}{(\epsilon_{c_1} - \epsilon_{c_2})^2} \int_{\epsilon_{c_2}}^{\epsilon_{c_1}} (\epsilon_x - \epsilon_{c_2}) F(\epsilon_x) d\epsilon_x$$

$$= m_o bt^2 \tag{7.5}$$

where $f_o = \frac{P}{bt}$ and $m_o = \frac{M}{bt^2} = \frac{P(e + \frac{t}{2})}{bt^2}$

Differentiating Eq. 7.5 with respect to ϵ_{c_1}, combining the resulting equation with Eq. 7.4 and rearranging, the following equation is obtained

$$f_{c_1} = (\epsilon_{c_1} - \epsilon_{c_2}) \frac{dm_o}{d\epsilon_{c_1}} + (f_o t - 2m_o) \frac{d\epsilon_{c_2}}{d\epsilon_{c_1}} + 2m_o \qquad (7.6)$$

In the above equations, f_{c_1} is the concrete stress in the maximum strained surface and ϵ_{c_1} and ϵ_{c_2} are the maximum and minimum compressive strains, respectively, in the specimen. (See Fig. 2.)

In like manner, the differentials can be approximated by the finite differences $\Delta m_o / \Delta \epsilon_{c_1}$ and $\Delta\epsilon_{c_2} / \Delta\epsilon_{c_1}$. The stress-strain curve for the maximum strained fiber of the specimen can be established from the load-strain curves of Group 1c static tests such as that shown in Fig. 2.

The corresponding stress-strain curve for the minimum strained fiber can be obtained by using the following equation

$$f_{c_2} = (\epsilon_{c_1} - \epsilon_{c_2}) \frac{dm_o}{d\epsilon_{c_2}} + 2m_o \frac{d\epsilon_{c_1}}{d\epsilon_{c_2}}$$

$$+ (f_o t - 2m_o) - \frac{d}{d\epsilon_{c_2}} \left[f_o (\epsilon_{c_1} - \epsilon_{c_2}) \right] \qquad (7.7)$$

It can be shown that for $f_{c_2} = 0$ ($\epsilon_{c_2} = 0$), Eq. 7.6 reduces to the form of Eq. 7.3 for $\epsilon_t = 0$ and $t = t'$.

8. APPENDIX B - EXAMPLE CALCULATION OF BEAM FATIGUE LIFE

The procedure for estimating beam fatigue life as developed in this investigation is illustrated by a numerical calculation using the data for Beam No. 2.

8.1 STRESS-MOMENT CALCULATIONS

8.1.1 Beam and Material Properties

b	= 6.25 in.	E_s	= 26.4×10^3 ksi
d	= 7.75 in.	m	= 5.9
h	= 12.00 in.	f'_c	= 5.32 ksi
e	= 1.75 in.	ϵ'_c	= 0.00240 in./in.
A_c	= 74.4 $in.^2$	F_{se}	= 92.4 kips
I_c	= 900 $in.^4$	ϵ_{se}	= 0.00540 in./in.
A_s	= 0.654 $in.^2$	ϵ_{ce}	= 0.00051 in./in.
p	= 0.0135		

8.1.2 First Loading Stage, $M \leq M_{oN}$

Transformed Section Properties

(a) C.G. of transformed section $\bar{x}$ measured from C.G.S.

$$\bar{x} = \frac{A_c\, e}{A_c + (m-1)\, A_s} \qquad (8.1)$$

$$= 1.68 \text{ in.}$$

(b) Moment of inertia I

$$I = A_c\left[\frac{h^2}{12} + (e - \bar{x})^2 + (m - 1)\,\frac{A_s}{bh}\,\bar{x}^2\right] \qquad (8.2)$$

$$= 902 \text{ in.}^4$$

Cracking Moment at N = 1, M_{o1}

Assume $f'_t = 0.10\, f'_c = 0.532$ ksi

$$M_{o1} = I\,\frac{f'_t + F_{se}\left[\frac{1}{A_c} + \frac{he}{2I_c}\right]}{\frac{h}{2} - e + \bar{x}} \qquad (4.4)$$

$$= 434 \text{ in-kips}$$

Stresses at Cracking Moment M_{o1}

(a) Concrete top fiber stress

$$f_{c1}^{t} = - F_{se}\left[\frac{1}{A_c} - \frac{he}{2I_c}\right] - \frac{M}{I}\left[\frac{h}{2} + e - \bar{x}\right] \qquad (4.1)$$

$$= -3.08 \text{ ksi} \quad (= 0.68\, k_3 f_c')$$

(b) Steel stress at C.G.S.

$$f_{s1} = \frac{F_{se}}{A_s} + m\,\frac{M}{I}\,\bar{x} \qquad (4.3)$$

$$= 145.8 \text{ ksi}$$

Stresses at Minimum Applied Moment, M_{min} = 79.1 in-kips

(a) Concrete top fiber stress

From Eq. 4.1 , $(f_c^t)_{min}$ = -0.69 ksi. This value is equal to $0.15\, k_3 f_c'$, for $k_3 = 0.85$.

(b) Concrete bottom fiber stress

$$(f_c^b)_{min} = - F_{se}\left[\frac{1}{A_c} - \frac{he}{2I_c}\right] + \frac{M_{min}}{I}\left[\frac{h}{2} - e + \bar{x}\right] \qquad (4.2)$$

$$= -1.80 \text{ ksi} \quad (= 0.40\, k_3 f_c')$$

(c) Steel stress at C.G.S.

From Eq. 4.3 , $(f_s)_{min}$ = 141.9 ksi

Cracking Moment at $N \geq 1$, M_{oN}

$$M_{oN} = I \frac{F_N\left[\frac{1}{A_c} + \frac{he}{2I_c}\right]}{\frac{h}{2} - e + \bar{x}} \qquad (4.5)$$

$$\cong 353 \text{ in-kips}^*$$

*Approximate because F_N may not be equal to F_{se} at $N \geq 1$.

8.1.3 Second Loading Stage, $M \geq M_{oN}$

The stress-moment calculations in the second loading stage were made for the following assumed values:

$\alpha = 2.0$ $\qquad$ $\epsilon_c' = 0.00240$ in./in.

$k_3 = 0.85$ $\qquad$ $\psi = 1.0$

Results of the computations are presented in tabular form and the procedure for obtaining the values listed under each column is explained as follows.

Column (1) Specify value of E_1

(2) From $E_1 = \frac{\epsilon_{c1}}{\epsilon_c'}$

(3) From concrete stress-strain relation as given by Eq. 4.10, $F_1 = 2E_1 - E_1^2$

(4) From Eq. 4.9, with $\alpha = 2.0$, reduced to the form,

$$k_2 = \frac{1 - 0.25\ E_1}{3 - E_1} \qquad (4.9a)$$

(5) From Eq. 4.13, with $\alpha = 2.0$ and $\psi = 1.0$, rearranged to the form

$$k^2 - \frac{J}{E_1 - \frac{E_1^2}{3}}(\epsilon_{se} + \epsilon_{ce} + \epsilon_{c1})k + \frac{J}{E_1 - \frac{E_1^2}{3}}\epsilon_{c1} = 0 \qquad (4.13a)$$

where $J = \dfrac{E_s A_s}{bd\ k_3 f'_c}$

Note that the unknown quantities in Eq. 4.13a are E_1 (hence ϵ_{c1}) and k. By specifying E_1, k is found by solving the quadratic equation.

(6) From Eq. 4.8 with ϵ_{c1} and k known, and $\psi = 1.0$

$$\epsilon_{s1} = \epsilon_{se} + \epsilon_{ce} + \frac{1-k}{k}\epsilon_{c1} \qquad (4.8a)$$

(7) From steel stress-strain relation as given by Eq. 4.12,

$$f_{s1} = E_s \epsilon_{s1}$$

(8) From Eq. 4.7 with k_2, k, and f_{s1} known,

$$M_1 = f_{s1}\ A_s\ d(1 - k_2 k)$$

Results of Stress-Moment Calculations, $M_1 = M_{oN}$

(1) E_1	(2) ϵ_{c1}	(3) F_1	(4) k_2	(5) k	(6) ϵ_{s1}	(7) f_{s1}	(8) M_1
0.45	0.00108	0.70	0.349	1.17	0.00571	150.5	452
0.50	0.00120	0.75	0.350	1.08	0.00573	151.5	477
0.60	0.00144	0.84	0.354	0.97	0.00591	156.0	520
0.70	0.00168	0.91	0.358	0.89	0.00603	159.5	551
0.80	0.00192	0.96	0.362	0.83	0.00621	164.0	581
0.90	0.00216	0.99	0.367	0.80	0.00637	168.0	603
1.00	0.00240	1.00	0.373	0.77	0.00648	171.0	620

Concrete Stress at Maximum Applied Moment, M_{max} = 522 in-kips

The stress-moment (F_1 versus M_1) curve from the calculations is plotted in Fig. 20 with $k_3 = 0.85$. The concrete top fiber stress corresponding to M_{max} = 522 in-kips is obtained from the curve and is equal to $0.85\ k_3 f'_c$.

Hence, for Beam No. 2 the applied repeated loads induced a range of stress in the top fiber of 15-85 percent of the static ultimate stress $k_3 f'_c$.

8.2 STRESS GRADIENT CALCULATIONS

The following data are obtained from the stress-moment

calculations:

$F^t_{min} = 0.15$ $\qquad$ $E^t_{min} = 0.080$

$F^b_{min} = 0.40$ $\qquad$ $E^b_{min} = 0.225$

$F^t_{max} = 0.85$ $\qquad$ $E^t_{max} = 0.614$

$k = 0.96$ $\qquad$ $(kd = 7.37 \text{ in.})$

Stress Gradient θ_k

$$\theta_k = \frac{E^t_{max}}{kd}\left(\frac{dF}{dE}\right)_{E^t_{max}} \qquad (4.15)$$

$$= \frac{E^t_{max}}{kd}\left(2 - 2E^t_{max}\right)$$

$$= 6.40 \times 10^{-2} \text{ per in.}$$

Modified Stress Gradient $\theta_{k'}$

$$k'd = \frac{kd}{2}\left[1 + \frac{1 - \dfrac{E^t_{min}}{E^t_{max}}}{1 + \dfrac{kd}{h}\left(\dfrac{E^b_{min} - E^t_{min}}{E^t_{max}}\right)}\right] \qquad (4.18)$$

$$= 6.52 \text{ in.}$$

$$\theta_{k'} = \frac{E^t_{max}}{k'd}\left(\frac{dF}{dE}\right)_{E^t_{max}} \qquad (4.19)$$

$$= 7.28 \times 10^{-2} \text{ per in.}$$

8.3 MEAN FATIGUE LIFE

The mean fatigue life of Beam No. 2 is obtained from the S-N-P-θ diagrams in Fig. 10 knowing the following information:

(a) Maximum stress level S:

$$S_{max} = 100\ F^t_{max} = 85$$

(b) Stress gradient θ:

$$\theta_k = 6.40 \times 10^{-2} \text{ per in.}$$

or

$$\theta_{k'} = 7.28 \times 10^{-2} \text{ per in.}$$

(c) Probability level P:

$$P = 0.37 \qquad \text{(From Art. 4.4.1)}$$

The procedure for using the S-N-P-θ diagram is as follows.

8.3.1 Procedure for Using S-N-P-θ Diagram

The point representing the computed values of $\theta_{k'} = 7.28\text{x}10^{-2}$

per in. and S_{max} = 85 for Beam No. 2 is plotted on the S-N-θ diagram for P = 0.37 in Fig. 10. An N-curve is drawn through this point and it intersects the θ vs. S_{max} curve of Group 2b at S_{max} = 86.5. The number of cycles corresponding to the N-curve is found by substituting the values of S_{max} = 86.5 and P = 0.37 into the S-N-P equation of Group 2b such as Eq. 2.13

$$\log(\log N) = 9.3083 - 4.4076\ (\log S) + 0.0435\ \log(-\log L) \qquad (2.13)$$

where L = 1 - P. A value of N = 320,000 cycles is obtained.

The S-N-P relation from either Group 2a or 2b may be used. However, in order to minimize the error that may be introduced in drawing the N-curve, the S-N-P equation for Group 2b was chosen because of the proximity of the point representing Beam No. 2 to the θ vs. S_{max} curve of Group 2b. It must also be pointed out that the other S-N-P relationships for Group 2b derived in Chapter 2, such as those given by Eqs. 2.5b and 2.6b (log-normal distribution) and Eqs. 2.10 (extreme value distribution), may be used instead of Eq. 2.13 (McCall's mathematical model). The use of Eq. 2.13 has the advantage of having the variables S, N, and P contained in a single equation, and therefore, does not involve additional graphical plots which the log-normal and extreme value distributions require.

In this example, the S-N-θ diagram for P = 0.37 was used for the sake of clarity. Note that the only information necessary from

the S-N-θ diagram is the value of S_{max} = 86.5 corresponding to a stress distribution (Group 2b) with a known S-N-P relation. The same value of S_{max} is obtained if the point representing Beam No. 2 is plotted on the S-N-θ diagram for P = 0.50. Therefore only <u>one</u> S-N-θ diagram is required.

8.3.2 Calculated Values of Fatigue Life

The mean fatigue life of Beam No. 2 calculated on the basis of the modified stress gradient $\theta_{k'}$ is therefore $\bar{N}_{k'}$ = 320,000 cycles. The mean fatigue life corresponding to the uncorrected stress gradient θ_k is determined by following a similar procedure as indicated above and a value of $\bar{N}_k$ = 150,000 cycles is obtained.

9. TABLES

Table 1. Details of Concrete Mixes -

Cylinders and Prisms

Batch	Date Prepared	Number		Concrete Mix*				
		Cyls.	Prisms	C lb.	W lb.	FA lb.	CA lb.	SL in.
AA	3-29-62	13	18	129	72	363	375	3-1/2
BB	4-11-62	14	19	129	69	393	405	2-1/4
CC	4-25-62	13	20	129	69	393	405	1-1/2
DD	5-21-62	14	18	120	76	402	402	1-7/8
EE	6- 7-62	14	19	120	74	402	402	2-1/4
FF	6-19-62	13	21	120	72	402	402	1-7/8
GG	6-29-62	12	21	120	70	402	402	1-3/4
HH	7-10-62	12	21	120	72	402	402	2
II	7-24-62	13	21	120	77	402	402	1-7/8
JJ	8- 7-62	13	21	120	74	402	402	2-1/4
KK	8-21-62	12	21	120	80	402	402	2

*C - cement W - water

FA - fine aggregate CA - coarse aggregate

SL - slump

Table 2. Distribution of Specimens into the Different Test Groups

Batch	Group 1 - Static Tests			Group 2 - Fatigue Tests		
	Group 1a	Group 1b	Group 1c	Group 2a	Group 2b	Group 2c
AA	P I L O T			T E S T S		
BB	P I L O T			T E S T S		
CC	6	2	0	9	3	0
DD	4	3	0	7	4	0
EE	3	2	0	8	6	0
FF	3	2	(1)	9	6	1
GG	2	2	(1)	7	7	3
HH	3	2	(2)	6	6	4
II	3	2	(2)	6	5	5
JJ	3	(2)	(2)	6	6	6
KK	4	(1)	(2)	3	1	7
Total	31	15	-	61	44	26

Notes: ( ) - Specimens not loaded to failure and were later tested in fatigue.

Groups 1a, 2a - e = 0

Groups 1b, 2b - e = 1"

Groups 1c, 2c - e = 1/3"

Group 1d - Cylinder static tests; not included in Table.

Table 3. Stress-Strain Properties of Cylinders

Batch	f'_c (ksi)		ϵ'_c	E_c	α	*F at E of			
	28 Days[1]	At Test[2]	(in/in)	(ksi)		0.2	0.4	0.6	0.8
AA	5.39	5.61	.0022	5180	2.03	.360	.648	.852	.970
BB	5.35	5.84	.0022	5500	2.07	.369	.660	.865	.972
CC	5.24	5.66	--	--	--	--	--	--	--
DD	4.84	5.49	.0022	5410	2.17	.383	.671	.862	.967
EE	4.62	5.26	.0021	5560	2.22	.393	.674	.862	.964
FF	4.55	5.44	.0022	5080	2.05	.375	.655	.856	.951
GG	4.84	5.74	.0021	5710	2.08	.370	.661	.858	.965
HH	4.91	5.89	.0022	5950	2.22	.374	.655	.861	.963
II	4.78	6.14	.0022	6000	2.15	.366	.652	.851	.965
JJ	4.52	5.41	.0022	5380	2.18	.389	.668	.852	.970
KK	4.50	5.47	.0022	5470	2.20	.392	.674	.864	.969
Ave.	4.87	5.59	.0022	5520	2.14	.377	.662	.858	.966

[1]Average of 3 cylinders

[2]Average of 8-9 cylinders

*Non-dimensionalized terms: $F = \frac{f_c}{f'_c}$, $E = \frac{\epsilon_c}{\epsilon'_c}$, and $\alpha = E_c \frac{\epsilon'_c}{f'_c}$

Table 4. Stress-Strain Properties of Prisms

Batch	Age At Test (days)[1]	f'_c (ksi) At Test[2]	ϵ'_c (in/in)	E_c (ksi)	α	*F at E of 0.2	0.4	0.6	0.8
AA	32-54	5.82	.0019	5320	1.74	.327	.625	.831	.951
BB	29-58	6.13	.0020	5600	1.82	.342	.618	.821	.945
CC	44-61	5.74	--	--	--	--	--	--	--
DD	49-63	5.66	.0019	5050	1.70	.320	.617	.831	.962
EE	46-61	5.69	.0020	5200	1.83	.339	.618	.831	.961
FF	47-63	5.85	.0020	5280	1.80	.330	.618	.831	.960
GG	49-67	5.95	.0019	5800	1.85	.352	.647	.853	.966
HH	56-69	6.49	.0020	5830	1.80	.324	.604	.817	.952
II	56-69	6.36	.0021	5600	1.85	.338	.618	.820	.952
JJ	59-71	6.00	.0021	5270	1.84	.330	.615	.830	.952
KK	57-77	6.02	.0020	5480	1.82	.340	.614	.820	.950
Ave.		5.97	.0020	5440	1.80	.334	.619	.828	.955

[1]Age at fatigue tests of prisms

[2]Average of 3-6 prisms from Groups 1a and 1b

*Non-dimensionalized terms: $F = \frac{f_c}{f'_c}$, $E = \frac{\epsilon_c}{\epsilon'_c}$, and $\alpha = E_c \frac{\epsilon'_c}{f'_c}$

Table 5. Compressive and Tensile Strains at Failure - Group 1b (e = 1")

Batch	Load (kips)	Strains (in/in) Maximum ϵ_c	Maximum ϵ_t
AA	102.0	0.002840	--
BB	100.0	0.002830	0.000430
	101.8	0.002910	--
CC	95.0	0.002150	--
	98.0	0.002190	--
DD	87.8	0.002850	0.000380
	89.5	0.003330	0.000380*
	92.5	0.002690	0.000280
EE	86.2	0.002350	--
	88.3	0.002850	0.000460
FF	91.3	0.002840	--
	92.0	0.003090	0.000420
GG	95.8	0.003110	--
	98.8	0.002940	--
HH	100.5	0.002500	0.000200*
	109.2	0.003200	0.000300*
II	(104.0)+	(0.002590)	--
	(105.0)+	(0.002800)	--
JJ	(90.0)+	(0.002240)	--
	(93.5)+	(0.002200)	--
KK	(93.0)+	(0.002260)	--

*Extrapolated ( )+ - Less than failure load

Table 6. Results of Group 2a (e = 0)

Spec. No.	Age (days)	Loads (kips) Min.	Max.	N	log N	$P_r = \frac{r}{n+1}$ *
	(a)	S_{max} = 80		S_{min} = 10		
CC-11	57	13.2	105.0	14,000	4.14613	--
JJ-12	64	12.9	103.0	2,000	--	--
JJ-6	69	13.5	107.5	16,000	4.20412	--
JJ-5	71	13.6	109.0	17,000	4.23045	--
	(b)	S_{max} = 77.5		S_{min} = 10		
DD-17	52	13.6	109.0	14,000	4.14613	--
DD-11	57	13.0	104.0	1,000	--	--
	(c)	S_{max} = 75		S_{min} = 10		
EE-3	46	13.8	102.0	17,000	4.23045	0.091
CC-3	52	13.2	98.8	24,000	4.38021	0.182
FF-16	52	13.6	102.0	36,000	4.55630	0.273
EE-8	51	13.1	105.0	39,000	4.59106	0.364
FF-5	48	13.6	102.0	40,000	4.60206	0.455
HH-14	59	15.1	109.7	47,000	4.67210	0.545
FF-13	56	13.6	102.0	53,000	4.72428	0.637
GG-2	59	13.9	103.9	59,000	4.77085	0.728
GG-11	57	13.9	103.9	65,000	4.81291	0.819
EE-5	59	13.4	101.0	70,000	4.84510	0.910

Table 6 - Continued

Spec. No.	Age (days)	Loads (kips) Min.	Max.	N	log N	$P_r = \frac{r^*}{n+1}$
	(d)	S_{max} = 72.5		S_{min} = 10		
DD-2	51	13.0	97.5	(5,000)	--	--
HH-10	58	15.1	109.7	39,000	4.59106	0.111
II-2	61	15.1	109.5	60,000	4.77815	0.222
HH-21	58	15.1	109.7	107,000	5.02938	0.333
DD-14	51	13.6	102.0	110,000	5.04139	0.445
KK-3	59	14.5	105.3	130,000	5.11394	0.556
CC-8	52	13.2	98.8	136,000	5.13354	0.667
CC-6	59	13.2	98.8	192,000	5.28330	0.778
II-18	61	15.1	109.5	275,000	5.43933	0.889
	(e)	S_{max} = 70		S_{min} = 10		
EE-6	47	13.1	98.2	(7,000)	--	--
JJ-10	59	13.7	95.9	55,000	4.74036	0.071
GG-5	53	13.9	97.0	106,000	5.02531	0.143
FF-2	47	13.6	95.5	135,000	5.13033	0.214
HH-2	58	15.1	106.0	152,000	5.18184	0.286
JJ-13	64	13.9	97.2	155,000	5.19033	0.357
KK-18	60	14.5	101.7	206,000	5.31387	0.429
GG-14	59	13.9	97.0	269,000	5.42975	0.500
FF-6	65	13.6	95.5	313,000	5.49554	0.571
HH-16	57	15.1	106.0	320,000	5.50515	0.642
II-14	67	14.8	104.0	356,000	5.55145	0.714
EE-13	50	13.1	98.3	429,000	5.63327	0.786
II-13	62	15.1	106.0	492,000	5.69197	0.858
FF-19	53	13.6	95.5	2,305,000+	--	0.929

Table 6 - Continued

Spec. No.	Age (days)	Loads (kips) Min.	Max.	N	log N	$P_r = \frac{r}{n+1}$ *
		(f) S_{max} = 67.5		S_{min} = 10		
FF-8	48	13.6	92.1	159,000	5.20276	0.077
JJ-2	60	13.7	92.7	256,000	5.40824	0.154
KK-6	58	14.5	98.2	270,000	5.43136	0.231
HH-15	59	15.1	102.1	655,000	5.81624	0.308
FF-12	48	13.6	92.1	779,000	5.89154	0.385
DD-20	50	13.4	94.0	970,000	5.98677	0.462
CC-15	57	13.2	92.1	1,048,000	6.02036	0.539
II-10	59	14.8	103.5	1,051,000	6.02160	0.615
EE-14	48	12.7	93.0	1,318,000	6.11992	0.692
FF-3	50	13.6	92.1	1,661,000	6.22037	0.770
CC-2	48	13.2	92.1	2,083,000+	--	0.847
GG-19	54	13.9	93.5	2,300,000+	--	0.923
		(g) S_{max} = 65		S_{min} = 10		
AA-6	68	13.6	95.2	2,030,000+	--	--
BB-4	42	14.4	93.8	2,000,000+	--	--
CC-4	44	13.2	85.3	2,808,000+	--	--
DD-15	52	13.4	90.5	2,879,000+	--	--
II-9	56	14.8	99.0	2,290,000+	--	--
		(h) S_{max} = 60		S_{min} = 10		
AA-2	40	10.6	85.0	2,245,000+	--	--
BB-11	35	14.6	88.0	4,050,000+	--	--

*Plotting position

+No failure

( ) - Premature failure by splitting. Not included in analysis.

Table 7. Results of Group 2b (e = 1")

Spec. No.	Age (days)	Loads (kips) Min.	Max.	N	log N	$P_r = \frac{r}{n+1}$ *
		(a) S_{max} = 95		S_{min} = 10		
CC-14	59	7.3	73.5	12,000	4.07918	--
EE-12	64	6.5	69.2	14,000	4.14613	--
FF-10	58	6.6	73.2	2,500	--	--
HH-17	64	7.8	82.0	11,000	4.04139	--
		(b) S_{max} = 92.5		S_{min} = 10		
GG-7	62	6.6	74.5	31,000	4.49136	--
GG-15	62	6.6	74.5	39,000	4.59106	--
JJ-9#	63	7.5	73.9	34,000	4.53148	--
		(c) S_{max} = 90		S_{min} = 10		
CC-13	53	7.5	67.8	28,000	4.44716	0.111
II-20	62	8.0	77.5	31,000	4.49136	0.222
II-21	63	8.0	77.5	35,000	4.54407	0.333
JJ-21	64	7.5	71.1	45,000	4.65321	0.445
FF-15	58	6.6	67.3	46,000	4.66276	0.556
FF-7	59	6.6	67.3	58,000	4.76343	0.667
DD-12	61	6.0	66.0	61,000	4.78533	0.778
HH-19	65	7.8	76.1	129,000	5.11059	0.889

Table 7 - Continued

Spec. No.	Age (days)	Loads (kips) Min.	Max.	N	log N	$P_r = \frac{r}{n+1}$*
	(d)	S_{max} = 87.5		S_{min} = 10		
EE-2	57	6.5	66.5	(---)	--	--
EE-15	57	6.5	66.5	(---)	--	--
HH-5	64	7.8	73.4	81,000	4.90849	0.077
II-4	62	8.0	75.5	120,000	5.07918	0.154
GG-1	62	6.6	68.9	131,000	5.11727	0.231
JJ-8	70	7.5	68.1	141,000	5.14922	0.308
EE-18	58	6.5	66.5	156,000	5.19312	0.385
HH-3	64	7.8	73.4	180,000	5.25527	0.462
FF-11	58	6.6	64.5	190,000	5.27875	0.538
DD-7	61	6.5	63.5	226,000	5.35411	0.615
DD-5	61	6.0	63.5	242,000	5.38382	0.692
KK-17#	76	7.2	70.0	317,000	5.50106	0.770
JJ-19#	62	7.0	68.0	351,000	5.54531	0.846
GG-9	61	6.6	68.9	527,000	5.72181	0.922
	(e)	S_{max} = 85		S_{min} = 10		
JJ-17	70	7.5	66.0	305,000	5.48430	0.100
GG-17	60	6.6	66.3	684,000	5.83506	0.200
II-8	63	8.0	72.5	730,000	5.86332	0.300
EE-16	53	6.5	64.2	859,000	5.93399	0.400
HH-4	66	7.8	71.0	860,000	5.93450	0.500
DD-8	59	6.0	61.0	1,045,000	6.01912	0.600
EE-17	54	6.5	64.2	2,105,000	6.32325	0.700
FF-17	59	6.6	61.8	2,751,000	6.43949	0.800
CC-20	54	7.5	64.0	2,000,000+	--	0.900

*Plotting position

+No failure

( ) - Premature failure due to misalignment. Not included in analysis.

#Statically loaded prior to application of repeated loading.

Table 8. Results of Group 2c (e = 1/3")

Spec. No.	Age (days)	Loads (kips) Min.	Max.	N	log N	$P_r = \frac{r^*}{n+1}$
	(a) S_{max} = 85			S_{min} = 10		
JJ-15	69	12.0	96.1	16,000	4.20412	0.143
II-17#	65	11.0	101.0	26,000	4.41497	0.286
II-11	67	10.8	98.7	35,000	4.54407	0.429
KK-7	64	11.0	95.3	37,000	4.56820	0.571
HH-6#	65	11.0	100.0	46,000	4.66276	0.712
GG-16#	63	11.0	90.5	65,000	4.81291	0.859
	(b) S_{max} = 80			S_{min} = 10		
KK-8	67	11.0	88.8	108,000	5.03342	0.111
JJ-18	69	12.0	89.2	206,000	5.31387	0.222
HH-20#	69	11.5	100.0	224,000	5.35025	0.333
GG-10	63	11.0	86.3	249,000	5.39620	0.445
HH-11	67	11.0	94.4	270,000	5.43136	0.556
HH-8	65	11.0	97.0	364,000	5.56110	0.667
II-7#	65	10.0	91.3	542,000	5.73400	0.778
KK-19#	64	11.0	88.2	2,155,000+	--	0.889
	(c) S_{max} = 77.5			S_{min} = 10		
JJ-14#	65	12.0	89.2	464,000	5.66652	--
II-6	66	10.8	90.0	888,000	5.94841	--
KK-10#	62	11.0	86.6	941,000	5.97359	--
GG-4	71	11.0	83.7	1,198,000	6.07809	--
KK-21	67	11.0	86.0	2,000,000+	--	--

*Plotting position +No failure

#Statically loaded prior to application of repeated loading.

Table 9. Summary of Small Concrete Specimen Fatigue Test Results

Test Group	S_{max},* % f'_c	No. of Spec.	Fatigue Life		Log Fatigue Life		
			$\bar{N}$	D_N	$\overline{\log N}$	$\log^{-1}(\overline{\log N})$	$D_{(\log N)}$
2a	80.0	3	15,700	--	4.19357	15,600	--
	75.0	10	45,000	17,200	4.61853	41,600	0.1940
	72.5	8	131,000	74,600	5.05126	112,500	0.2678
	70.0	12**	249,000	136,000	5.32410	210,900	0.2800
	67.5	9**	890,000	460,000	5.87940	757,500	0.2857
	65.0	5	2,000,000+	--	--	--	--
2b	95.0	3	15,700	--	4.08890	12,300	--
	92.5	3	34,700	--	4.53797	34,500	--
	90.0	8	54,000	32,500	4.68224	48,100	0.2114
	87.5	12	222,000	125,000	5.29062	195,300	0.2256
	85.0	8**	1,167,000	825,000	5.97913	953,100	0.2964
2c	85.0	6	37,500	16,900	4.53450	34,200	0.2091
	80.0	7**	280,400	138,400	5.40288	252,900	0.2171
	77.5	4**	872,800	--	5.91665	825,400	--

*S_{min} = 10 **Run-outs discarded +No failure (Run-out)

$\bar{N}$ - Mean fatigue life

$\overline{\log N}$ - Mean of log N

D_N - Standard deviation of N

$D_{(\log N)}$ - Standard deviation of log N

Table 10. Ultimate Static Strength of Prisms Surviving Over Two Million Cycles - Group 2a

Spec. No.	S_{max}	N Cycles	$(f'_c)_N$ ksi	$\frac{(f'_c)_N}{f'_c}$
AA-2	60.0	2,245,000	6.35	1.09
AA-6	65.0	2,030,000	6.48	1.11
BB-11	60.0	4,050,000	6.75	1.10
CC-4	65.0	2,808,000	6.36	1.11
CC-2	67.5	2,083,000	6.04	1.05
DD-15	65.0	2,879,000	6.14	1.09
FF-19	70.0	2,305,000[1]	6.05	1.03
GG-19	67.5	2,300,000	6.11	1.03
II-19	65.0	2,290,000	6.91	1.09

[1]Cracks had formed under repeated loads

Table 11. Comparison of Geometric Standard Deviation (Linear Theory)

Test Group	S_{max} % f'_c	V_S	$\frac{D_N}{V_S}$	$D_{(\log N)}$ Estimated	$D_{(\log N)}$ Observed
2a	75.0	51,900	0.3017	0.1704	0.1940
	72.5	156,000	0.4782	0.2882	0.2678
	70.0	320,000	0.4250	0.2531	0.2800
	67.5	1,366,000	0.3367	0.1939	0.2857
2b	90.0	63,000	0 5159	0.3123	0.2114
	87.5	254,000	0.4921	0.2972	0.2256
	85.0	1,608,000	0.5130	0.3105	0.2964

Note: Values of D_N and Observed $D_{(\log N)}$ taken from Table 9.

Table 12. Summary of Test Beam Properties

Beam No.	Age (Days)	f'_c* (ksi)	Total F_{se} (kips)	b in.	d in.	h in.	$p = \frac{A_s}{bd}$
1	31	5.00	954	6.06	7.88	12.12	0.0137
2	43	5.32	924	6.25	7.75	12.00	0.0135
3	28	5.23	975	6.12	7.88	12.12	0.0136
4	37	4.84	939	6.09	7.94	12.19	0.0135

*Average cylinder f'_c in test section

Table 13. Details of Concrete Mixes - Beams

Test Section*		Cement	Water	Aggregates (lb)		Slump
Beam	Mix	lb.	lb.	Fine	Coarse	in.
1	I	134	77	420	435	2-1/2
-	II	134	77	420	435	4-1/2
2	III	134	70	420	435	3-1/4
3	IV	134	71	420	435	2-3/4
4	V	134	70	420	435	3

*Concrete from only one mix was placed in the test section of each beam.

Table 14. Mechanical Properties of Concrete - Beams

Mix	f'_c (ksi)	ϵ'_c (in/in)	E_c (ksi)	α	*F at E of 0.2	0.4	0.6	0.8
(a) Cylinders - At Release of Prestress								
I	4.37	.0020	4100	1.88	.366	.635	.828	.949
II	4.34	.0021	3570	1.73	.337	.631	.833	.960
III	4.62	.0022	3720	1.77	.376	.640	.831	.951
IV	5.04	.0022	4000	1.74	.337	.605	.810	.948
V	4.50	.0020	4080	1.81	.365	.635	.830	.956
Ave.	4.57	.0021	3890	1.79	.357	.629	.826	.953
(b) Cylinders - At Test[1]								
I	5.00	.0024	4500	2.17	.378	.660	.858	.968
II	4.95	.0024	4560	2.21	.364	.648	.839	.960
III	5.32	.0025	4320	2.03	.335	.604	.810	.942
IV	5.23	.0024	4950	2.27	.378	.642	.840	.962
V	4.84	.0024	4360	2.17	.384	.664	.852	.962
Ave.	5.07	.0024	4540	2.17	.368	.644	.840	.960
(c) Prisms - At Test[1]								
I	5.20	.0023	4500	1.99	.373	.660	.850	.966
II	5.04	.0023	4250	1.94	.363	.643	.840	.960
III	5.26	.0023	4700	2.05	.368	.650	.850	.925
IV	5.20	.0023	4560	2.02	.372	.678	.852	.955
V	--	--	--	--	--	--	--	--
Ave.	5.18	.0023	4500	2.00	.369	.658	.848	.952

*Non-dimensionalized terms: $F = \frac{f_c}{f'_c}$, $E = \frac{\epsilon_c}{\epsilon'_c}$, and $\alpha = E_c \frac{\epsilon'_c}{f'_c}$

[1]Age at test as given in Table 12.

Table 15. Prestress Data

Beam No.	Steel Level	ϵ_c	$\Delta\epsilon_c$	ϵ_{se}	F_{se} (kips)	Loss %
1	(a)	44	47	569	48.6	14.3
2		45	73	552	47.1	16.9
3	Upper	46	31	583	49.5	12.2
4		45	55	560	47.7	15.9
1	(b)	49	51	560	95.4	15.9
2		51	69	540	92.4	18.5
3	C.G.S.	51	35	574	97.5	13.8
4		50	60	550	93.9	17.2
1	(c)	54	56	550	46.8	17.5
2		56	75	529	45.3	20.2
3	Lower	56	38	566	48.0	15.4
4		55	65	540	46.2	18.5

Notes: Steel strain due to initial prestress force, ϵ_{si} = 660, for all strands.

All strains in in/in x 10^{-5}

Table 16. Elastic Strains at Release of Prestressing Force , C.G.S. Line

Beam No.	Elastic Strains, ϵ_{ce} South (S)	North (N)	Average	$\frac{S-N}{2}$	% Difference
1	55	43	49	6	12.2
2	56	46	51	5	9.8
3	53	49	51	2	3.9
4	56	44	50	6	12.0

All strains in in /in x 10^{-5}

Table 17. Summary of Beam Test Results

Beam No.	Type of Test	P_{crk}	Loads[1] P_{min}	P_{max}	N (Cycles)	Failure Mode
1	Fatigue	11.9	1.8	15.3	80,000	Compression
2	Fatigue	11.5	2.2	14.5	350,000	Compression
3	Static	11.9	(P_u = 20 kips)		--	Compression
4	Fatigue	11.9	1.8	14.3	525,000	--
	(Static)[2]		(P_u = 18 kips)		--	(Compression)

Notes: [1]Loads in kips per jack

[2]Static ultimate test after 525,000 cycles

Table 18. Comparison of Estimated and Observed Beam Fatigue Lives

Beam No.	Stresses[1]		Stress Gradient[2]		Fatigue Life[3]		
	S_{min}	S_{max}	θ_k	$\theta_{k'}$	$\bar{N}_k$	$\bar{N}_{k'}$	N_{obs}
1	14	87.5	6.21	7.12	48	88	80
2	15	85.0	6.40	7.28	150	320	350
4	14	81.5	6.18	7.22	580	1800	525*

Notes:

[1]Calculated top fiber concrete stresses in % $k_3 f'_c$

[2]Stress gradient $\theta = \frac{E^t_{max}}{t}\left(\frac{dF}{dE}\right)_{E^t_{max}}$ in 10^{-2} per in.

θ_k: $t = kd$ $\theta_{k'}$: $t = k'd$

[3]Number of cycles in thousands

$\bar{N}_k$, $\bar{N}_{k'}$: Estimated mean fatigue lives corresponding to θ_k and $\theta_{k'}$, respectively.

N_{obs} : Observed beam fatigue life.

*Beam No. 4 tested statically to failure after N = 525,000

10. FIGURES

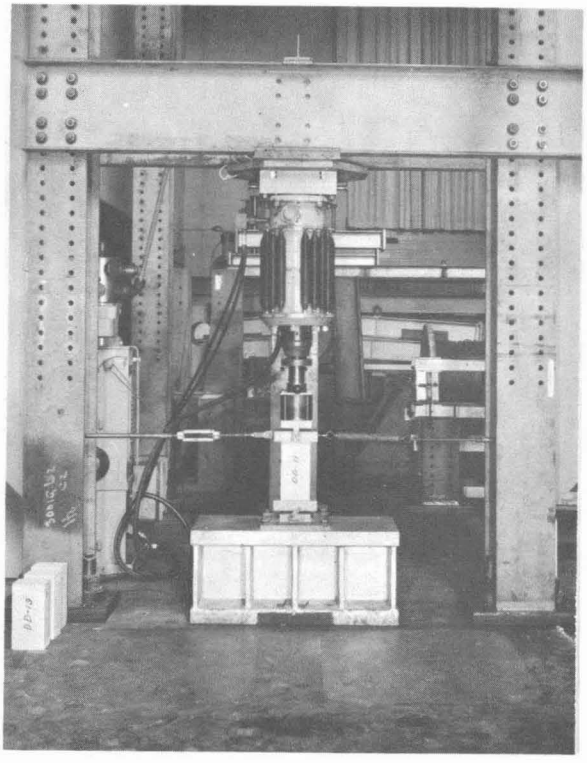

(a) Overall View

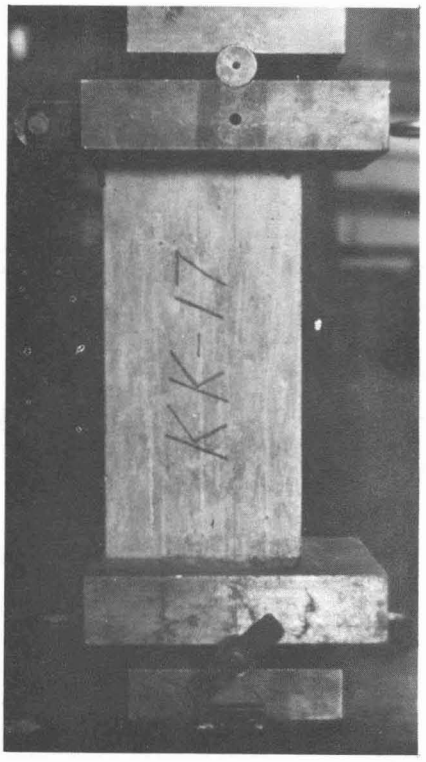

(b) Close-up View

Fig. 1 Concrete Specimen Fatigue Test Setup

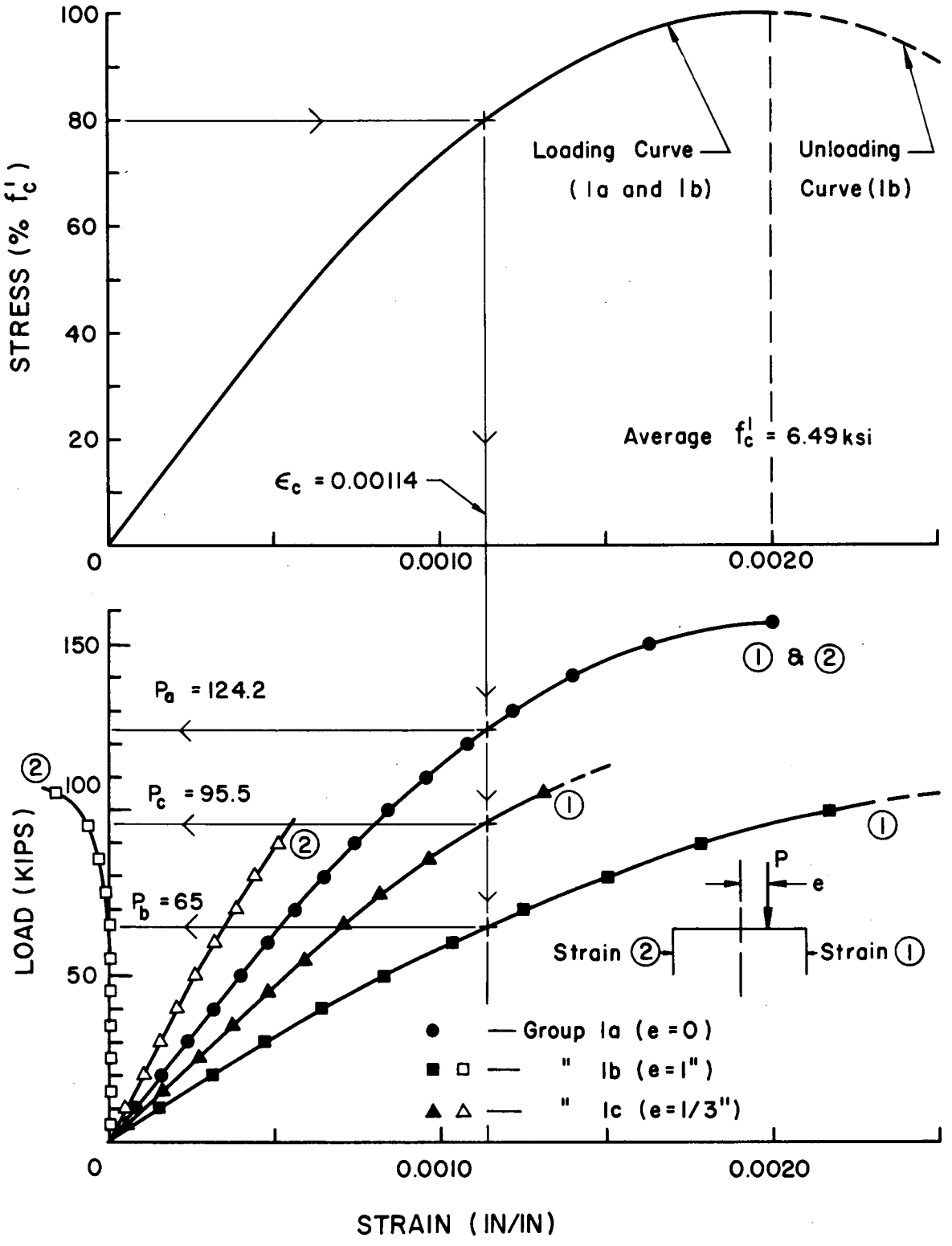

Fig. 2 Load-Stress-Strain Curves (Specimen HH)

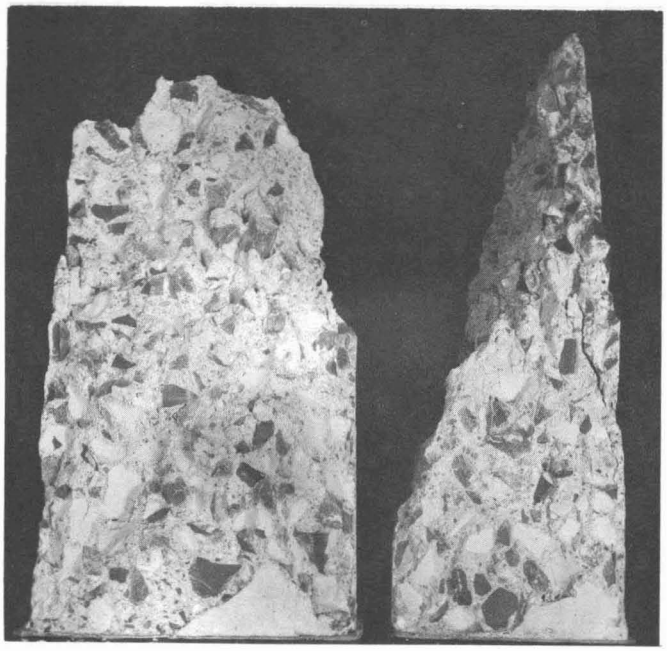

(a) Axially Loaded Specimen

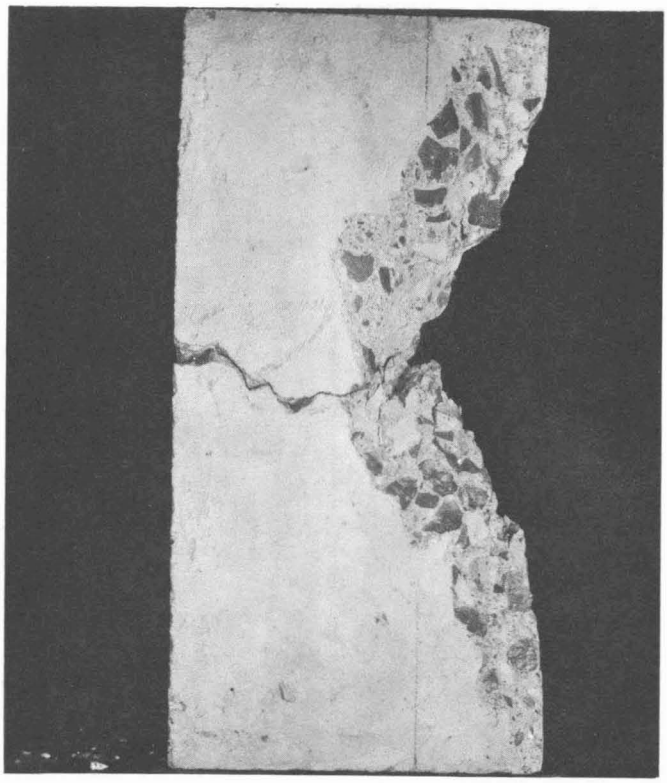

(b) Eccentrically Loaded Specimen

Fig. 3 Typical Concrete Specimen Fatigue Failures

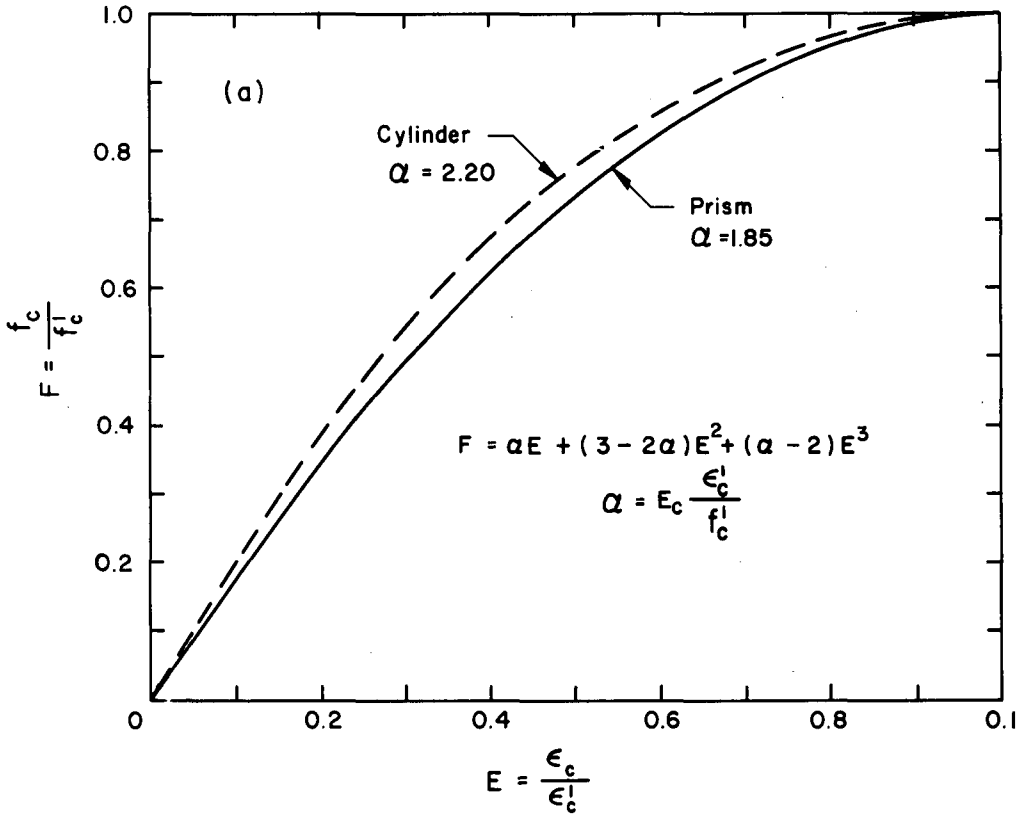

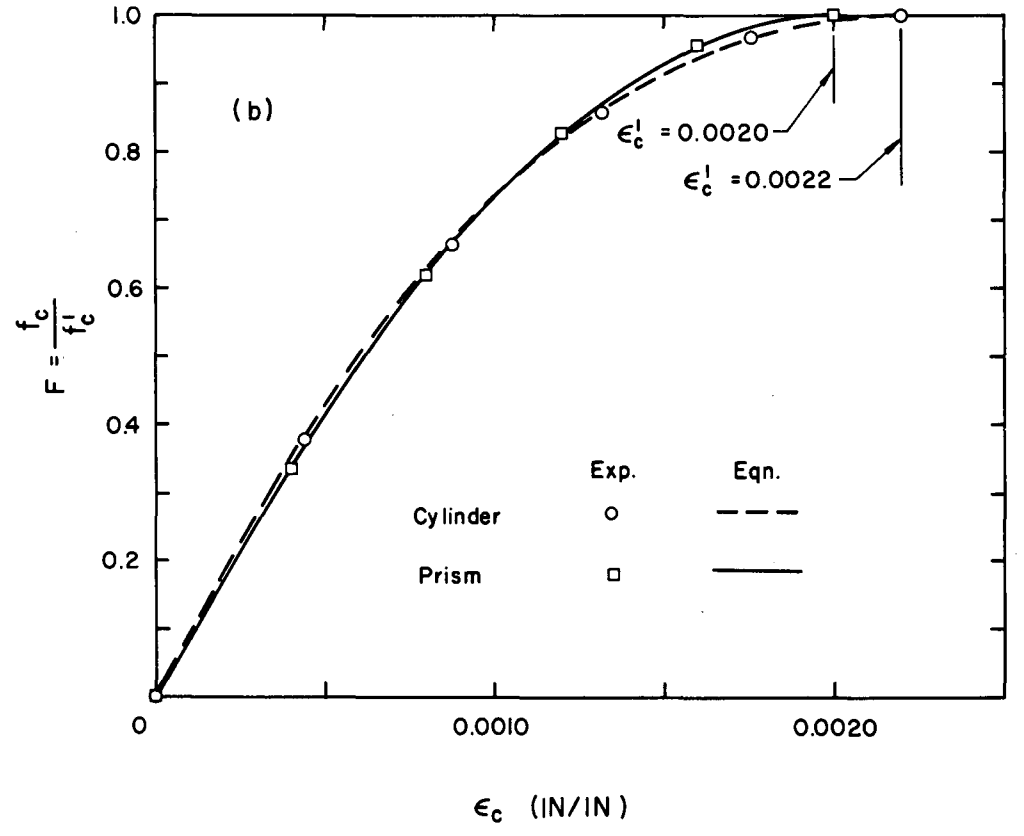

Fig. 4 Concrete Stress-Strain Curves

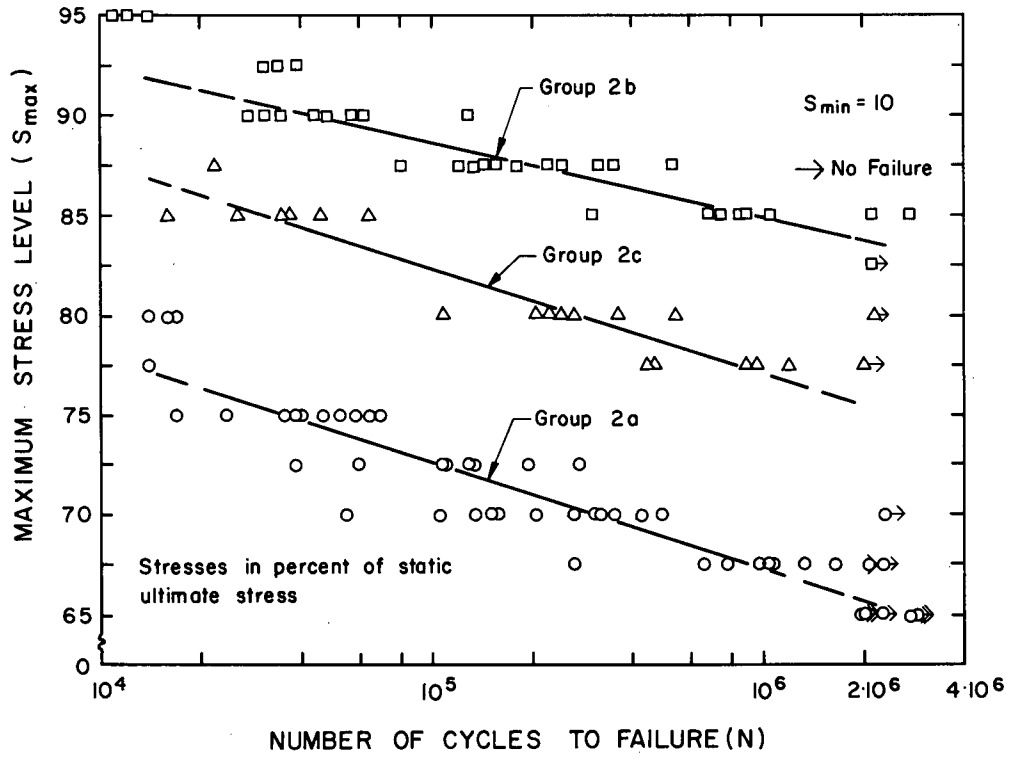

Fig. 5 Maximum Stress vs. Fatigue Life

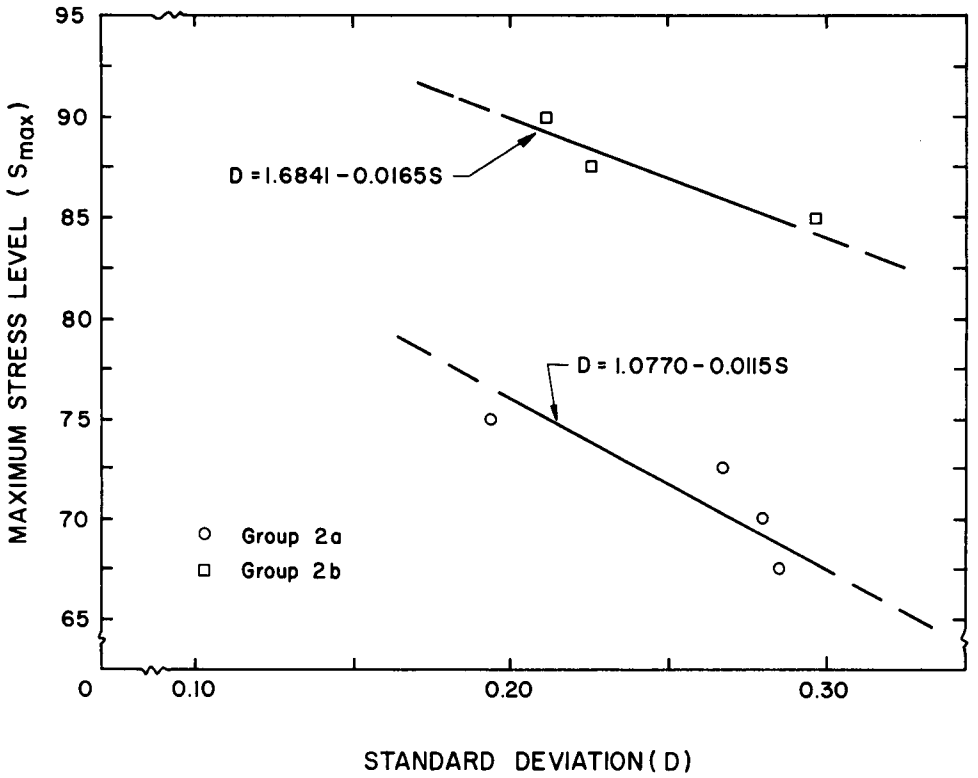

Fig. 6 Maximum Stress vs. Standard Deviation

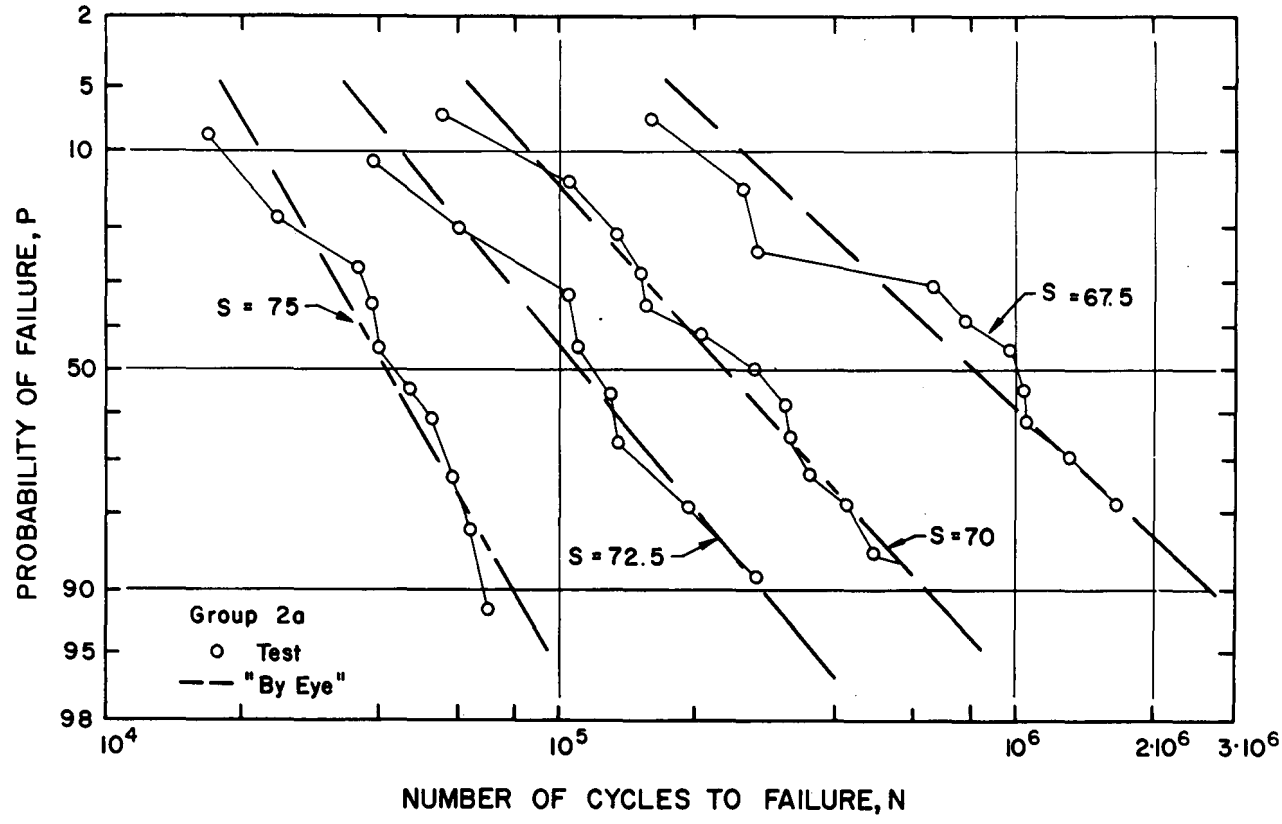

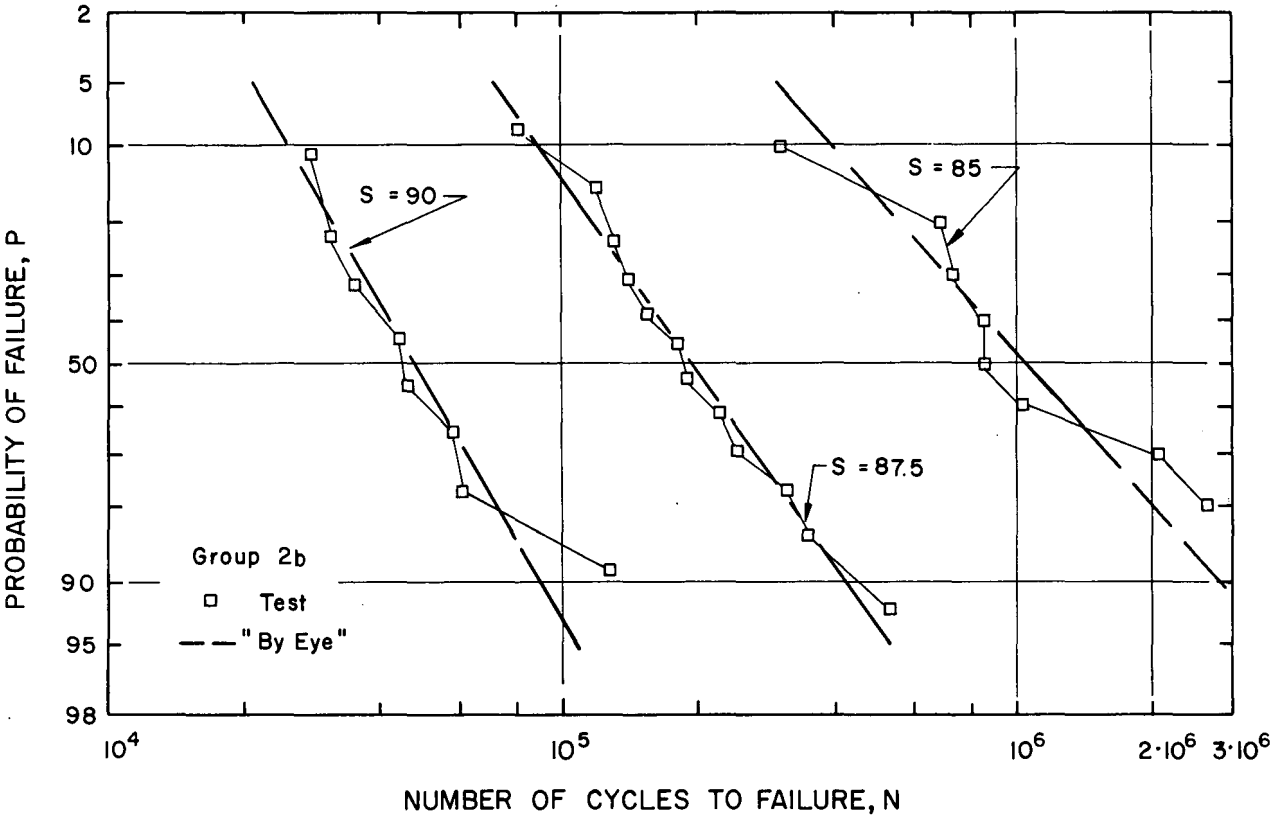

Fig. 7 S-N-P Diagrams - Logarithmic-Normal

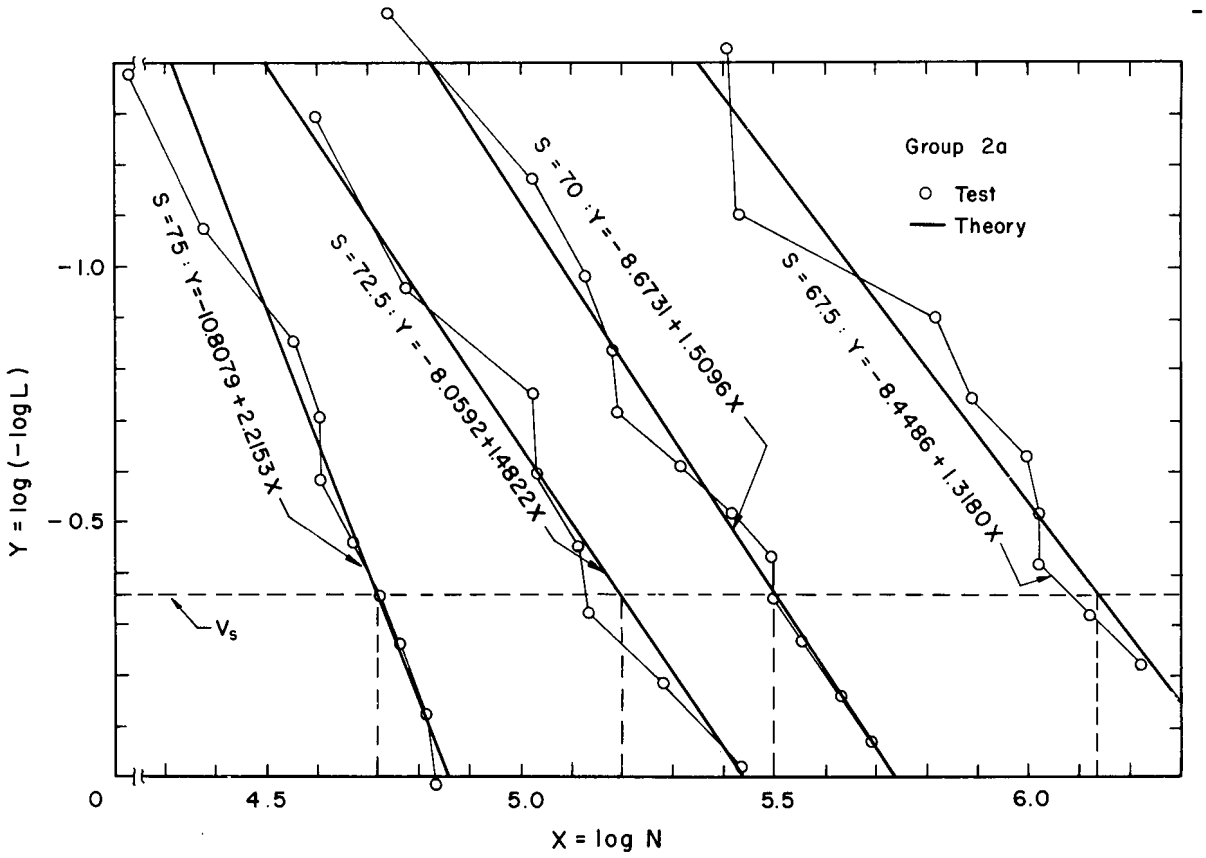

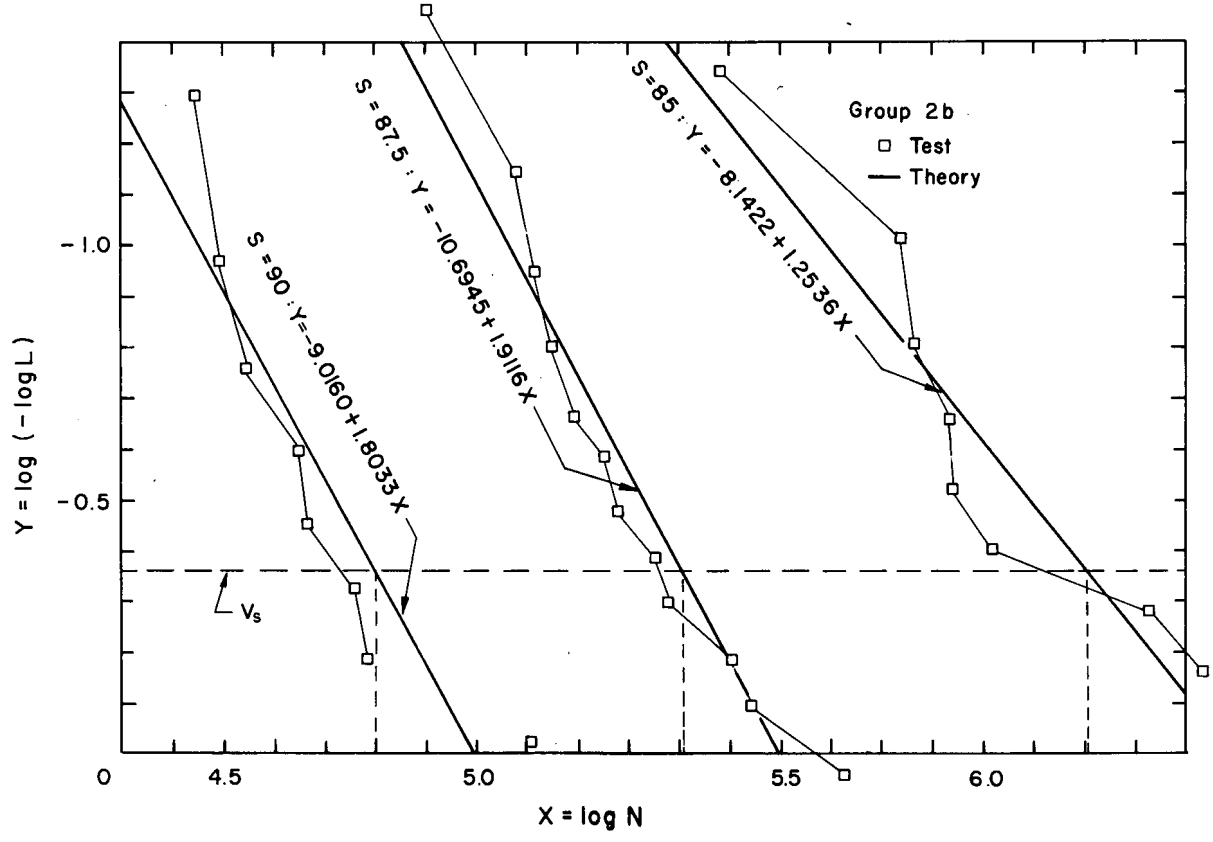

Fig. 8 S-N-P Diagrams - Extreme Value (Linear Theory)

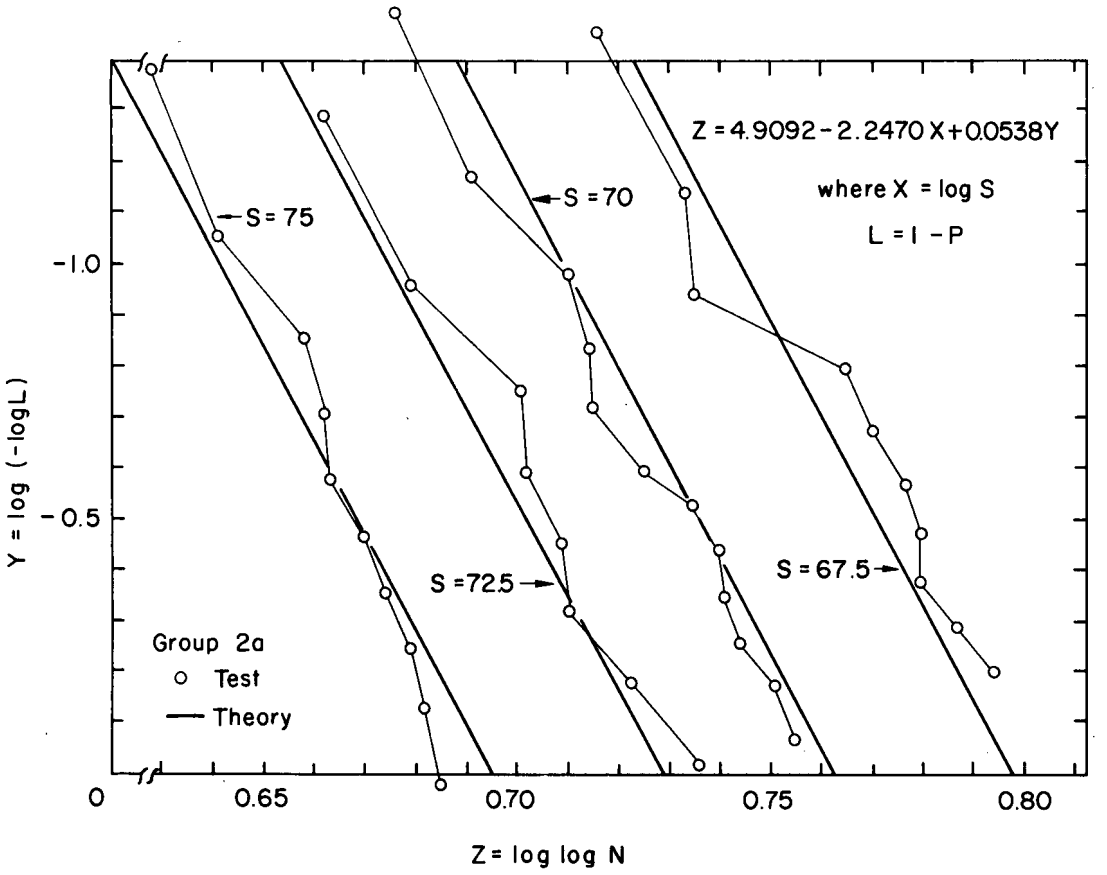

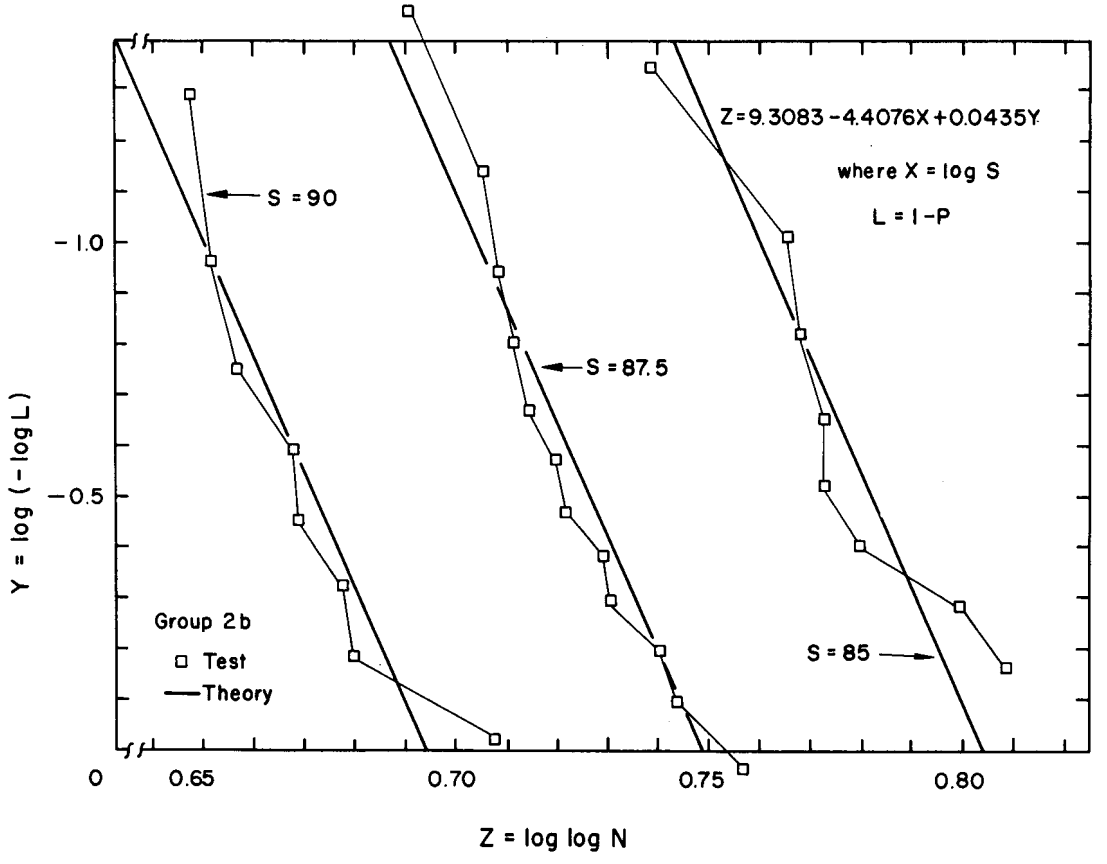

Fig. 9 S-N-P Diagrams - Mathematical Model (McCall)

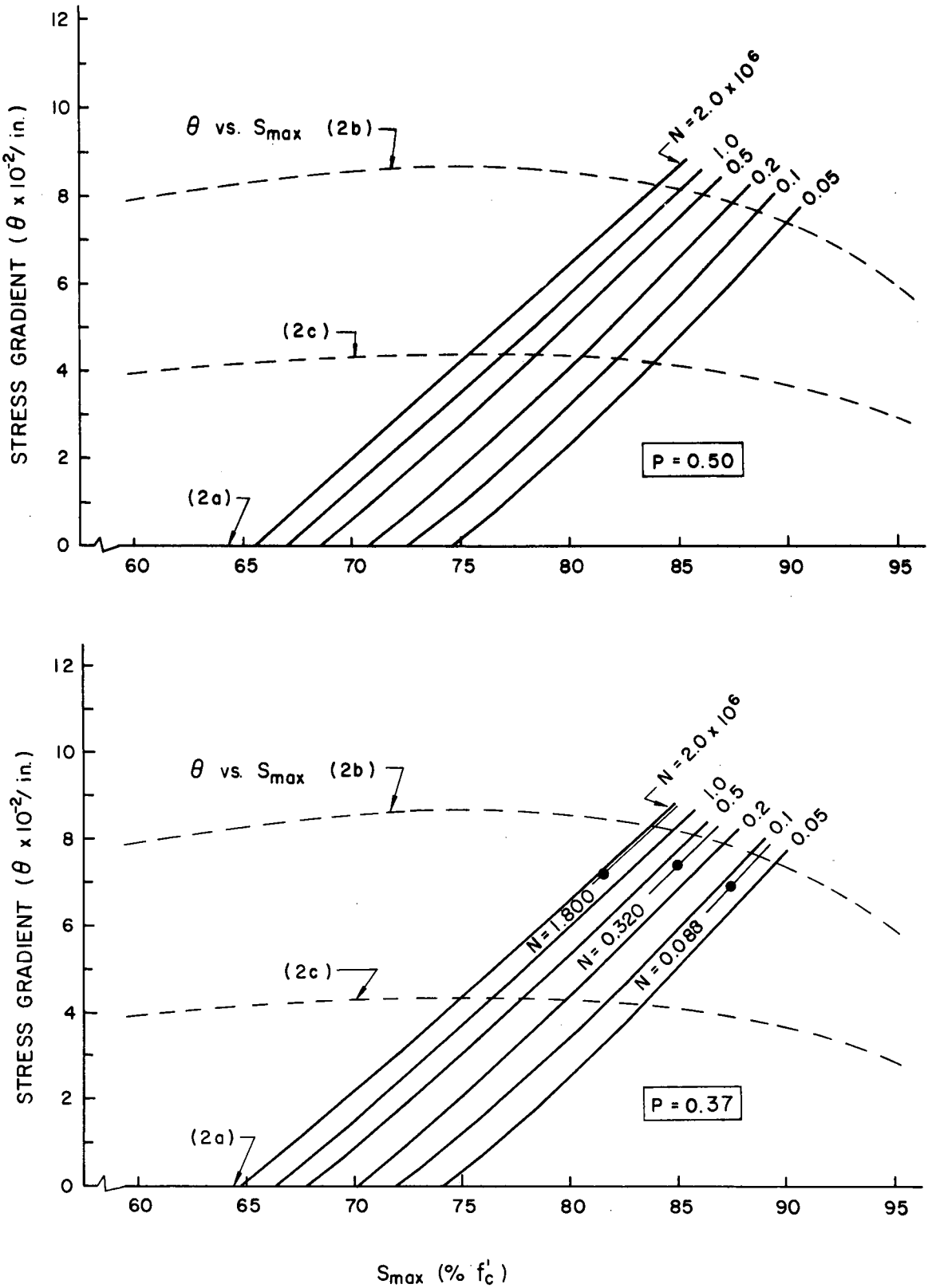

Fig. 10 S-N-θ Diagrams for P = 0.50 and P = 0.37

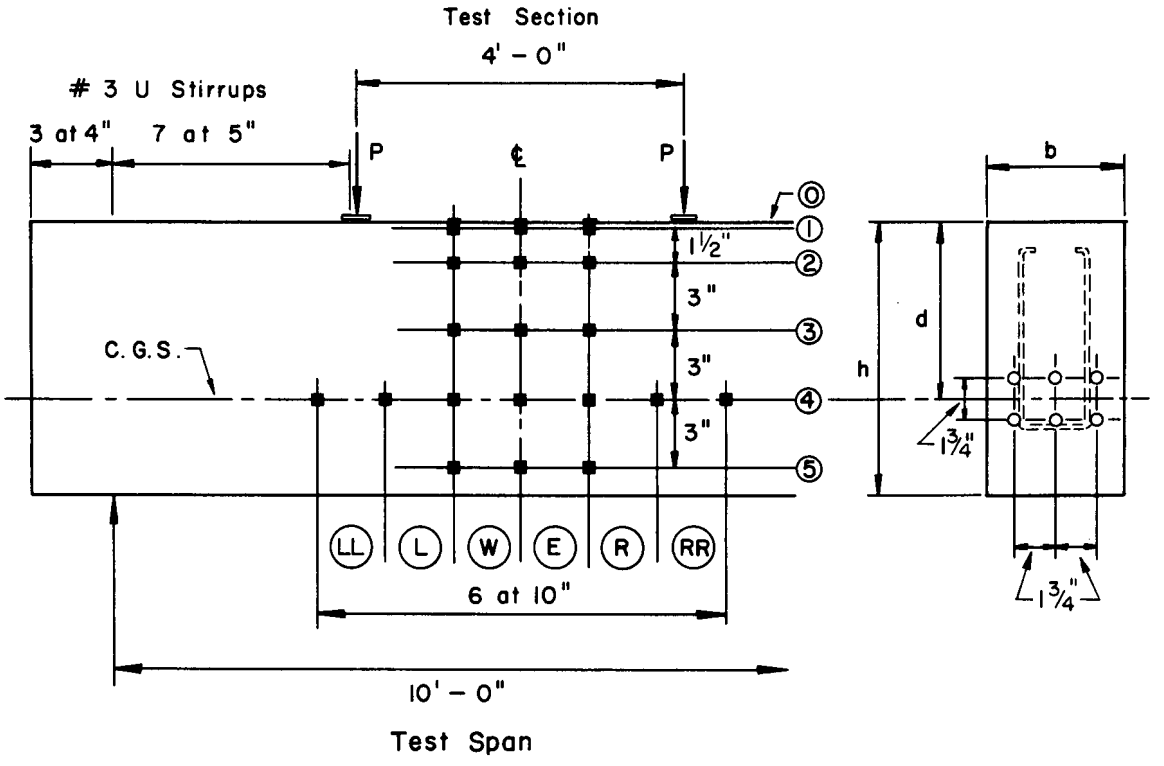

Fig. 11 Beam Details and Whittemore Target Layout (South Face)

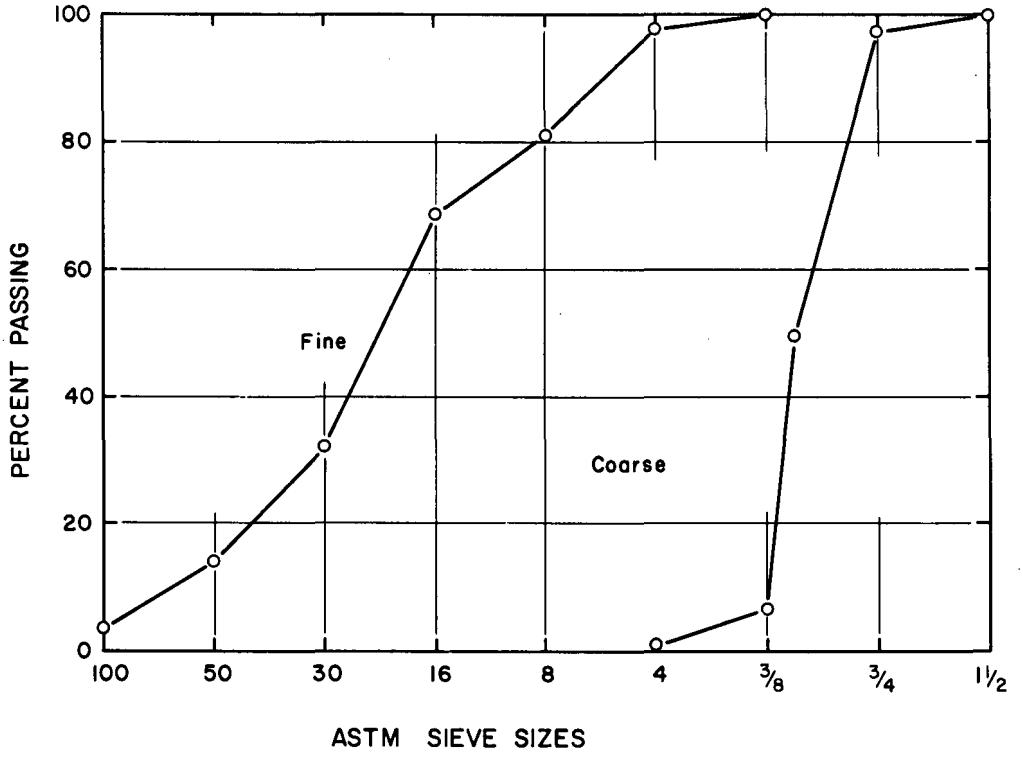

Fig. 12 Grading Curves for Aggregates

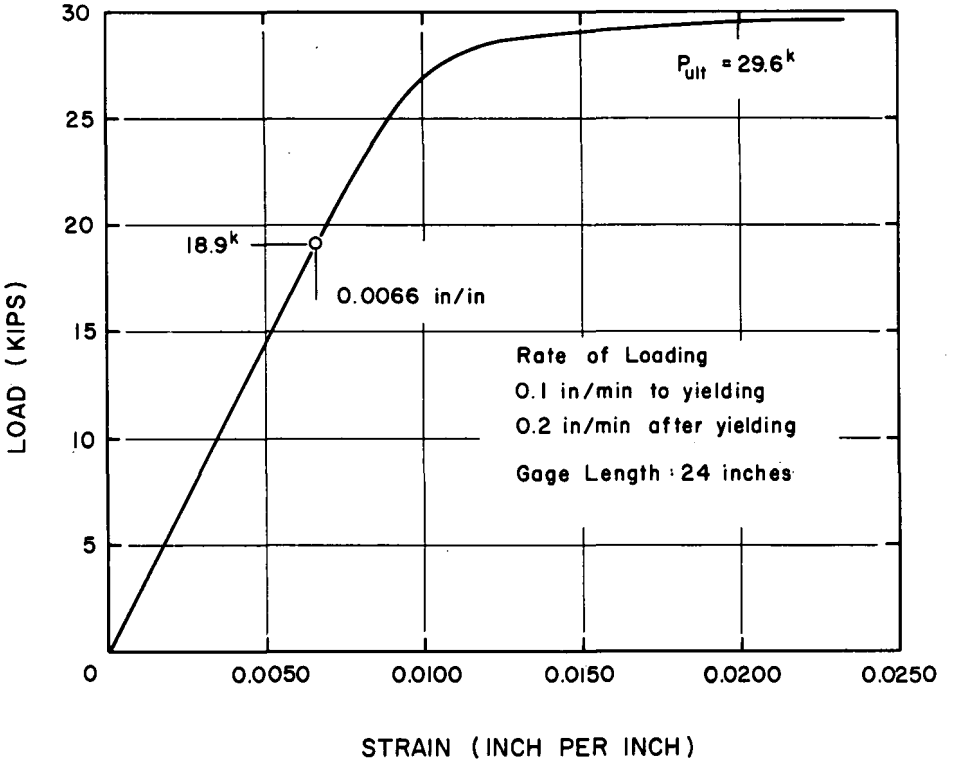

Fig. 13 Load-Strain Curve for Prestressing Strand

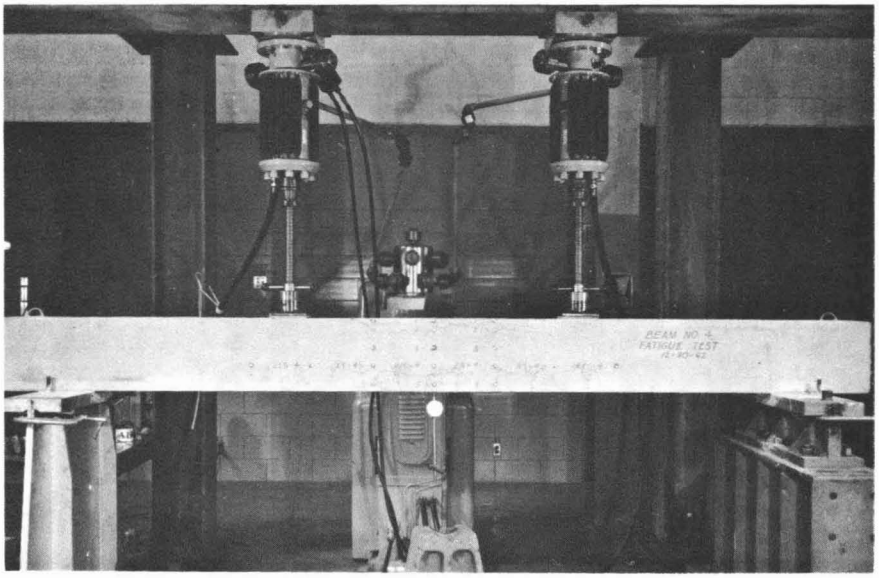

Fig. 14 Beam Fatigue Test Setup

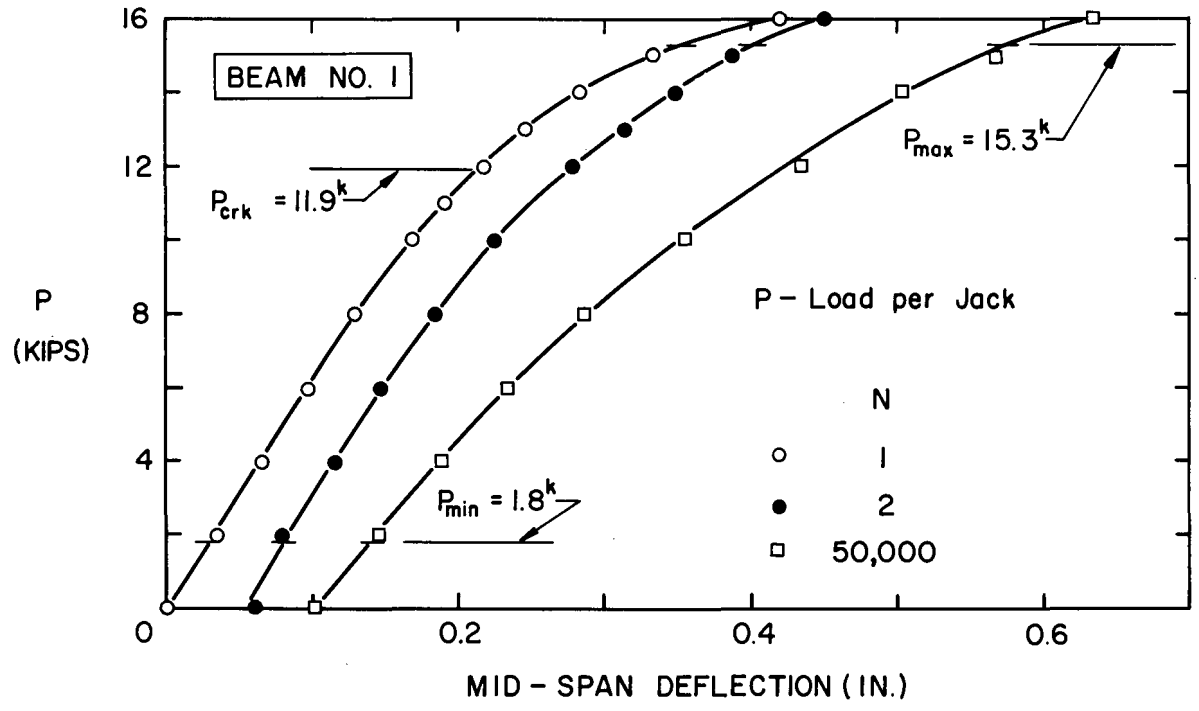

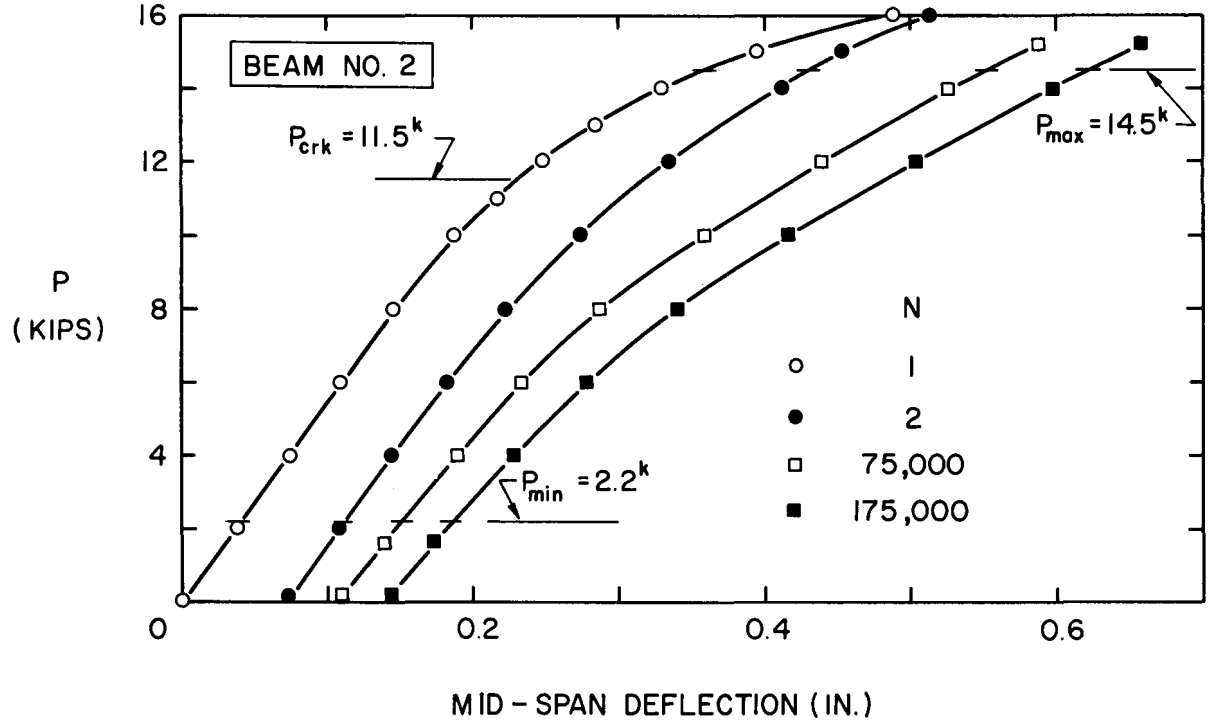

Fig. 15 Mid-span Deflection Curves (Beams 1 & 2)

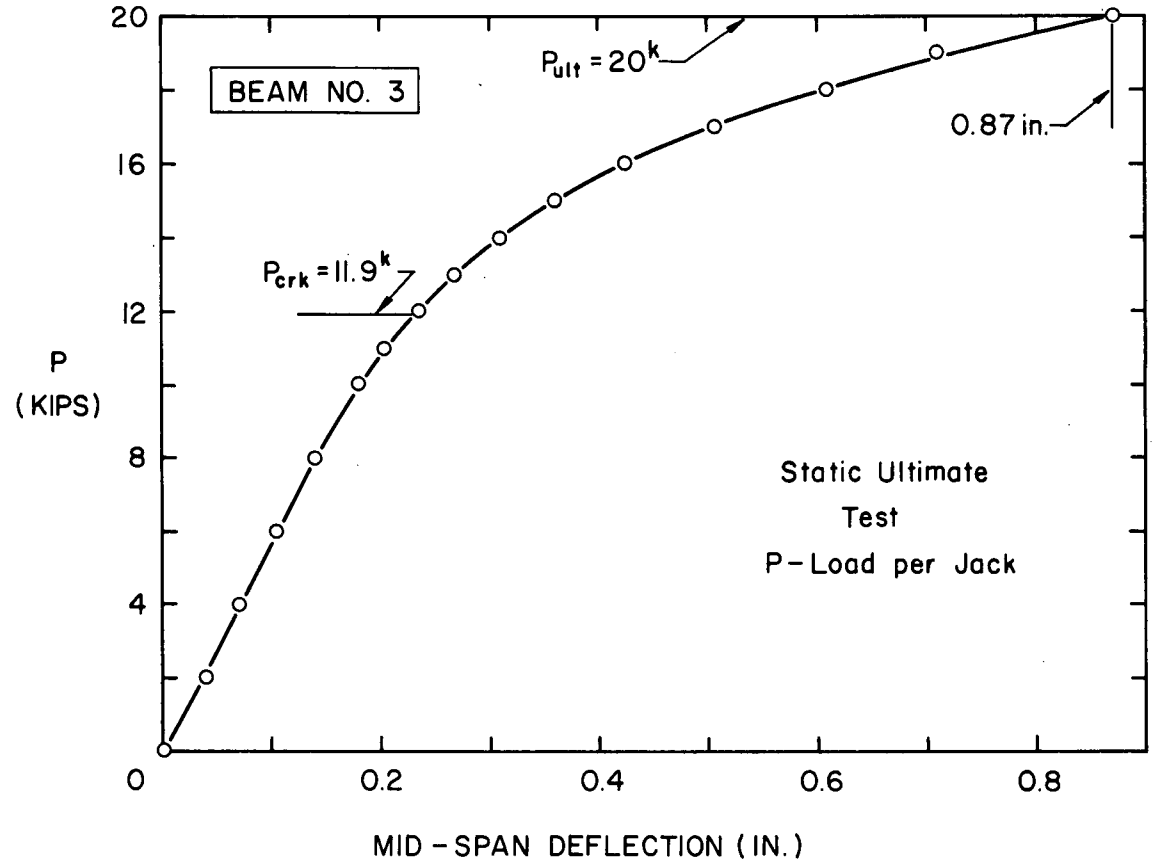

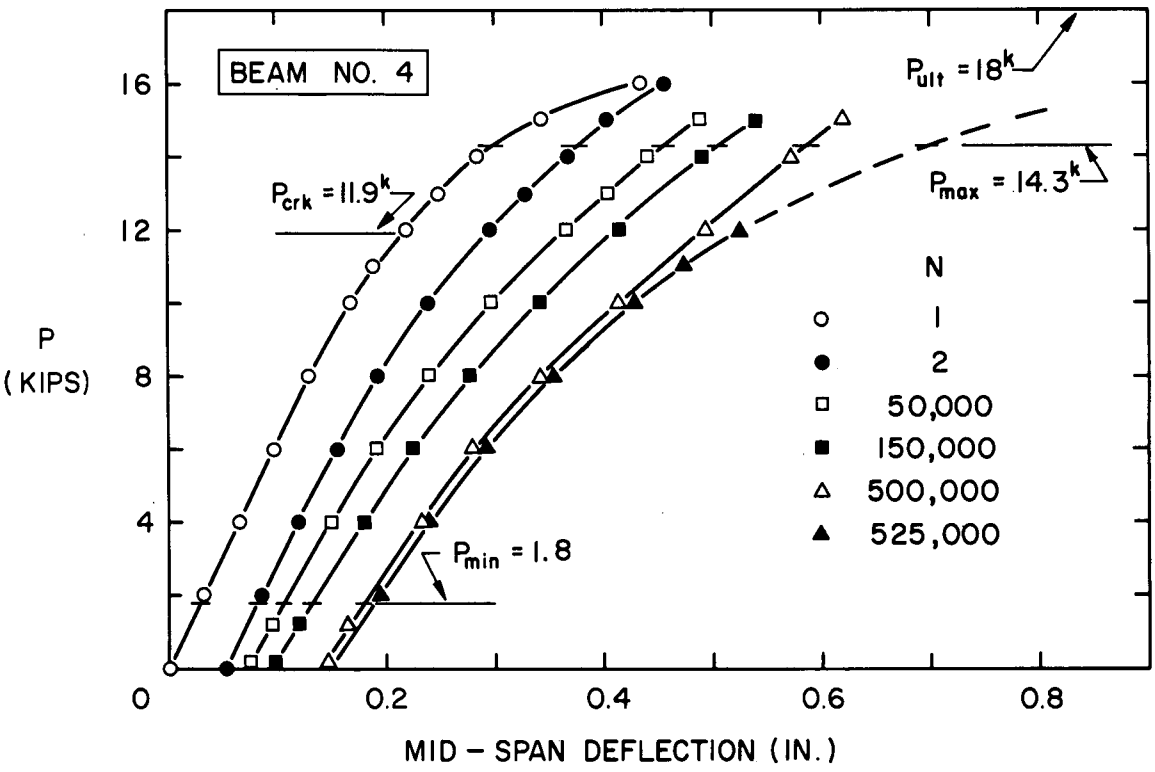

Fig. 15 Mid-span Deflection Curves (Beams 3 & 4)

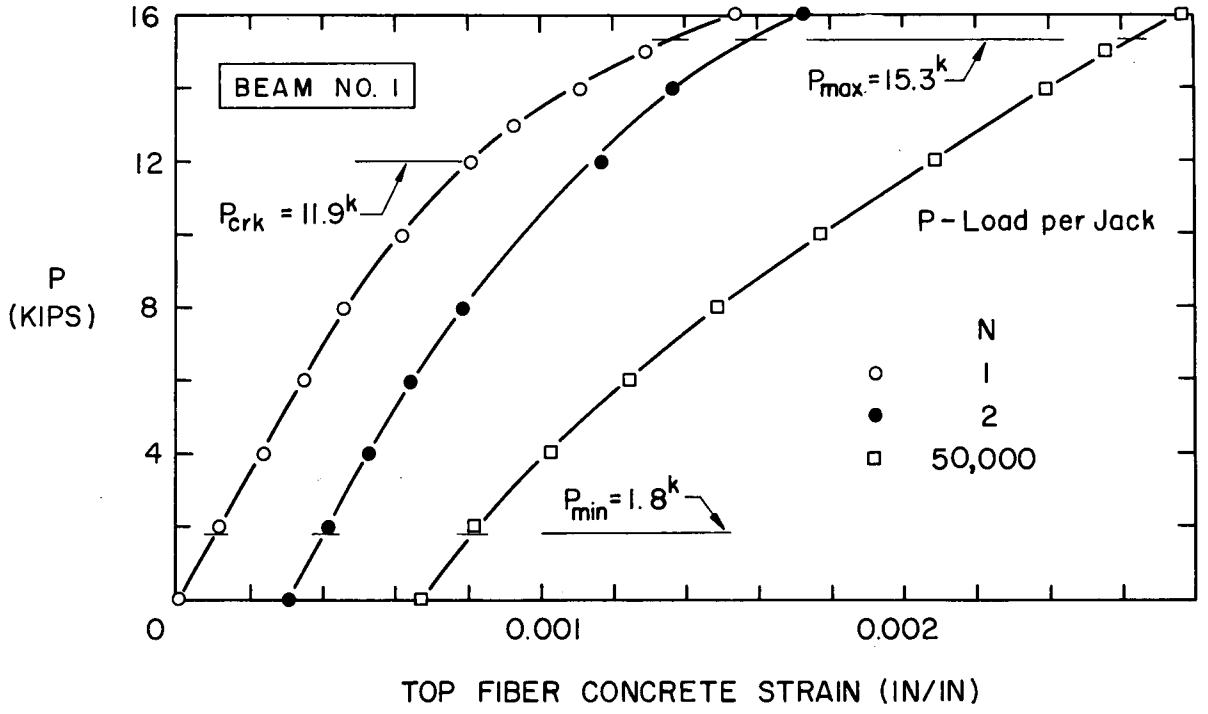

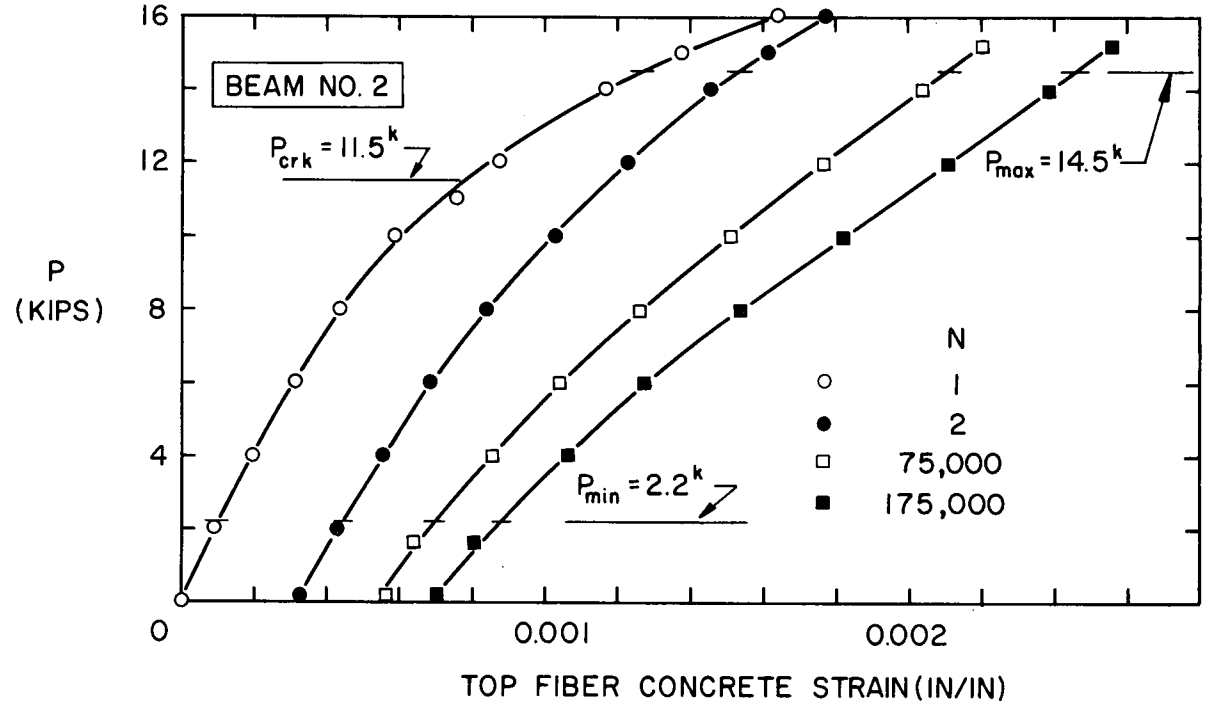

Fig. 16 Top Fiber Concrete Strain Curves (Beams 1 & 2)

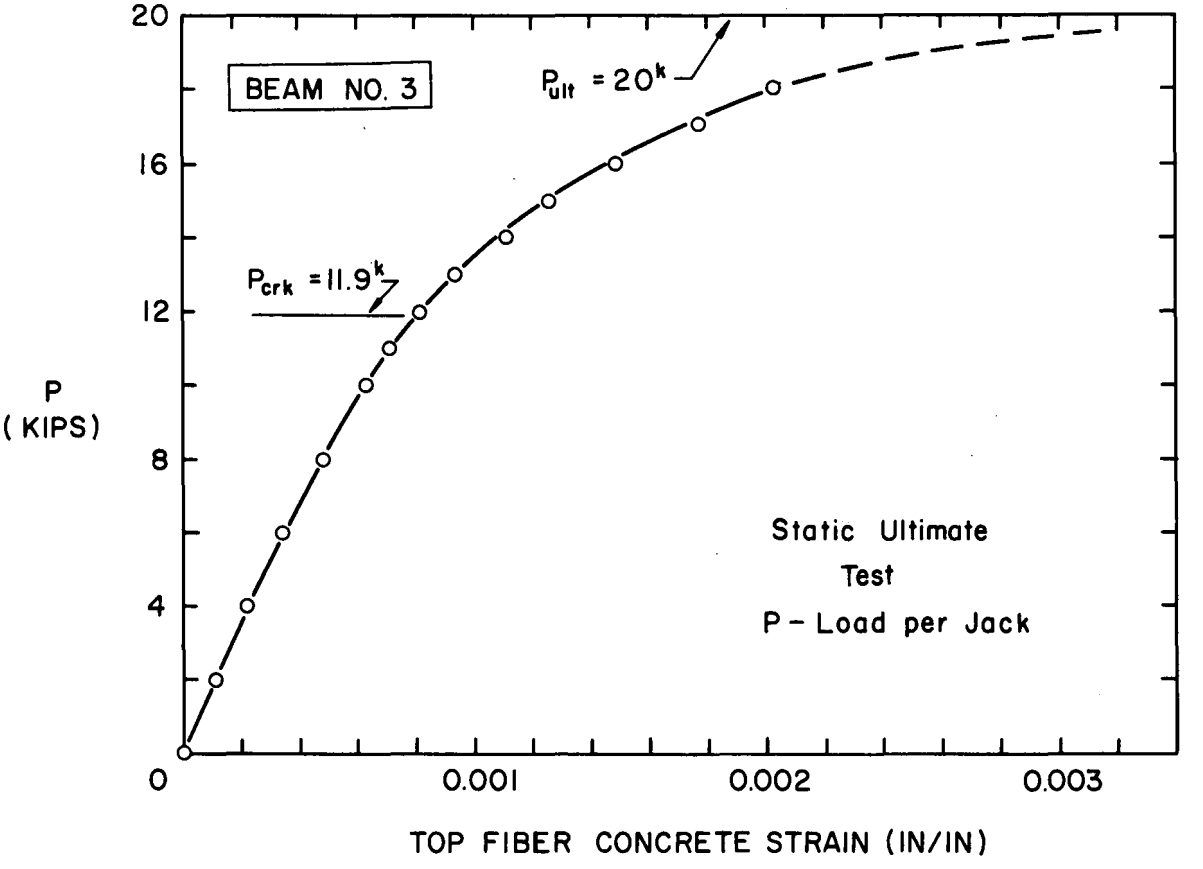

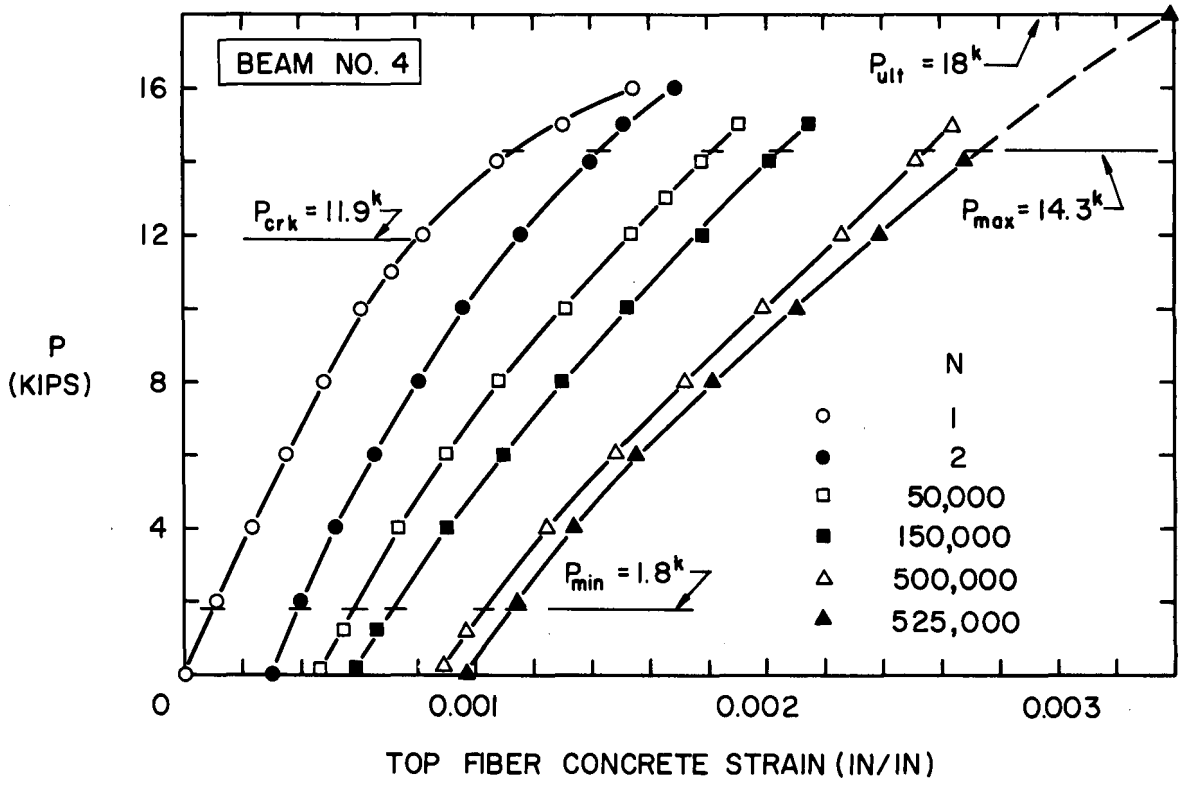

Fig. 16 Top Fiber Concrete Strain Curves (Beams 3 & 4)

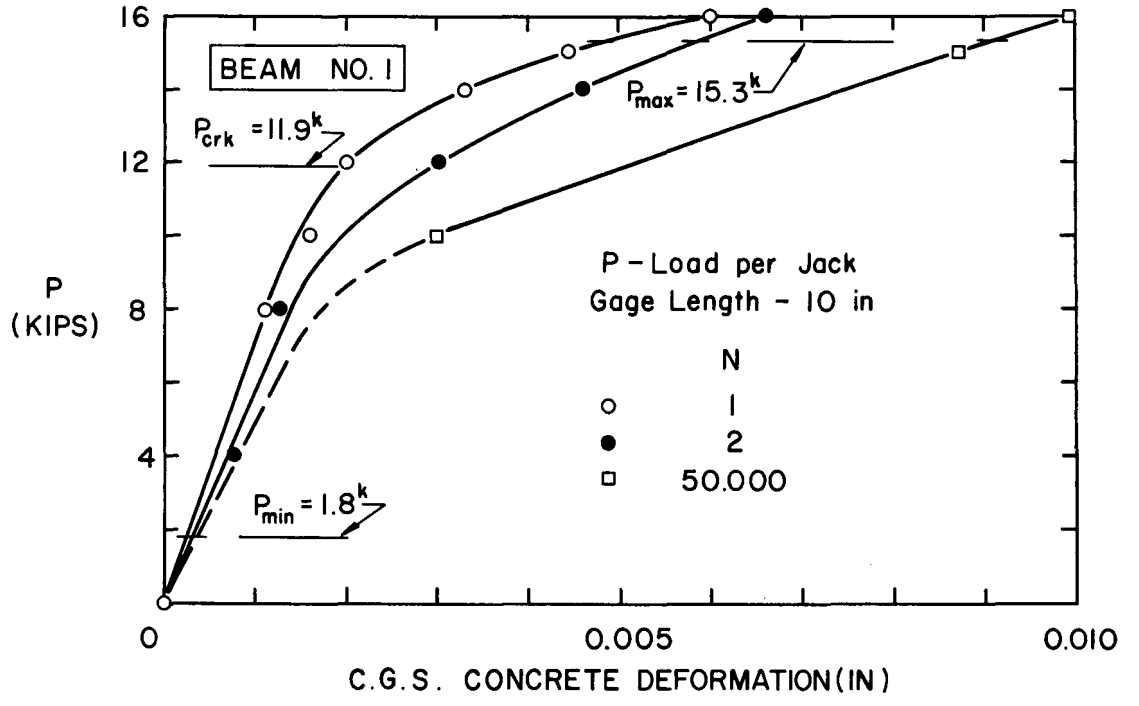

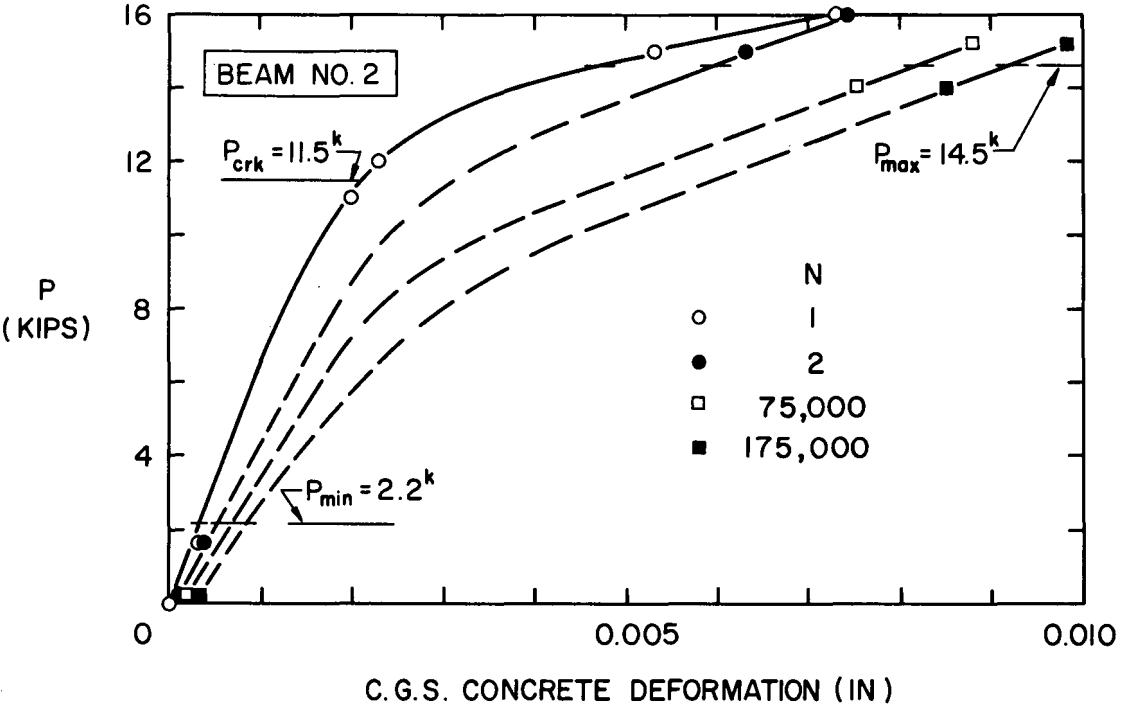

Fig. 17 C.G.S. Concrete Deformation Curves (Beams 1 & 2)

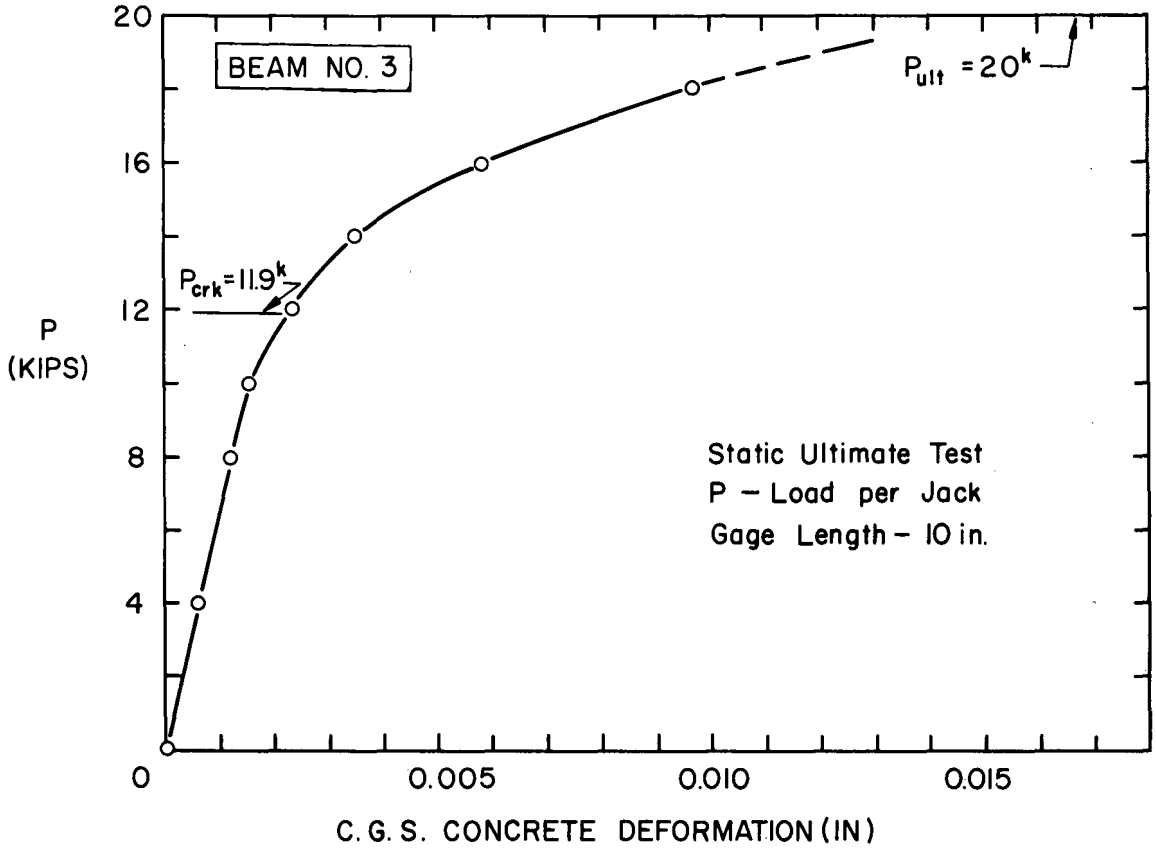

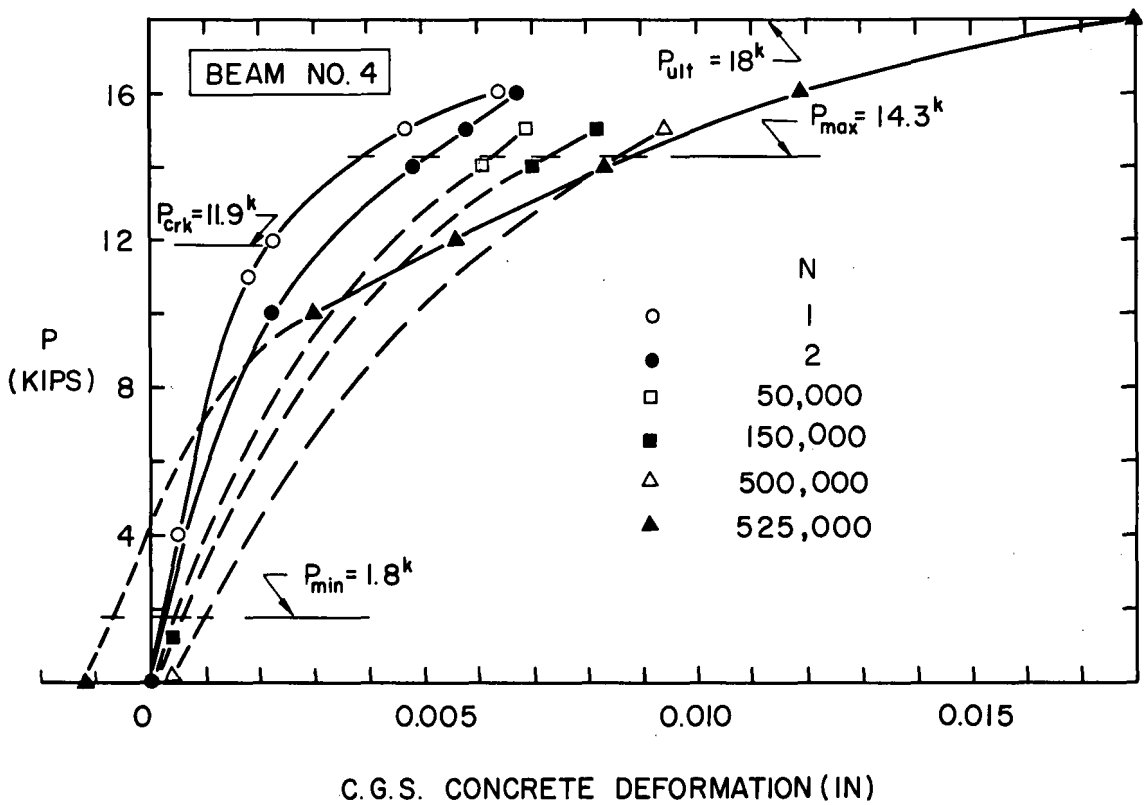

Fig. 17 C.G.S. Concrete Deformation Curves (Beams 3 & 4)

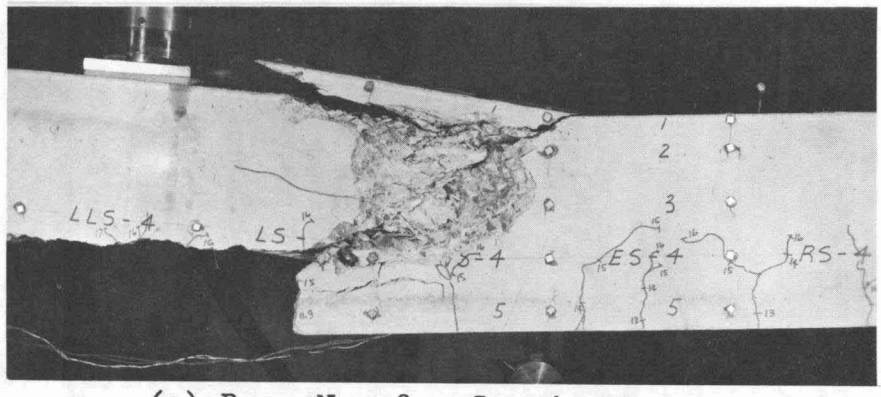

(a) Beam No. 3 - Static Test

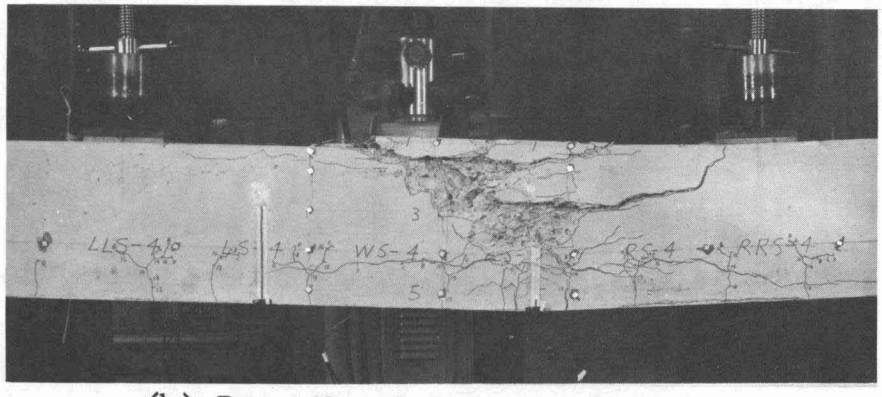

(b) Beam No. 2 - Fatigue Test

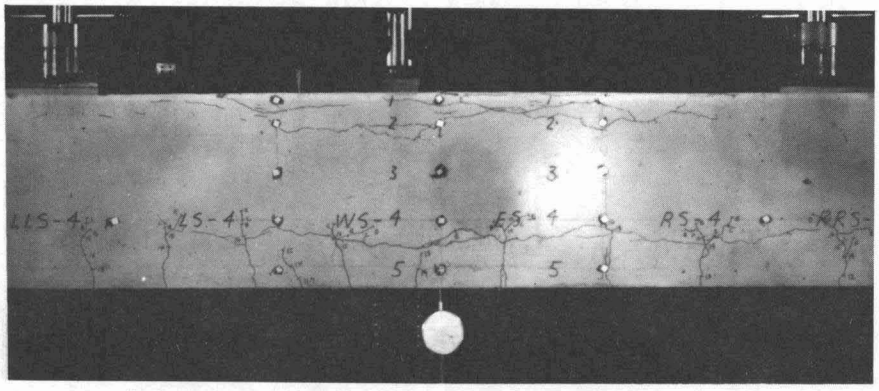

(c) Beam No. 4 - After N = 525,000

Fig. 18 Beam Failures and Beam No. 4 Crack Patterns

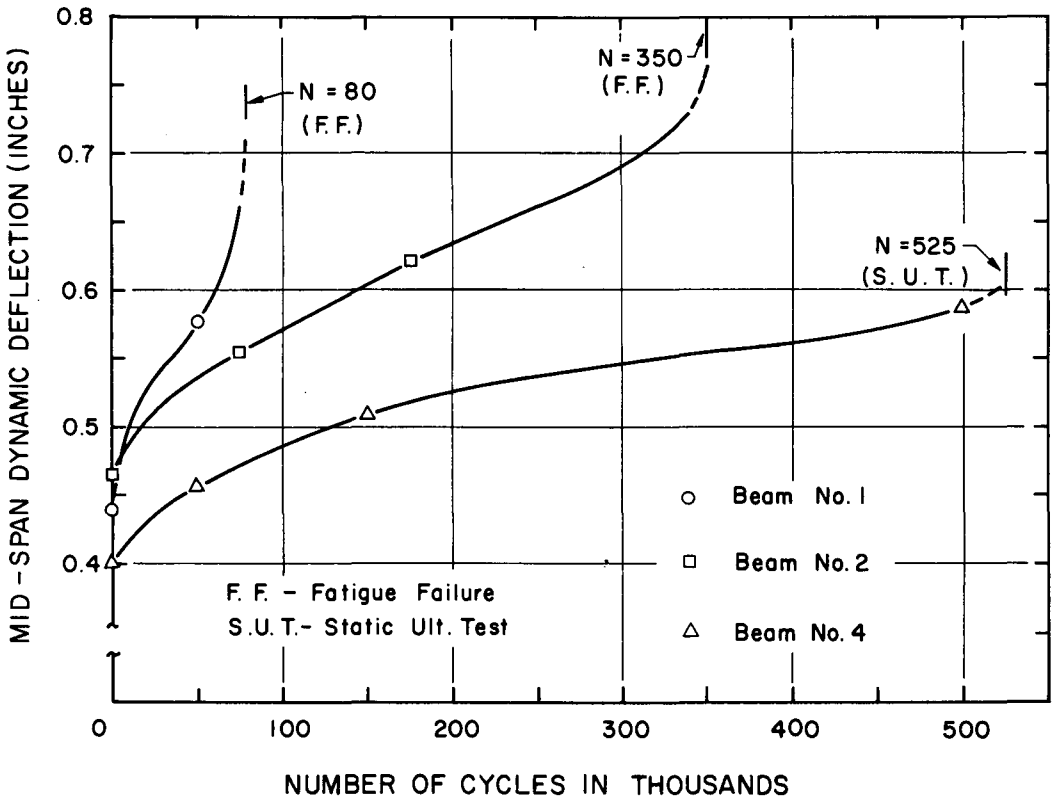

Fig. 19 Dynamic Deflection - Load Cycle Curves

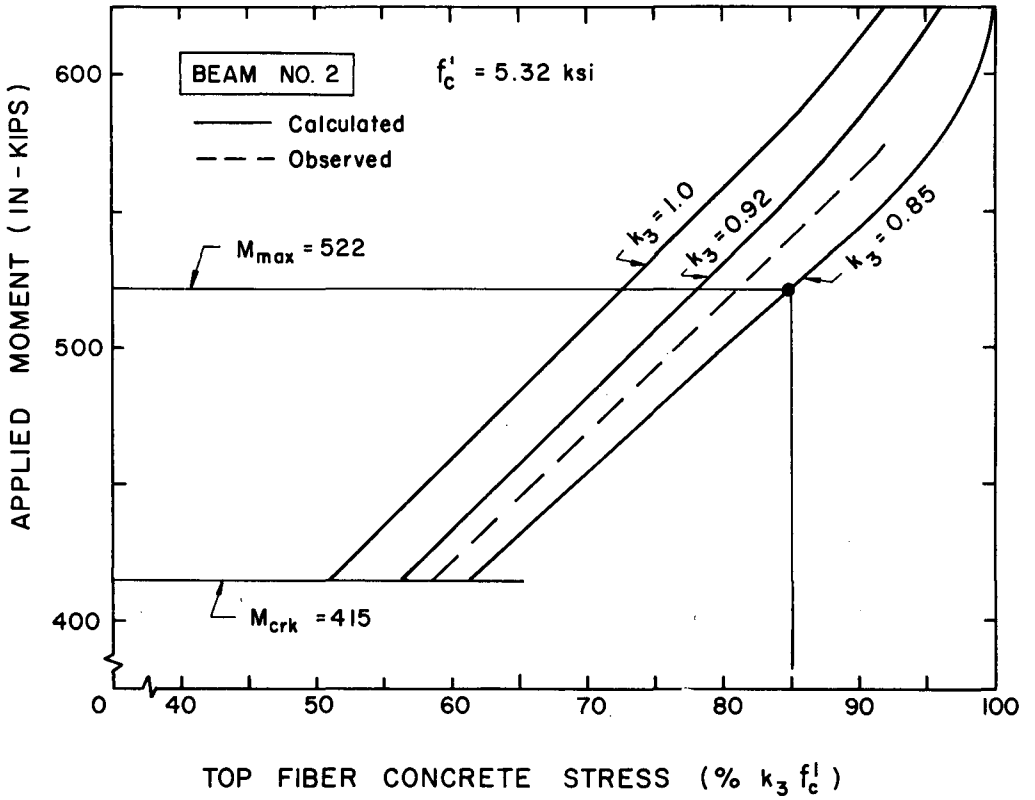

Fig. 20 Stress-Moment Curves (Beam No. 2)

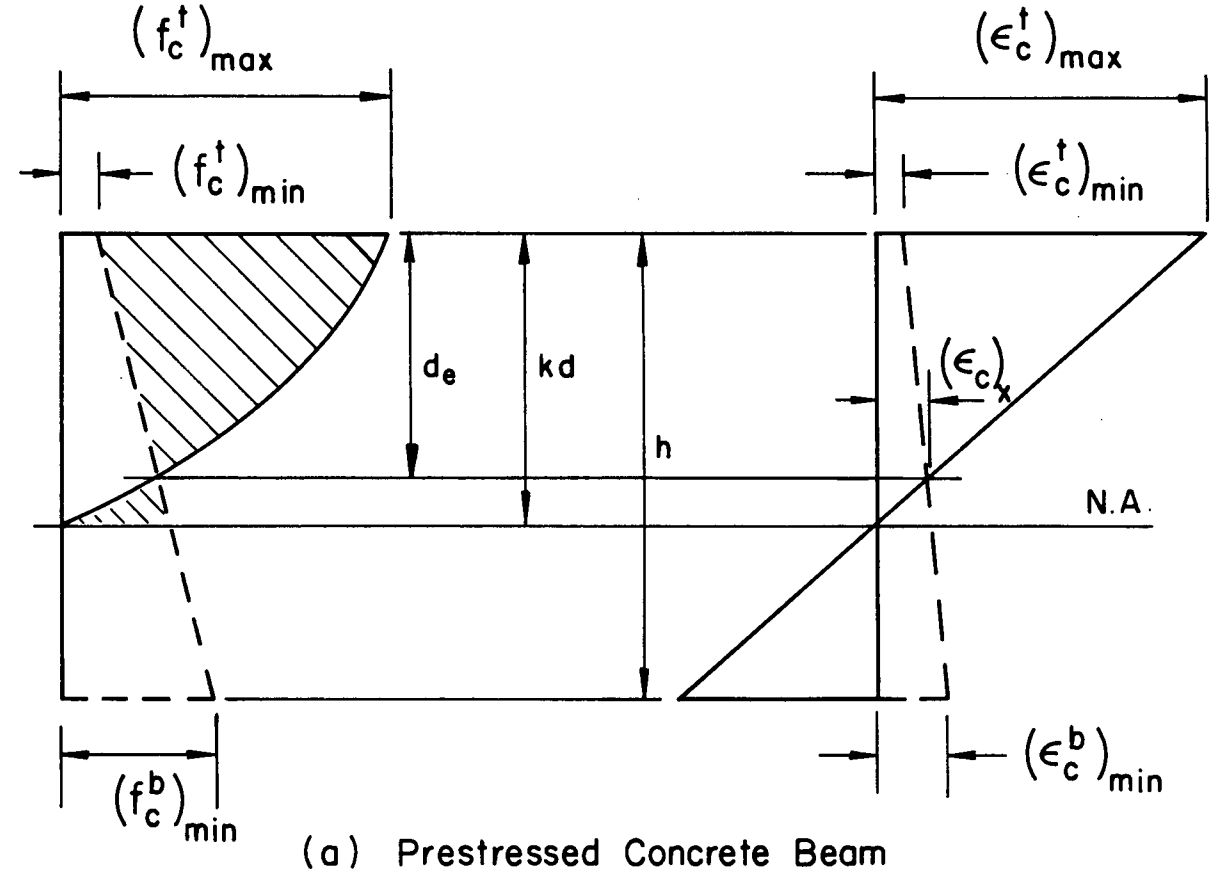

(a) Prestressed Concrete Beam

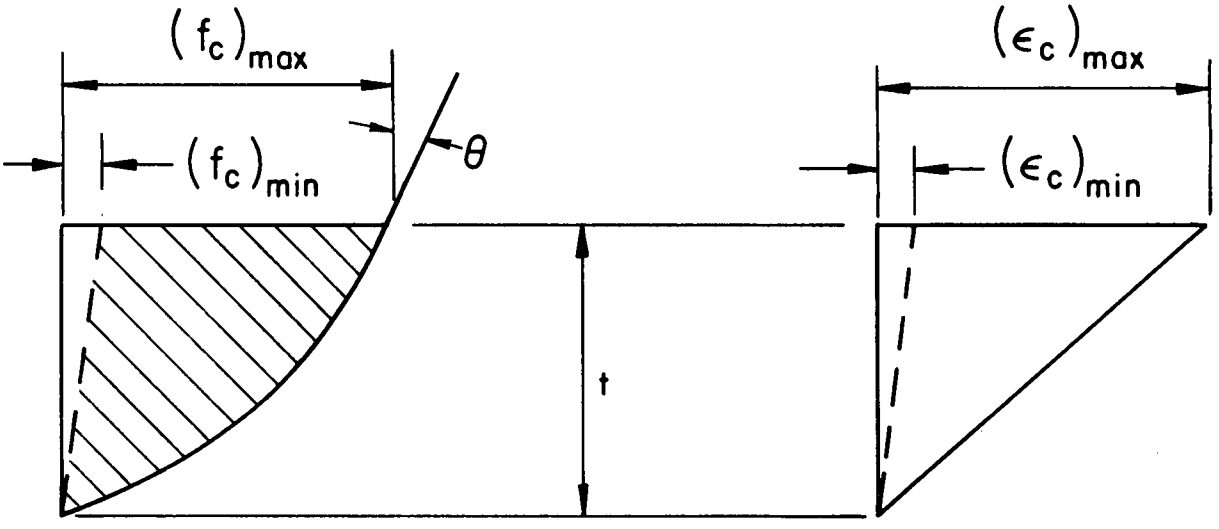

(b) Concrete Test Specimen

Fig. 21 Stress and Strain Distributions

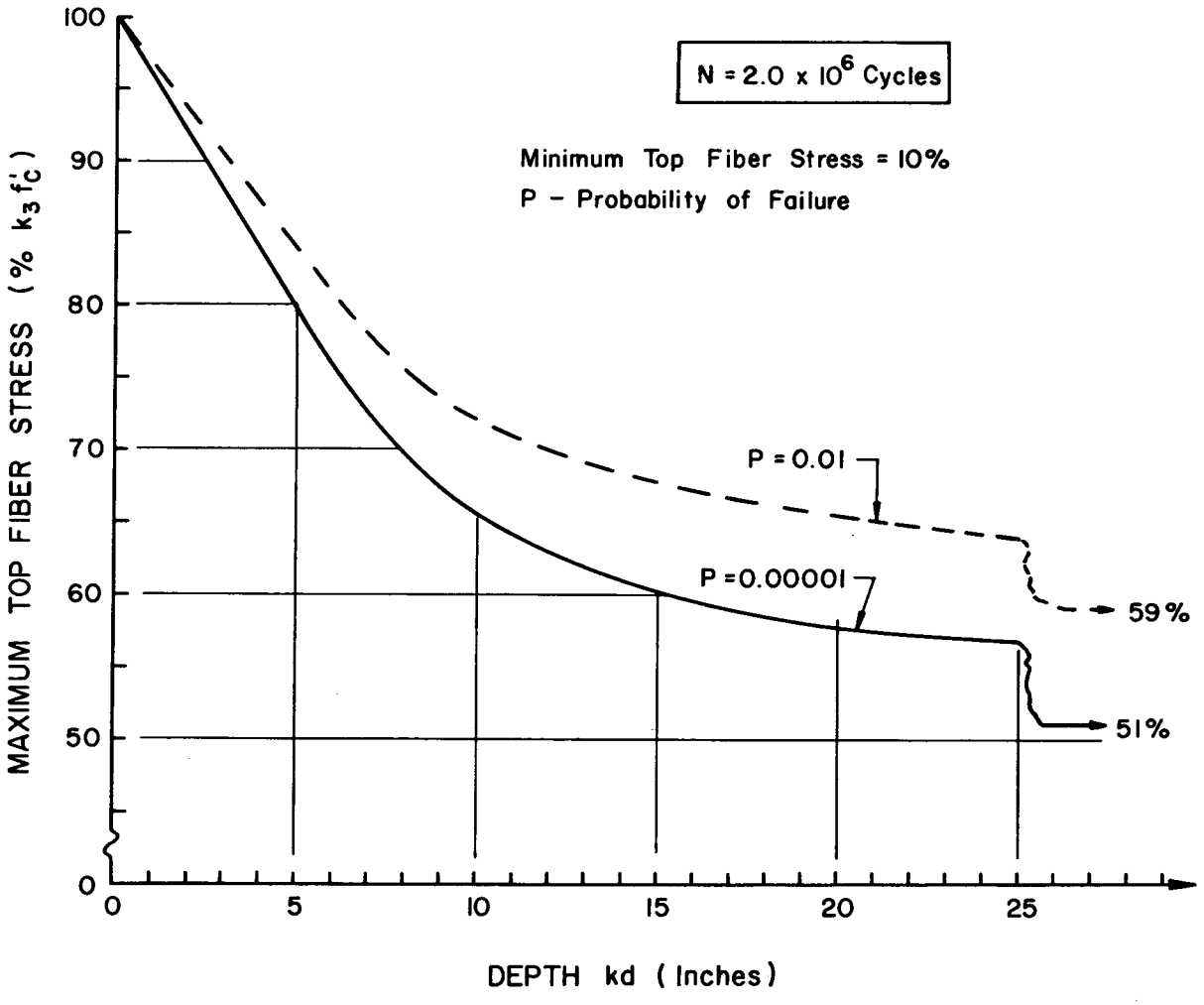

Fig. 22 Fatigue Strength vs. Compressive Depth kd

11. REFERENCES

1. ACI Committee 215
   FATIGUE OF CONCRETE
   ACI Bibliography No. 3, American Concrete Institute, Detroit, 1960

2. Nordby, G.M.
   FATIGUE OF CONCRETE - A REVIEW OF RESEARCH
   Journal, American Concrete Institute, Vol. 30, No. 2, August 1958, pp. 191-219

3. Venuti, W.J.
   PROBABILITY OF FATIGUE FAILURE OF BONDED-TYPE PRE-STRESSED CONCRETE BEAMS
   Technical Report No. 20, Department of Civil Engineering, Stanford University, February 1963

4. Considere, M.
   INFLUENCE DES ARMATURES METALLIQUES SUR LES PROPRIETES DES MORTIERS ET BETONS
   Compte Rendu de l'Academie des Sciences, Vol. 127, 1898, pp. 992-995

5. De Joly
   LA RESISTANCE ET L'ELASTICITE DES CIMENTS PORTLAND
   Annales des Pontes et Chaussees, Memoires, Vol. 16, Series 7, 1898, pp. 198-244

6. Van Ornum, J.L.
   FATIGUE OF CEMENT PRODUCTS
   Transactions, American Society of Civil Engineers, Vol. 51, 1903, p. 443

7. Van Ornum, J.L.
   FATIGUE OF CONCRETE
   Transactions, American Society of Civil Engineers, Vol. 58, 1907, pp. 294-320

8. Probst, E.
   EINFLUSS WIEDERHOLTER BELASTUNGEN AUF ELASTIZITAT UND FESTIGKEIT VON BETON UND EISENBETON
   Bauingenieur (Berlin), Vol. 6, No. 33, 1925, pp. 931-935

9. Graf, O.; Brenner, E.
VERSUCHE ZUR ERMITTLUNG DER WIDERSTANDSFAEHIGKEIT VON BETON GEGEN OFTMALS WIEDERHOLTE DRUCKBELASTUNG
Deutscher Ausschuss fuer Eisenbeton (Berlin), No. 76, 1934, pp. 1-13

10. Fowler, F.H.; Caldwell, N.J.
ON FATIGUE FAILURE UNDER TRIAXIAL STATIC AND FLUCTUATING STRESSES AND A STATISTICAL EXPLANATION OF SIZE EFFECT
Transactions, American Society of Mechanical Engineers, Vol. 67, 1945, p. 213

11. Weibull, W.
A STATISTICAL REPRESENTATION OF FATIGUE FAILURES IN SOLIDS
Transactions, Royal Institute of Technology (Stockholm), No. 27, 1949

12. Freudenthal, A.M.
PLANNING AND INTERPRETATION OF FATIGUE TESTS
Symposium on Statistical Aspects of Fatigue, Special Technical Publication No. 121, American Society for Testing Materials, June 1951, pp. 3-13

13. Stulen, F.B.
ON THE STATISTICAL NATURE OF FATIGUE
Symposium on Statistical Aspects of Fatigue, Special Technical Publication No. 121, American Society for Testing Materials, June 1951, pp. 23-40

14. Freudenthal, A.M.; Gumbel, E.J.
ON THE STATISTICAL INTERPRETATION OF FATIGUE TESTS
Proceedings, Royal Society (London), Vol. 216, Series A, February 10, 1953, pp. 309-332

15. Freudenthal, A.M.; Gumbel, E.J.
MINIMUM LIFE IN FATIGUE
Journal, American Statistical Association, Vol. 49, 1954, pp. 575-597

16. McCall, J.T.
PROBABILITY OF FATIGUE FAILURE OF PLAIN CONCRETE
Journal, American Concrete Institute, Vol. 30, No. 2, August 1958, pp. 233-244

17. Ekberg, C.E.; Walther, R.E.; Slutter, R.G.
FATIGUE RESISTANCE OF PRESTRESSED CONCRETE BEAMS IN BENDING
Proceedings, American Society of Civil Engineers, Vol. 83, No. ST4, July 1957, pp. 1304.1 - 1304.17

18. Slutter, R.G.; Ekberg, C.E.
STATIC AND FATIGUE TESTS ON PRESTRESSED CONCRETE RAILWAY SLABS
Bulletin, American Railway Engineering Association, Vol. 60, No. 544, June-July 1958, pp. 3-50

19. Assimacopoulos, B.M.; Warner, R.F.; Ekberg, C.E.
HIGH SPEED FATIGUE TESTS ON SMALL SPECIMENS OF PLAIN CONCRETE
Journal, Prestressed Concrete Institute, Vol. 4, No. 2, September 1959

20. Lane, R.E.; Ekberg, C.E.
REPEATED LOAD TESTS ON 7-WIRE PRESTRESSING STRANDS
Progress Report No. 223.21, Fritz Engineering Laboratory, Lehigh University, January 1959

21. Warner, R.F.; Hulsbos, C.L.
PROBABLE FATIGUE LIFE OF PRESTRESSED CONCRETE FLEXURAL MEMBERS
Fritz Engineering Laboratory Report No. 223.24A, Lehigh University, July 1962

22. Miner, M.A.
CUMULATIVE DAMAGE IN FATIGUE
Journal of Applied Mechanics, Vol. 12, P.A-159, September 1945

23. Hognestad, E.; Hanson, N.W.; McHenry, D.
CONCRETE STRESS DISTRIBUTION IN ULTIMATE STRENGTH DESIGN
Journal, American Concrete Institute, Vol. 27, No. 4, December 1955 (Proceedings Vol. 52, p. 455)

24. Chen, W.F.
A STUDY OF LIMIT DESIGN IN STRUCTURAL CONCRETE
Master's Thesis, Department of Civil Engineering, Lehigh University, 1963

25. Brownlee, K.A.
INDUSTRIAL EXPERIMENTATION
Chemical Publishing Co., Inc., New York, 1953, p.51